THE ROLE OF PHOSPHORYLATION OF THE MUMPS VIRUS PHOSPHOPROTEIN IN VIRAL PATHOGENESIS

by

ADRIAN KATHRYN PICKAR

(Under the Direction of Biao He)

ABSTRACT

Mumps virus (MuV) is a human pathogen that causes acute parotitis and is highly neurotropic. Even though the mumps vaccine has dramatically reduced disease incidence, large outbreaks have recently occurred in vaccinated populations. There is no antiviral drug for MuV infection. MuV is a paramyxovirus containing a negative-sense nonsegmented RNA genome. The RNA-dependent RNA polymerase of MuV minimally consists of the phosphoprotein (P) and the large protein (L). While P does not have intrinsic enzymatic activity, it is an essential cofactor for the viral polymerase, and has a variety of functions, including enabling binding of the P-L complex to the nucleocapsid template and preventing self-assembly of nascent nucleoprotein (NP). The P protein is heavily phosphorylated. The importance of P phosphorylation in paramyxovirus transcription and replication has been studied in numerous viruses, and it has been shown to play a role in regulating viral mRNA synthesis. We hypothesized that phosphorylation of MuV P plays roles in viral transcription and replication. Understanding functions of viral proteins will aid development of antiviral strategies. In this study, a strain of MuV

from a recent outbreak in Iowa in 2006, $MuV^{Iowa/US/06}$, was used to examine the role of phosphorylation of MuV P in viral RNA synthesis. Using mutational analysis and a minigenome system, the roles of the MuV P domains was investigated. We found that the functions of the N-terminal and C-terminal domains can be trans-complemented and that this complementation requires the oligomerization domain. To investigate the roles of serine (S) and threonine (T) residues of P in viral RNA synthesis, P was subjected to mass spectrometry and mutational analysis. We found ten critical S/T residues for minigenome activity, and analysis of a recombinant virus containing a P-T101A mutation suggests that phosphorylation of MuV-P-T101 plays a negative role in viral RNA synthesis. We also identified a host kinase, PLK1, that phosphorylates MuV P and this phosphorylation negatively regulates viral transcription. Together, these results show a role for phosphorylation of MuV P in regulating viral RNA synthesis and provide insight into potential targets for development of antiviral strategies and vaccines.

INDEX WORDS: Paramyxovirus, mumps virus, P protein, oligomerization, phosphorylation, PLK1, animal models

THE ROLE OF PHOSPHORYLATION OF THE MUMPS VIRUS PHOSPHOPROTEIN IN VIRAL PATHOGENESIS

by

ADRIAN KATHRYN PICKAR

BS, University of Richmond, 2010

A Thesis Submitted to the Graduate Faculty of The University of Georgia in Partial Fulfillment of the Requirements for the Degree

DOCTOR OF PHILOSOPHY

ATHENS, GEORGIA

2015

THE ROLE OF PHOSPHORYLATION OF THE MUMPS VIRUS PHOSPHOPROTEIN IN VIRAL PATHOGENESIS

by

ADRIAN KATHRYN PICKAR

Major Professor:	Biao He
Committee:	Ralph A. Tripp
	Zhen Fu
	Mark Jackwood
	Ming Luo

Electronic Version Approved:

Suzanne Barbour
Dean of the Graduate School
The University of Georgia
August 2015

DEDICATION

This work is dedicated to my parents, Mike and Kathy Pickar, for their love and support. Thank you for believing that I can achieve my dreams, I hope to make you proud.

ACKNOWLEDGEMENTS

I would like to thank my major professor, Biao He for his helpful advice and for always pushing me to improve. Thank you for your guidance and for providing the opportunity to explore my own ideas and to learn from my own mistakes. I would also like to thank my committee members Ralph A. Tripp, Zhen Fu, Mark Jackwood, and Ming Luo for their guidance and insight throughout my graduate degree.

I appreciate the encouragement, helpful discussion and technical assistance from all members of our lab specifically including Yuan Lin, Zhuo Li, Pei Xu, Jimmy Zengel, Stephanie Foster, and Ligon O'Kelly. I specifically would like to thank Yang Yang for sharing his ideas, providing laughter, and for being an amazing friend that I can count on for support in any circumstance. Thank you to Shannon Phan for sharing your knowledge, for helping to optimize conditions, and for listening when I needed encouragement. Thank you to Andrew Elson for all your friendship and assistance with my various projects. It was a privilege to mentor you and then to watch you gain independence in the lab following your undergraduate commencement. Thank you to Samantha Tucker for your feedback and encouragement and for being an incredible roommate. Your friendship has made my graduate experience more enjoyable.

Thank you to Nicole Josleyn for providing my first opportunity to be a scientist, for being a great mentor, and for believing in me. You taught me how to persevere when science is challenging, and your mentorship helped build the foundation of my career.

Thank you to Kat Cashman for your expertise and for encouraging me to seek out the information I needed. Your mentorship prepared me well for graduate school.

Thank you to my family for your support and for being interested when I was excited to share a discovery with you. I appreciate you making an effort to understand my passion and to learn about my research.

Thank you to Emily Taylor for your encouragement and friendship since we were young. Having a childhood friend to explore common interests with while growing up has fortified my love for science. Thank you for pushing me to share my knowledge with the public, and for encouraging me to push my limits.

Finally, thank you to Matt Oliver for your love and support throughout this endeavor. Thank you for increasing my awareness and for pushing me to explore more topics. You have strengthened my passion for science and I'm thankful to share this curiosity with you.

TABLE OF CONTENTS

Page

LIST OF TABLES

Page

LIST OF FIGURES

Page

CHAPTER 1

INTRODUCTION

Mumps virus (MuV) is a human pathogen that causes acute parotitis and is highly neurotropic, with infection of the central nervous system evident in almost half of all clinical cases (1). Even though the measles, mumps, rubella (MMR) vaccine, which contains the attenuated Jeryl Lynn MuV strain, has dramatically reduced disease incidence, large outbreaks still occur even in vaccinated populations (2, 3). There is no specific antiviral therapy for mumps infection. The development of MuV therapeutics and better vaccines is needed. Viral RNA synthesis is a potential process to be targeted for combating this affliction. MuV is a member of the family *Paramyxoviridae*. The phosphoproteins (P) of paramyxoviruses play numerous roles in viral RNA synthesis. While P does not have intrinsic enzymatic activity, it is an essential cofactor for the viral polymerase, and has a variety of functions, including enabling binding of the P-L complex to the nucleocapsid template and preventing self-assembly of nascent nucleoprotein (NP) (4, 5). The phosphoproteins (P) of paramyxoviruses are highly phosphorylated. The importance of P phosphorylation in paramyxovirus transcription and replication has been studied in numerous viruses, and it has been shown to play a role in regulating viral mRNA synthesis (6–10). The role of MuV P phosphorylation remains to

be examined. The central hypothesis of these studies is that phosphorylation of MuV P plays roles in viral transcription and replication. The study includes the following aims:

Specific Aim 1. To determine the roles of the MuV P domains in viral RNA synthesis. A novel minigenome system was developed to study the functional domains of P using trans-complementation. The roles of the P domains were investigated using mutational analysis and a minigenome system to provide structure-function insights. The working hypothesis is that the MuV P domains are biologically active by trans-complementation through the oligomerization domain.

Specific Aim 2. To determine the phosphorylated residues of MuV P that are critical for viral transcription and replication. The working hypothesis is that phosphorylation of these 10 residues is critical for viral RNA synthesis. Phosphorylated MuV P residues were detected by mass spectrometry analysis and mutation of 10 of these residues resulted in changes in transcription and replication in the MuV minigenome system.

Specific Aim 3. To determine the role of host kinases in MuV P phosphorylation. The working hypothesis is that phosphorylation of MuV P is completed by a host kinase. PLK1 is known to negatively regulate viral transcription in the closely related virus, parainfluenza virus 5 (PIV5). MuV growth kinetics were enhanced with the addition of a PLK1 inhibitor, and MuV P has been found to interact with PLK1 via coimmunoprecipitation. The working hypothesis is that MuV P is phosphorylated by the host kinase, PLK1, and this phosphorylation negatively regulates viral transcription.

These specific aims will provide a better understanding of the role of MuV P phosphorylation in viral pathogenesis. Understanding the viral and host proteins involved in viral RNA synthesis will be a vital approach in the elucidation of potential antiviral strategies. Over 5700 mumps cases were reported in a 2006 outbreak that originated at a university in Iowa and spread to 11 other states and the complete genome of an isolate, $MuV^{Iowa/US/06}$ (referred to as MuV), from this epidemic has been sequenced (2, 11). Therefore, the $MuV^{Iowa/US/06}$ strain functions as a model to examine viral RNA synthesis in more detail. No small animal model has been established for a systemic infection with MuV (12). Development of a small animal model will be a useful tool to study the role of phosphorylation in MuV pathogenesis. The rationale for these studies is that successful completion will provide possible anti-viral targets as well as recombinant viruses that will aid in vaccine development strategies against MuV.

CHAPTER 2

LITERATURE REVIEW

Classification and history

MuV has a nonsegmented, negative-stranded RNA genome of 15,384 nucleotides and is a member of the family *Paramyxoviridae* (1). The family includes many important human and animal pathogens and is further divided into the paramyxovirinae, pneumovirinae, and unclassified paramyxovirus subfamilies (Fig. 2.1). MuV belongs to the subfamily *Paramyxovirinae*, and genus *Rubulavirus* (1). Parainfluenza virus 5 (PIV5) is a prototypic virus for this family and is the most closely related virus to MuV.

Hippocrates described mumps in the first book of the *Epidemics* in the 5th century BCE (13). He included characterizations of parotitis complicated by orchitis in both children and adults. In the late 18th century, central nervous system (CNS) involvement with MuV was first associated together by the physician, Hamilton (14). Early etiology investigations for mumps were conducted using bacteriological methods, however suggestions of a filterable and transmissible agent led to a study by Johnson and Goodpasture that resulted in the proposal of a viral infection in 1934 ((15), reviewed in (1)). This hypothesis was later confirmed with the successful isolation, propagation, and characterization of MuV through the use of embronated eggs in 1945 (16, 17). The introduction of tissue culture was critical for advancing studies of viruses. This system

was then adopted as a more practical alternative for propagating and studying MuV in 1955 (18). These systems permitted the development of the first live virus vaccine for MuV in 1958 which has enabled the dramatic reduction of mumps cases throughout the world (19–21).

Virion structure and morphology

Mumps virions are pleomorphic particles that are roughly spherical in shape and range from 100 to 600 nm in size (22, 23). A schematic representation of the *Rubulavirus* virion structure and incorporation of the viral proteins in the virion is provided in Figure 2.2. The viral RNA genome is encapsidated by the nucleoprotein (NP) to form the left-handed helical nucleocapsid with a unit length of 0.98 μm (24). This coiled inner structure produces a hollow filamentous tube that has a central core of 5 nm and a diameter of 17 to 20 nm (23–26). Each nucleocapsid ring consists of 13 NP subunits and RNA with a length of 78 nucleotides (27). This is consistent with the rule of six found in related viruses where the viral genome is a multiple of six for full encapsidation of the RNA since each NP subunit binds to six nucleotides (27–30). The ribonucleoprotein complex is linked to the virion by the matrix (M) protein that forms a structured layer under the host cell-derived lipid envelope. The viral glycoproteins, hemagglutinin-neuraminidase (HN), fusion (F), and small hydrophobic (SH), project 12 to 15 nm from the envelope surface to produce a studded appearance (22).

Mumps virus genome

The nonsegmented negative-stranded RNA genome of mumps virus contains 15,384 nucleotides which make up a series of tandemly-linked genes separated by non-transcribed sequences in the order of 3'-Leader-NP-V/P-M-F-SH-HN-L-Trailer 5'(Fig. 2.3) (1, 31). The RNA genome of MuV contains seven open reading frames (ORF) but encodes nine viral proteins. The V/P gene encodes three proteins, V, P, and I. The V mRNA is faithfully transcribed by this gene, and the I and P mRNA is produced through the insertion of one or two non-template guanine residues, respectively, at site 155 via RNA editing (32). Thus, these proteins have the same N-terminal regions, but have different C-terminal ends due to a frame shift in the ORF.

The viral genes are separated by untranslated regions of variable lengths that include a gene start sequence upstream (3'- $U^{U}_{C}C^{GG}_{UU}N^{CU}_{UC}U$) and a gene end sequence downstream ($A^{AU}_{UA}U^{C}_{A}U_{6\text{-}7}$) that signal for mRNA synthesis termination and polyadenylation by the viral RNA dependent RNA polymerase (vRdRP) (31). The untranslated regions also contain intergenic regions with one nucleotide between P and M (A), M and F (A), and HN and L (G), two nucleotides between NP and P (AA), and SH and HN (CG), and seven nucleotides between F and SH (GAUUUUA) (31).

A 3' promoter leader region containing 55 nucleotides and a 5' trailer region containing 24 nucleotides are located at the genome termini. The vRdRP initiates RNA synthesis at these sequences (31, 33, 34). The *cis*-acting elements described above are responsible for regulating transcription and replication levels of the virus.

Mumps viral proteins

Nucleocapsid protein

The nucleocapsid protein (NP) is the first translated transcription unit of MuV. This protein is 549 amino acid residues in length, 61kD to 73kD in size, and is divided into two regions, an N-terminal domain and a C-terminal tail (35, 36). The N-terminal domain is also referred to as the assembly domain because the first 400 amino acid residues are responsible for RNA encapsidation and formation of the nucleocapsid (36, 37). This domain is also responsible for P protein binding, which differs from measles virus (MeV) and Sendai virus (SeV) in that the C-terminal tail of NP encompasses the P protein binding site (36, 38, 39). The viral polymerase is able to associate with NP through its interaction with the P protein. The N-terminal domain sequence is well-conserved among viruses, however the C-terminal domain is hypervariable and has an intrinsically disordered structure (40).

The main function of NP is to form the nucleocapsid, which functions as the template for viral RNA synthesis. NP binds to both the viral genome and antigenome during transcription and replication, without sequence specificity (41). The nucleocapsid is the hallmark for nonsegmented negative-stranded RNA viruses. This nuclease-resistant structure is thought to aid the integrity of the viral RNA, as well as to protect it from host innate immune detection. The vRdRP is able to access the viral genomic RNA through the P-NP interaction on the nucleocapsid. Electron microscopy revealed uncoiling of the helical nucleocapsid by the N-terminal domain of MuV P (42).

In addition to forming the nucleocapsid structure, nascent NP (NP^o) is found in a soluble form within the cell. NP^o molecules assemble to form the new nucleocapsid

during viral RNA synthesis. The P protein binds to the NP monomer to form the NP°-P complex, and acts as a chaperone to prevent it from encapsidating non-specific cellular RNA (43). The accumulation of the NP°-P complex is thought to trigger the switch between viral transcription and replication (44–46).

Phosphoprotein and I protein

A shift in the ORF of the mumps virus V/P gene produces the phosphoprotein (P) mRNA by the insertion of two non-template guanine residues at site 155 (32). The translated polypeptide from this edited RNA is 391 amino acid residues in length and 41 to 47 kD in size (35). The P protein has numerous functions in virus transcription and replication (4). P is highly phosphorylated, and P phosphorylation is thought to regulate viral RNA synthesis. Phosphorylation of MuV P has been shown to play a negative role in viral transcription (47). The P protein does not have intrinsic enzymatic activities, but it is an essential cofactor for the vRdRp and enables binding of the P-L complex to the nucleocapsid template. P also prohibits self-assembly of nascent NP and prevents NP from encapsidating cellular RNA (43, 48).

The mumps I protein is also translated from a shift of the V/P gene ORF. The 171 amino acid residue and 19 kD I protein is translated from mRNA with an additional single guanine residue at this same editing site. Even though the I polypeptide has been identified in virus infected cells, it has yet to be identified in the virion (49). The function of the I protein remains to be determined.

V protein

The V protein contains 224 amino acid residues and is 25 kD to 28 kD in size. The V mRNA is faithfully transcribed by the V/P gene. Thus, the P, I and V proteins have the same N-terminal regions, but have different C-terminal ends due to a frame shift in the ORF. The unique C-terminal domain sequence of the V protein contains seven cysteine residues and is conserved among paramyxoviruses. The V protein is thought to be important in viral pathogenesis. This cysteine-rich domain is essential for binding to both MDA5 and LGP2, but is absent for V binding to RIG-I (50). MDA5 is an RNA helicase that functions in interferon (IFN) expression activation during viral infection. The MuV V protein is able to block this IFN activation through its interaction with MDA5 (50–52). A tryptophan-rich motif within the cysteine-rich domain is able to bind to STAT1 and subsequently leads to the ubiquitination and degradation of this IFN-induced signaling molecule (53–56). Besides direct targeting to STAT1, MuV V has been shown to interact with RACK-1 (adaptor for STAT1 binding to the IFN receptor) and to interfere with IFN signaling by competing with RACK-1 for the disruption of the complex formed from STAT-1, RACK1, and the IFN receptor (53).

The V protein of MuV is also able to cause degradation of STAT3 and reduces IL-6 expression (57, 58). Similar to PIV5, the MuV V protein is incorporated into virions (59, 60). Since the N-terminal domain of P is known to interact with NP, it is thought that this shared domain in V also interacts with NP for incorporation into the virion.

Matrix protein

The M gene encodes the structural matrix protein (M) which contains 375 amino acid residues and is 39 kD to 40 kD in size (61). The M protein assembles as a layer beneath the membrane to provide structural support to the virus particle. Based on studies with SeV M, it is thought that the folding of this basic protein creates a surface of positively charged domains that interact with the negatively charged lipid membrane surface (62). *Paramyxovirus* M proteins have also been shown to interact with the cytoplasmic tails of the viral glycoproteins, as well as with the viral ribonucleoproteins within the cytoplasm (63–66). The M, NP, and fusion proteins for MuV are required for efficient production of virus-like particles. The two MuV glycoproteins do not contribute equally to virus particle formation, with the fusion protein being the major contributor and the hemagglutinin-neuraminidase protein being the minor contributor. Co-transfection experiments showed that addition of the fusion protein resulted in enhanced particle release, whereas this was not observed with addition of the hemagglutinin-neuraminidase protein.. The M protein completes its essential role in inducing virus budding through interactions with the glycoproteins and nucleocapsid. The M protein functions by gathering the viral components at the plasma membrane for viral particle egress from the host cell. Studies with MuV and PIV5 revealed a FPVI and FPIV motif in the M proteins of MuV and PIV5, respectively, that are essential for viral budding (67, 68). M proteins have also been shown to recruit and interact with host proteins to assist in virus assembly and budding (69, 70).

Fusion protein

The fusion glycoprotein (F) is synthesized as an inactive precursor (F_0) that contains 538 amino acid residues and is 64 kD to 74 kD in size. The F protein is a type I transmembrane protein that mediates virus-to-cell and cell-to-cell membrane fusion for viral infectivity. A cleaved 19 amino acid residue signal peptide targets the F_0 inactive precursor to the rough endoplasmic reticulum where it undergoes N-glycosylation (71). As this protein travels through the *trans*-golgi network, it is cleaved by the cellular endoprotease furin following the last Arg residue of the cleavage site, Arg-Arg-His-Lys-Arg (amino acid residues 98 to 102), thus producing the subunits F1 and F2 (71–74). Formation of the disulfide-linked F1+F2 heterodimer is required for the F protein to be fusogenically active (75). The transmembrane subunit F1 is comprised of 436 amino acid residues and is 48-61 kD in size. The cleavage event exposes a hydrophobic domain in the N-terminus of the F1 subunit that makes up the fusion peptide. The distal subunit F2 contains 83 amino acid residues (following cleavage of the signal sequence) and is 10-16 kD in size.

Conservation of hydrophobic residues following the fusion peptide of enveloped glycoproteins is found among paramyxoviruses. In the F1 ectodomain of MuV, at least two heptad repeat (HR) domains of hydrophobic residues are found. The first heptad repeat, HR1, is located at the N-terminus and is followed by a longer spacer domain, and a second heptad repeat, HR2, is located at the carboxy terminus, followed by a shorter spacer domain, and is adjacent to the transmembrane anchor (76). MuV HR1 and HR2 form a stable six-helix bundle, however the specific processes involved in MuV fusion remain to be elucidated (77, 78). Conformational changes in the active F protein are

initiated by binding of the HN protein to the receptor, which lead to F fusion activity (79, 80). The HR domains function by bringing the viral and cellular membranes together due to a high affinity for each other, thus permitting membrane fusion to take place (77).

Small Hydrophobic protein

The small hydrophobic protein (SH) contains 57 amino acid residues and is 6 kD in size. The SH protein is a type I integral membrane protein and it is named due to comprising many hydrophobic amino acid residues, including a stretch of 25 hydrophobic residues located near the N-terminus which acts as a membrane anchor domain (31, 81, 82). Unlike the SH protein of PIV5 where the N-terminal faces the cytoplasm and the C-terminal is toward the cell surface, MuV SH is oriented so that the C-terminal faces the cytoplasm (82, 83).

Nucleotide sequences of the SH gene are hypervariable and have been used to identify MuV strains (84–86). A point mutation in the putative F gene polyadenylation signal of the Enders and Rubini strains results in F-SH bicistronic mRNA so that only the F protein is translated (85). Since the SH protein has not been detected in all MuV strains, this protein is not essential for virus replication. The function of the SH protein has been studied by replacing the PIV5 SH gene with that of MuV, as well as by altering the ORF of the MuV SH gene to generate a recombinant MuV that does not express SH, rMuVΔSH. Experiments using both of these methods have found that the SH protein of MuV functions similarly to that of PIV5 in that it can inhibit TNF-α and interfere with viral pathogenesis during infection (11, 87). rMuVΔSH increases NFkB activation and apoptosis in L929 cells and it is attenuated in an animal model using intracranial

injections of newborn rats to score neurotoxicity (11). The ataxin-1 ubiquitin-like interacting protein (A1Up) has been identified as a cellular target of the MuV SH protein (88). The interaction between these proteins was confirmed by co-immunoprecipitation and A1Up was found to redistribute the SH protein to the cellular proteasome, however the biological significance of these findings remains unclear.

Hemagglutinn-neuraminidase protein

The hemagglutinn-neuraminidase protein (HN) contains 582 amino acid residues and is 74 kD to 80 kD in size. The HN protein is a type II transmembrane glycoprotein. The N-terminal contains a 30 amino acid residue cytoplasmic tail, followed by a single hydrophobic transmembrane domain consisting of 23 amino acid residues, and a 78 amino acid residue membrane-proximal stalk domain that supports the large C-terminal globular six-blade propeller head structure (89–94). The HN protein contains nine potential glycosylation sites and comparison of HN proteins with other strains shows two major homology regions near the middle and in the C-terminal half of the protein (95). On the cell surface, the HN protein forms dimers through disulfide bonds in the hydrophilic stalk regions and by hydrophobic bonds at the bases (96). These linked dimers are believed to form symmetric tetramers by non-covalent interactions (93).

The HN protein has various functions during virus entry and egress. The HN protein recognizes sialylated glycoconjugates and since it can bind sialic acid as a receptor, the HN protein is responsible for MuV hemagglutination and hemadsorption (4). The HN protein also has enzymatic activity as a neuraminidase/ sialidase by removing neuramic acid/ sialic acid moieties from budding virus particles. Removing

these molecules from progeny virus eliminates aggregation caused by interactions between the potential virus receptors and the glycoproteins that would limit virus spread (4, 96). It has been proposed that the main receptor binding domain is located at the same site as the neuraminidase activity (97, 98). Interestingly, a HN-E335K mutation of the Urabe AM9 vaccine strain has been associated with neurovirulence and studies have shown that this mutation has a higher affinity of HN toward α2,6-linked sialic acid residues which are more abundantly exposed on the membrane of human neuroblastoma cells (99). The HN-E335K mutation caused changes in protein surface properties with minimal conformation changes and the HN-E335K virus has 11x higher neuraminidase activity (99, 100).

The HN protein also aids in entry of viral particles by activating F for fusion of the host cell and viral membranes (4). MuV HN has been critically linked to cell fusion in studies showing that selective proteolysis of the HN protein results in loss of F protein fusion activity (101).

Large protein

The large protein (L) contains 2261 amino acid residues and is 160 kD to 200 kD in size. Expression of the L protein is relatively low in infected cells since it is translated from the most distal gene in the MuV genome (102). Together, P and L make up the viral RNA dependent RNA polymerase, and the L protein is responsible for the enzymatic activities and capable of initiation, elongation, and termination of RNA synthesis (103–106). The L protein also adds the 5' cap and 3' poly(A) sequence to transcribed viral mRNA (107–109). Studies on VSV have found that L also has methyltransferase activity

(104, 110, 111). L is critical for viral transcription and replication and this is highlighted by its extreme sensitivity to mutations (112).

The L protein is made up of highly conserved stretches that are separated by variable regions. There is a high degree of homology within the conserved motifs, and these have been designated domains I through VI (113–115). The functions of these domains have been studied in various viruses. Domain II is positively charged and may contain a putative RNA binding site. Domain III has been proposed to be an active site for phosphodiester bond formation. Together, domains II and III constitute the polymerase module of the L protein (114–117). The capping addition is found in domain V and domain VI contains the methyltransferase activity (103, 106, 118, 119). Domains I, II, and IV do not have clear individual functions, but studies from mutagenesis analysis suggest that they may be involved in regulation of the transcription to replication switch (119, 120).

The L protein also functions through interactions with other viral proteins, as well as with itself. Self-oligomerization is independent of P, and occurs in the N-terminal half of the protein (121–124). The P-L complex makes up the viral polymerase, and P is needed to dock L to the nucleocapsid for viral RNA synthesis. P also helps stabilize L since L has been shown to be highly unstable in the absence of P (125). Studies investigating the putative P binding site on L have located interacting regions in the N-terminal of SeV, PIV5, human parainfluenza virus 3 (hPIV3), and measles virus L proteins (120, 126–129). The SeV C protein and human parainfluenza virus 2 (hPIV2) V protein have been shown to inhibit virus replication through their interactions with the L protein (125, 130). The part of MuV L that interacts with P has not been determined.

Virus entry

MuV enters the target cell by interacting with sialic acid, the acyl derivative of neuramic acid, as a receptor that is found on host glycoproteins and lipids. The HN protein is a specific sialic-acid-binding lectin that permits attachment of the virus to the host cell membrane (100, 131). Binding of HN to the receptor induces conformational changes in the F protein, which leads to F fusion activity (79, 80). MuV attachment and fusion results in dissociation of the helical nucleocapsid and delivery of the viral genetic content to the cytoplasm of the cell. The presence of MuV in infected cell cultures can be detected by the induction of syncytia (132–134).

Viral transcription and replication

Upon entry into the host cell, MuV undergoes viral RNA synthesis inside the cytoplasm. The proteins NP, P, and L are packaged inside the infectious virion, therefore these proteins are present upon infection. The packaged NP, P and L proteins function to initiate transcription so that additional viral proteins can be translated within the host cell. The linear, single-stranded RNA of the MuV genome represents a succession of individual protein-encoding genes. Each gene is defined by an upstream gene start signal and a downstream gene end signal. The intergenic regions of the 3' and 5' ends contain short nontranslated sequences. These sequences contain important *cis*-acting signals for viral transcription and replication. Synthesis of all viral mRNAs initiates at the 3' end sequence, termed the leader sequence, where the viral RNA-dependent RNA polymerase (vRdRp) transcribes the viral RNA genome into mRNAs, containing a 5' cap structure and 3' poly(A) tail, in a sequential manner. As the vRdRp moves across intergenic

regions, it must reinitiate at the downstream gene start site. Failure by the polymerase to reinitiate contributes to a 3'-5' gradient of transcripts that is produced from the sequential synthesis of individual viral mRNAs (135). Because of this, the gene order of MuV roughly reflects the viral protein amounts.

The V/P gene encodes three proteins, V, I and P. The V mRNA is faithfully transcribed by this gene, and the I and P mRNAs are produced via RNA editing, when the vRdRp recognizes a specific RNA sequence and 'stutters' thus causing an insertion of one or two non-template guanine residues in the I or P mRNA, respectively (136). This causes the V/P gene to be transcribed into two mRNAs at similar levels that are then translated into two proteins. Thus, these proteins have the same amino-terminal regions, but have different C-terminal ends due to a frame shift in the ORF.

To replicate vRNA (the negative sense viral RNA), an anti-genome sense RNA (cRNA or positive sense anti-genomic RNA) is first replicated starting at the 3' leader sequence and then the cRNA is replicated into the vRNA by the vRdRp, starting at the 5' trailer sequence (4). The functional template for viral RNA synthesis (viral mRNA transcription and viral RNA replication) of MuV, like other non-segmented, negative-sense RNA viruses, is contained in the ribonucleocapsid. This helical nucleocapsid structure is comprised of the viral genomic RNA encapsidated by the nucleoprotein (4). Only encapsidated RNA, not naked RNA, can be transcribed. This encapsidation not only protects the viral RNA as described above, but also functions to have anti-termination properties by causing the vRdRp to ignore the transcription signals in the intergenic junctions of the genome so that a full length replication product can be synthesized. Also, since MuV is a negative-sense RNA virus, a positive-sense antigenomic copy must first

be produced to function as the template for synthesizing additional negative-sense genomes. Similar to the 3' cis-acting leader signal for transcription, a 5' trailer sequence functions as the antigenomic RNA promoter for the vRdRp (17, 18). It has been found that the antigenomic promoter is stronger for RNA replication than the genomic promoter (17). In addition to the leader and trailer sequences, nucleotide sequences in the promoter of PIV5 have been found to be a second factor in replication efficiency. Three non-continuous sequence-dependent RNA segments, identified as CRI, CRII, and RIII, are separated by sequence independent spacer regions and are required for optimal RNA replication with the antigenomic promoter (18).

A transition occurs from transcription to replication during viral RNA synthesis of paramyxoviruses. There is an optimal ratio between the proteins NP, P, and L, and accumulation of the soluble NP-P complex is thought to trigger the switch from RNA transcription to genome replication (44–46). In the 3' terminal region, promoter elements have been identified (PrE-I and PrE-II) that may also play a role in regulating viral replication. These elements have been proposed to serve as an initial encapsidation site of the nascent RNA for NP to bind as the RNA emerges from the vRdRp. This may then provide an anti-termination signal for the viral polymerase at the leader-NP gene junction (137).

Virion assembly, budding, and egress

Replication and encapsidation of the viral genome occur alongside virion assembly. The newly synthesized negative sense genome is encapsidated by the nucleoprotein and is associated with the P-L polymerase complex in the cytoplasm. At

the same time, the viral glycoproteins are translated and then transported through the exocytic pathway to the plasma membrane. The M protein functions as the key organizer of virus assembly by binding to the nucleocapsid, cytoplasmic tails of the glycoproteins, as well as the lipid membrane. These interactions help to gather the viral components at the cell membrane for viral particle budding and egress. The M protein of measles virus has been shown to be responsible for preferential budding from the apical membranes of polarized cells (65, 138). Studies using virus-like particles (VLPs) have found that the M, NP and F proteins of MuV are required for efficient production. Studies examining the role of the MuV glycoproteins in VLP production showed that the F protein is the major contributor while the HN protein does not enhance particle release (68). Instead, the HN protein has enzymatic activity and functions to remove sialic acid moieties from budding virus particles to block aggregation.

Structural and functional characterization of the phosphoprotein

Paramyxovirus phosphoprotein characterization

The P proteins of paramyxoviruses are modular and consist of N-terminal, oligomerization, and C-terminal domains with flexible linkers between adjoining domains. P oligomerizes and forms complexes with L, NP, and the assembled nucleocapsid for its various roles in viral RNA synthesis. Self-association of P is observed throughout negative-stranded RNA viruses (NSVs). With the use of various sequence alignment and secondary structure prediction tools, numerous paramyxovirus P sequences from the parainfluenzavirus (SeV, hPIV3, human parainfluenza virus 1, and bovine parainfluenza virus 3), morbillivirus (canine and phocine distemper virus, measles

virus, and rinderpest virus), and rubulavirus (hPIV2, PIV5, human parainfluenza virus 4, Newcastle disease virus, and mumps virus) genera were predicted to oligomerize through a central coiled coil domain (139). Hydrophobic side chains at the alpha-helix interface of coiled coils can result in formation of dimers, trimers, or tetramers (140). Based on an epitope dilution assay, the P proteins of SeV, MuV, and Newcastle disease virus were originally suggested to form trimers (139, 141). However, more recent crystallization studies revealed differing oligomer formations and suggest that the P proteins can form tetramers.

The oligomerization domain of SeV P was the first to be crystallized and revealed a parallel coiled-coil tetramer (Fig. 2.4) (139, 142). Each SeV P monomer is composed of three short N-terminal helices, that form a small helical bundle at the N-terminal end, and a very long C-terminal helix (142). Deletion of the SeV P oligomerization domain inhibited transcription and replication of the viral genome RNA, thus demonstrating that self-association of P is required for transcriptional activity (142–144). This dependency of P oligomerization on biological function has been found for numerous other viruses as well (145–147). Tetrameric P structures have also been observed for other paramyxoviruses with crystallization of the P oligomerization domains for measles virus, human metapneumovirus, and mumps virus (148–154).

The modular structure of the SeV P protein domains have made alterations and deletions possible for functional characterization of the P domains without affecting the function of the other domains (139). The P protein of SeV is larger than that of mumps virus, consisting of 568 amino acid residues in length and it is divided into an N-terminal domain and a C-terminal domain. The NP^{o}-binding domain of P is in the N-terminus at

residues 33-41 and acts as a chaperone to prevent NP from assembling without the nascent viral genome (155, 156). The SeV P oligomerization domain has been defined as residues 320-446, and within this region is the binding site for SeV L (residues 412-445) (139, 142, 157, 158). The C-terminal residues 479-568 of SeV P are predicted to form a triple alpha-helical bundle that binds to the nucleocapsid (139, 144, 159, 160). An extreme C-terminal nucleocapsid-binding domain has also been found in other paramyxovirus P proteins (159, 161, 162).

The SeV P component of the vRdRP is thought to migrate down the NP-RNA template in steps of six nucleotides since it interacts with the NP protein which encapsidates six nucleotides per NP monomer. Since the L protein must progress over the viral RNA template in steps of one nucleotide, it has been proposed that the P protein cartwheels over the NP-RNA template as L transcribes the RNA in such a way that the tetrameric P and monomeric L interactions are continuously broken and remade (144). This model has also been used to explain viral RNA synthesis for measles virus, with additional insights on the coupling of catalysis and movement of the viral polymerase. Analysis of the measles virus P and NP interactions have revealed fast binding kinetics and a weak binding affinity between the two proteins (38). These kinetics are likely due to the necessity of the vRdRP to travel rapidly along the nucleocapsid during viral RNA synthesis.

Rhabdovirus phosphoprotein characterization

The P proteins of viruses that belong to the *rhabdoviridae* family have also been extensively studied. Crystallization of the P protein of vesicular stomatitis virus (VSV), a

member of the *rhabdoviridae* family, revealed formation of a dimer consisting of two parallel alpha-helices that are held together through hydrophobic interactions (147). The oligomerization domain of VSV P is also needed for P activity as observed by a VSV minigenome assay (146, 163). The crystal structure of the rabies virus P dimerization domain reveals that each monomer consists of a helical hairpin between two alpha-helices that permits interactions between the N-terminal helix of one monomer with the C-terminal helix of the other monomer (164). The N-terminal domain of rabies virus P interacts with the nascent NP and L, whereas the C-terminal domain binds to NP-RNA (165–167). This structural difference may be important for rabies virus P function since the N-terminal and C-terminal domains of P are positioned on the same side, whereas these domains are at opposite ends of the oligomerization domains for VSV and SeV P proteins.

Mumps virus phosphoprotein characterization

The oligomerization domain of MuV P has been defined as residues 213 to 277 and crystallization of this domain revealed two pairs of parallel alpha-helices that are antiparallel to each other (Fig. 2.4) (154). This unique tetramer orientation positions two N-terminal and two C-terminal domains on each end of the oligomerization domain, which likely has functional significance. The last 49 amino acid residues of MuV P (aa 343-391) were found to directly mediate binding to the nuclecocapsid through its interaction with the assembly domain of NP (36). An extreme C-terminal nucleocapsid-binding domain has also been found in other paramyxovirus P proteins (159, 161, 162). The N-terminal domain of MuV P also binds to the nucleocapsid (154). Electron

microscopy revealed uncoiling of the helical nucleocapsid by the N-terminal domain of P, which resulted in enhanced viral RNA synthesis in a minigenome system (42). Since both the N-terminal and C-terminal domains of MuV P bind to NP, its novel tetramer orientation may be required. However, the function of the MuV P oligomerization domain has not been examined for viral RNA synthesis. The L binding domain in MuV P has not been examined, however the L protein of RSV and human PIV2 have been shown to interact with the C-terminal domains of the respective P proteins (168, 169).

Paramyxoviridae P phosphorylation and host kinases

The virus family *Paramyxoviridae*, that contains MuV, also contains many human and animal pathogens such as Sendai virus (SeV), respiratory syncytial virus (RSV), parainfluenza virus 5 (PIV5), Measles virus (MeV), Hendra virus (HeV), and Nipah virus (NiV) (4). The P proteins of paramyxoviruses are highly phosphorylated and phosphorylation of these proteins in transcription and replication has been shown to play a role in regulating viral mRNA synthesis (6–10). The most heavily phosphorylated P protein of paramyxoviruses belongs to RSV, which contains two clusters of phosphorylation sites (170–174). Approximately 80% of RSV P protein phosphorylation is localized to S232, while the remaining is distributed among S116, S117, S119, and S232 (173). These major phosphorylation sites were found to reduce virus replication *in vitro* by 20% upon mutation and testing in an RSV minigenome system (175). Incorporation of these five sites in a recombinant RSV virus did not appear to activate alternative phosphorylation sites, and phosphorylation was reduced by 90%. Peak titers were reduced in cells infected with this recombinant virus, and it was highly attenuated in

mice and cotton rats. Thus, demonstrating that phosphorylation of the RSV P protein is required for efficient virus growth *in vitro* and *in vivo* however further studies are needed to determine if phosphorylation of RSV P plays a role in viral RNA synthesis (175). Mass spectrometry was used to identify T108 as an additional phosphorylation site in the RSV P protein and minigenome activity was diminished upon mutation of this residue (6). Viral RNA synthesis is mediated by P and M2-1 interactions via the dynamic dephosphorylation-phosphorylation at T108, which controls the M2-1 protein incorporation into the vRdRp, however this was not examined with a recombinant virus (6). It is important that minigenome observations are also examined in the context of virus infection for broader application of the results from P protein phosphorylation studies.

With the use of recombinant viruses, P protein residues of PIV5, a prototypical paramyxovirus, were found to play both negative and positive roles in mRNA synthesis (7–9). A phosphorylation site at S157 was found in the P protein of PIV5-infected cells (7). Further studies found that polo-like kinase 1 (PLK1) associated with S157 and phosphorylated the PIV5 P protein at S308 (7, 8). Phosphorylation of both of these residues reduced viral gene expression and prevented cytokine induction and cell death. This is the first report that P protein phosphorylation negatively regulated viral gene expression, suggesting that PIV5 limits its gene expression to avoid induction of innate immune responses (8). Further studies of the PIV5 P protein by mass spectrometry identified T286 as a phosphorylation site and mutation of this residue reduced minigenome activity (9). A recombinant virus containing the T286 mutation grew slower than wild-type PIV5 and had delayed viral mRNA synthesis and protein expression,

demonstrating that phosphorylation at T286 plays a positive role in virus growth and viral gene expression by upregulating viral mRNA transcription (9). These studies suggest a role of P protein phosphorylation in viral mRNA synthesis, however a detailed mechanism remains to be elucidated.

It is commonly believed that phosphorylation of the P proteins is carried out by host kinases (176). The host kinases, casein kinase II (CKII), protein kinase c isoform zeta (PKC-ζ), protein kinase B (AKT) and PLK1, have been identified so far as the main host kinases that phosphorylate paramyxovirus P proteins. CKII is thought to phosphorylate the P proteins of RSV (171, 177) and measles virus (178). PKC-ζ is reported to phosphorylate the P proteins of hPIV3 (179) and Sendai virus (180). The P protein of canine distemper virus is phosphorylated by both PKC-ζ and CKII (181). AKT phosphorylates the P protein of PIV5 to up-regulate its gene expression whereas PLK1's phosphorylation of P of PIV5 down-regulates its gene expression. It has been proposed to target host kinases that are critical for viral RNA synthesis as an anti-viral strategy for these paramyxoviruses (182).

Detailed examination of MuV P phosphorylation has not been completed. Characterization of MuV polypeptides was completed in the 1970s (35, 183–185), and at this time, phosphorylation was only found with MuV NP (186). However, when immunoprecipitation was used to reduce the high background of host cell proteins from virus-specific phosphoproteins, all the major mumps polypeptides were found to be phosphorylated (74). An identified 45 kD protein (p45), corresponding to MuV P, was found to be phosphorylated and on rare occasions, unphosphorylated. Interestingly, a minor 47 kD protein species (p47) was identified and found to be phosphorylated at least

20-fold more than p45. It is believed that p47 is a more highly phosphorylated form of p45 and that the band shift may be due to migration behavior depending on the electrophoretic conditions (74). Thus, a major MuV P species (p45, lower molecular weight) and a minor MuV P species (p47, highly phosphorylated form) have been identified. Further characterization of MuV P phosphorylation and its role in viral transcription and replication is needed to elucidate the significance of MuV P phosphorylation.

Transmission and pathogenesis

MuV infection is restricted to humans and is moderately to highly contagious. Transmission of natural infections occurs through direct contact, droplet spread, or contaminated fomites (187). During the 15 to 24 day incubation period, MuV propagates in the upper respiratory mucosa, spreads to draining lymph nodes, and can become viremic, where it can then infect virtually all tissues and organ systems (188–190). Systemic viral spread can occur via infected mononuclear cells, or possibly T cells (191). The hallmark for MuV infection is parotitis, and even though viral involvement with the parotid gland is thought to be a primary feature of all types of mumps infection (192), about one third occur without recognized symptoms (193, 194). MuV is also highly neurotropic where invasion of the central nervous system is evident in almost half of all clinical cases, with asceptic meningitis occurring in approximately 10% of cases and encephalitis in less than 1% (1).

A bat virus has been recently identified with high phylogenetic relatedness to human MuV at the nucleic acid level. The functional activities of the HN and F proteins

of the bat virus (batMuV) were compared to those of human MuV and were found to be serologically and functionally related (195). This discovery raises questions regarding whether bats may be a reservoir for interspecies transmission of MuV and whether neutralizing antibodies generated against MuV can protect humans from batMuV.

Treatment and vaccination

There is no specific antiviral therapy for mumps infection and treatment is generally provided to alleviate disease symptoms. At least 12 strains of MuV are used as live attenuated vaccines throughout the world (196). The mumps vaccines are available as monovalent vaccines or in combination with other vaccines. At present, the trivalent measles, mumps, and rubella vaccine (MMR) containing the Jeryl Lynn mumps strain (JL) is the most widely used and has been the licensed vaccine used in the United States since 1967 (1). The recommendation for MMR and varicella vaccination by the Advisory Committee on Immunization Practices (ACIP) is 12–15 months of age for the first dose and 4–6 years of age for the second dose (197). The JL vaccine strain was originally isolated from a mumps patient in 1963 and was then attenuated through continuous passages in hen eggs and chick-embryo cell cultures (198). The steady decline in reported mumps cases following introduction of the live attenuated mumps vaccine can be seen in Figure 2.5. Even though the JL vaccine has been shown to be safe and efficacious (1, 199–203), recent large outbreaks have occurred in the United States and worldwide (204–207). Over 5700 mumps cases were reported in a 2006 outbreak that originated at a university in Iowa and spread to 10 other states (2). A mumps outbreak occurred in New York and New Jersey in 2009-2010 where 88% of the patients had one-dose of mumps

vaccine and 75% of patients had two doses (3). Recently concerns have been raised as to the efficacy of the current vaccine program in the United States since both of these outbreaks occurred among highly vaccinated populations.

There is no established mumps neutralizing antibody titer predictive of protection against infection or disease. The lack of immune correlates to protection makes it difficult to standardize the efficacy of the current vaccine program. There are currently 13 MuV genotypes classified based on the sequence of the small hydrophobic (SH) gene (208). JL is a genotype A strain, and recent circulating wild-type strains are genotype G, therefore there may be antigenic differences between the vaccine and outbreak strains. Serum from individuals vaccinated with JL neutralized the outbreak-associated genotype G $MuV^{Iowa/US/06}$ strain in vitro by one-half of the geometric mean titer associated with their ability to neutralize the JL strain (209). Neutralization epitopes of the hemagglutinin and fusion envelope glycoproteins were not compared, supporting the existence of antigenic differences that may influence individual immunity (209). Antibodies directed against SH have not been detected in human sera, therefore it is unlikely that this protein is a target for antibody-mediated virus neutralization (210). Thus, the current MuV genotype classification system may not be ideal for comparing vaccine versus outbreak MuV strains.

B cell responses have been examined early after vaccination, but cell-mediated immunity should also be considered for evaluating vaccine efficacy. Certain MuV strains may be capable of escaping vaccine-induced T cell responses which may be important in the long term, after the B cell immunity has waned (210). T cell-mediated cytotoxic activity has been associated with mumps (211–214) and should also be considered for

vaccine development. It has been reported that some vaccinated individuals were still protected even though they lacked an antibody response, thus suggesting that a T cell response is sufficient for protection (215). Even though JL has had great success in reducing disease incidence, the attenuation method for this vaccine has resulted in two major components of the vaccine which differ by over 400 nucleotides as well as differences between different isolates of the minor vaccine component (216–218). The development of MuV therapeutics, more effective vaccines, and/or review of current vaccination policies are needed to prevent future outbreaks. Biological characterization of future vaccine candidates must be considered for standardization and safety testing. A better-defined vaccine will also help distinguish the live attenuated vaccine strain from virulent strains. Attenuation directed through genetic modification of an outbreak strain will be ideal for genotype matching circulating mumps strains, and for eliciting more specific protective immune responses (219).

Animal models

The only natural host of MuV is the human, and a small animal model that reflects the human disease has not been established. Experimental infections have been induced in numerous species, however each candidate model has had limitations. Mice are the most cost-efficient model, with a broad availability of reagents, however MuV is not known to replicate well or cause illness in adult mice (212, 220). MuV also tends to be abortive in this model system (131), however a mouse fibroblast cell-adapted strain was shown to replicate in the lung by a natural route of infection and further replicated in salivary glands, heart, and spleen, therefore demonstrating the potential to cause a

systemic infection in the mouse model (220). In most studies with mice, immune responses induced by different attenuated MuV strains (212), or by a recent outbreak strain (12), have been examined. Humoral and cell-mediated immune responses have also been evaluated for the MMR vaccine (221), as well as for MuV vaccine candidates (219, 222).

Ferrets are thought to be an attractive model for MuV pathogenesis because they have a respiratory tract that resembles the lung physiology and sialic acid composition on the upper airway epithelia in humans (223). However, ferrets intranasally infected with a high dose of a chicken-adapted mumps Enders strain did not show virus propagation in respiratory tissues and the infected ferrets only shed viruses during the first few days post-infection (224). In a different study, ferrets intranasally infected with attenuated and vaccine MuV strains, had no virus replication detected in nasal washes, oral swabs, urine, feces, or tissues homogenates (225). In ferrets intranasally infected with an outbreak strain, virus replication was self-limiting in the upper respiratory tracts (12). Even though immune responses were induced in these ferrets, no animals exhibited clinical signs (12, 225).

Mumps pathogenesis in the parotid glands and CNS has been extensively studied in rhesus macaques. Infiltration of mononuclear cells and lymphocytes was histologically characterized in animals injected with MuV inoculum directly into the parotid gland via Stenson's duct, or into the thyroid gland (15, 226, 227). No significant systemic phase has been found with this model, as the infection remains localized to the parotid gland (226), however, this infection model may be used to study biochemical mediators that evoke the protective inflammatory cell infiltration at the parotid gland infection site

(227). Infection of rhesus macaque via intranasal and intratracheal routes with a recent outbreak strain resulted in typical mumps clinical signs 2 to 4 weeks post infection, however no fever or neurological signs developed in these animals (12). Also, mumps viral antigen was detected in parotid glands by immunohistochemistry, suggesting that infection via the respiratory tract better reflects progression of mumps disease in humans (12). Therefore rhesus macaques represent the best animal model for the study of mumps viral pathogenesis, however a small animal model is more attractive as non-human primate experiments are expensive and labor intensive.

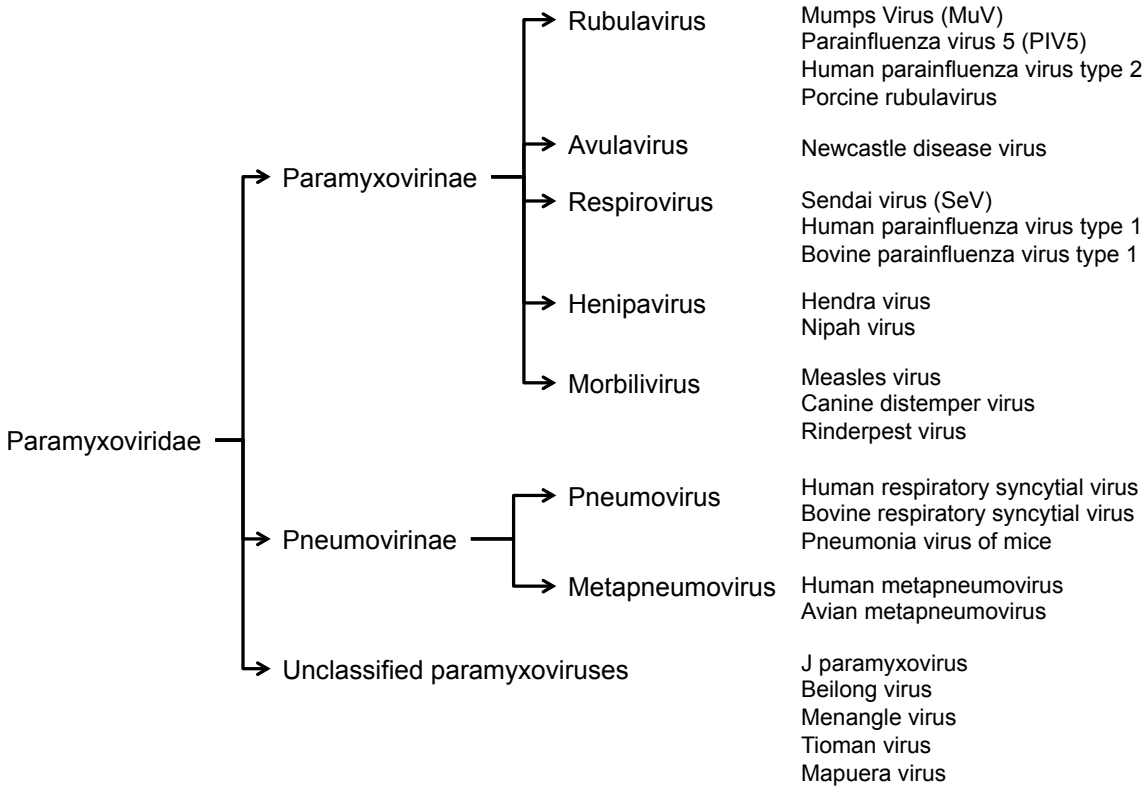

Figure 2.1. Classification of paramyxoviruses. The paramyxoviridae family is divided into the paramyxovirinae, pneumovirinae, and unclassified paramyxovirus subfamilies. The paramyxovirinae and pneumovirinae subfamilies are further divided into 5 and 2 genera, respectively. Modified from Goodbourn et al, 2009 (228).

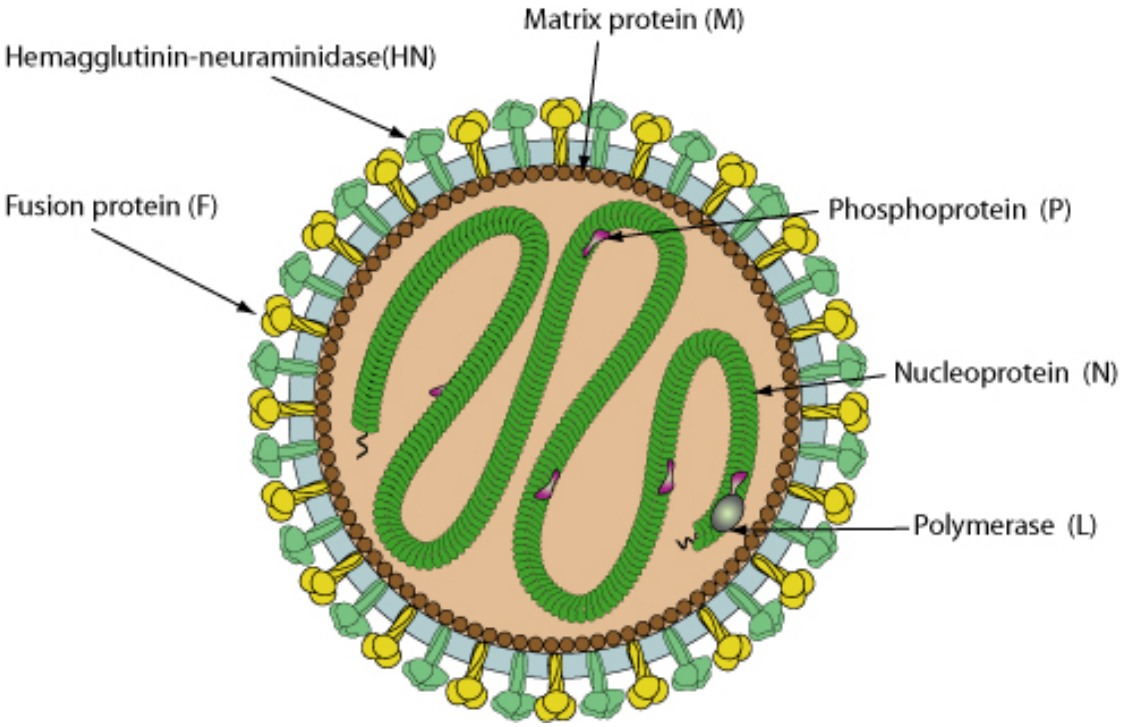

Figure 2.2. Representation of Rubulavirus virion structure. Modified from ViralZone 2009 Swiss Institute of Bioinformatics (http://viralzone.expasy.org).

Figure 2.3. Schematic of the MuV genome. The MuV negative-sense, single-stranded RNA genome contains 7 genes that encode 9 proteins. The P, V, and I proteins are produced from the P/V gene by RNA editing.

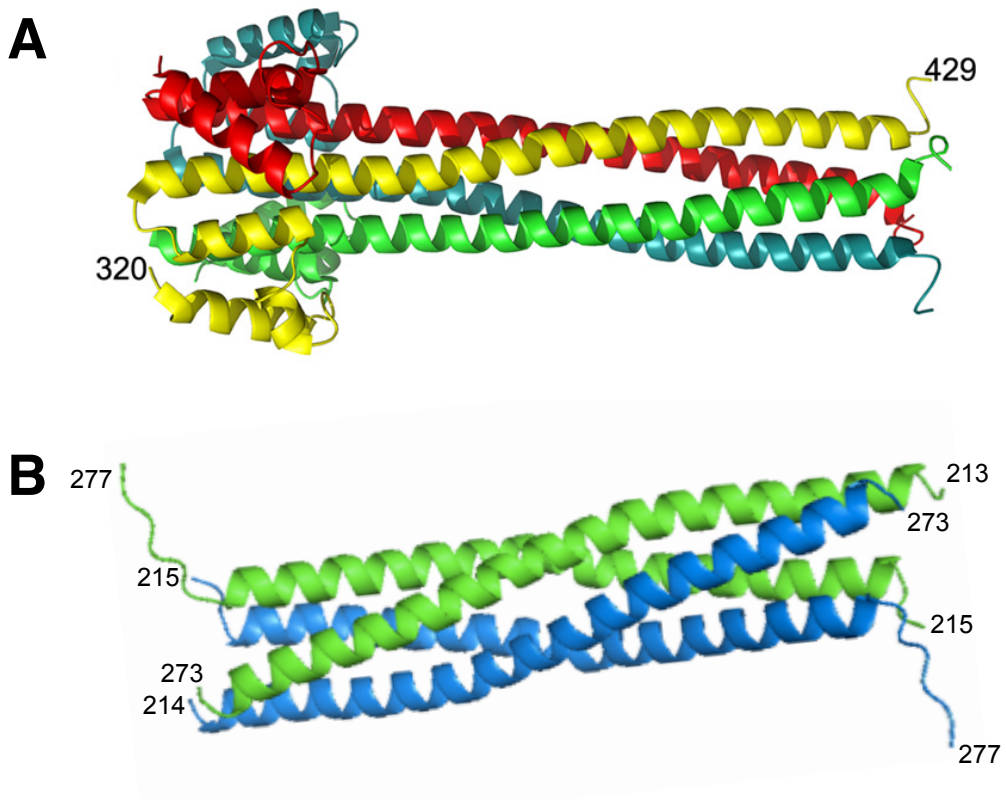

Figure 2.4. Oligomerization domain orientations of paramyxovirus phosphoproteins. (A) The crystal structure of the SeV P oligomerization domain reveals a tetramer of parallel α-helices. Each independent polypeptide chain is a different color. (B) The crystal structure of the MuV P oligomerization domain reveals two pairs of parallel α-helices (in green or cyan) that are in an antiparallel orientation to each other. Modified from Cox et al, 2013 (154).

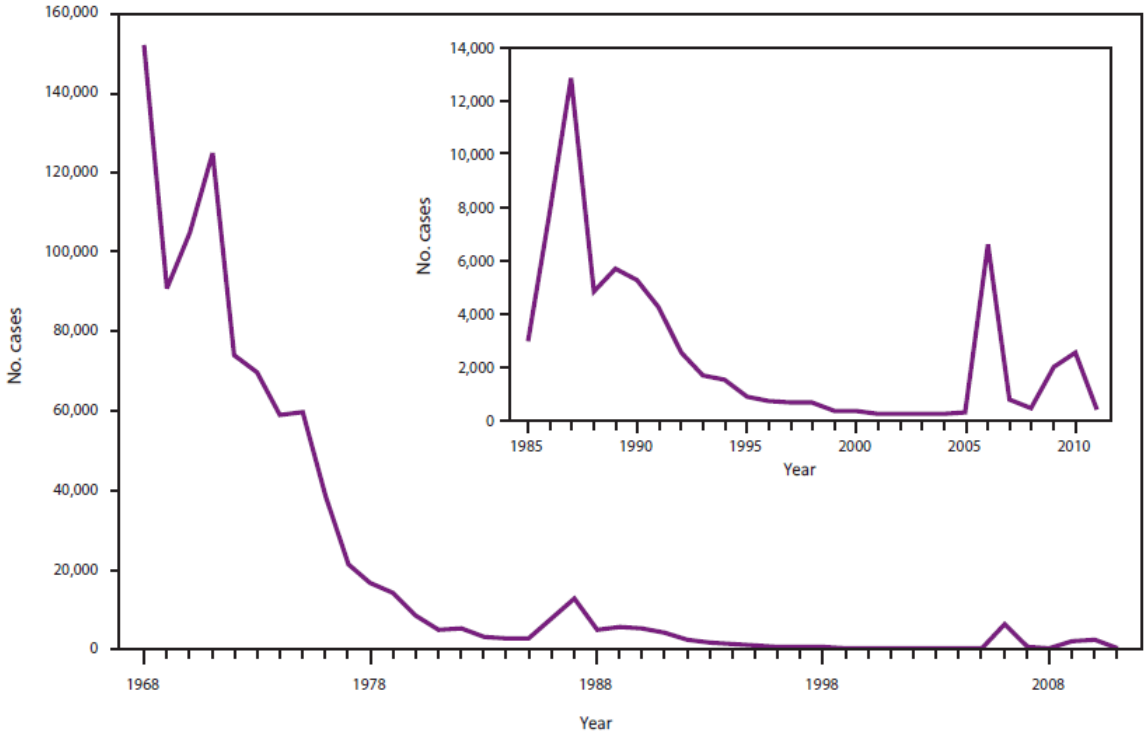

Figure 2.5. The number of mumps cases in the United States from 1968 to 2011. Following the introduction of the live mumps vaccine in 1967 and the recommendation for routine vaccination beginning in 1977, the reported number of mumps cases steadily decreased. Over 5,700 cases were reported in a 2006 outbreak at a university in Iowa of the $MuV^{Iowa/US/06}$ strain. Since then, numerous smaller outbreaks have occurred on college campuses throughout the United States. Modified from the CDC Morbidity and Mortality Weekly Report for June 14, 2013 (229).

CHAPTER 3

OLIGOMERIZATION OF THE MUMPS VIRUS PHOSPHOPROTEIN[1]

[1] Pickar A., Elson A., Yang Y., Xu P., Luo M., He B. Submitted to *Journal of Virology*, 7/5/2015.

Abstract

Mumps virus (MuV) encodes a phosphoprotein (P) that is important for viral RNA synthesis. P forms the viral RNA-dependent RNA polymerase with the large protein (L). P also interacts with the viral nucleocapsid protein (NP) and self-associates to form a homotetramer. The P protein consists of three domains, the N-terminal domain (P_N), oligomerization domain (P_O) and C-terminal domain (P_C). While P_N is known to relax the NP-bound RNA genome, the roles of P_O and P_C are not clear. In this study, we investigated the roles of P_O and P_C in viral RNA synthesis using mutational analysis and a minigenome system. We have found that P_N and P_C functions can be trans-complemented. However, this complementation requires P_O, indicating that P_O is essential for P function. Using this trans-complement system, we have found that P forms parallel dimers (P_N to P_N and P_C to P_C). Furthermore, we have found that residues R231, K238, K253 and K260 in the Po were are for P's functions. We have identified P_C as the domain that interacts with L. These results provide structure-function insights into the role of MuV P.

Significance

MuV, a paramyxovirus, is an important human pathogen. The P protein of MuV is critical for viral RNA synthesis. In this work, we established a novel minigenome system that allows domains of P to complement in trans. Using this system, we confirmed that

MuV P forms parallel dimers. Understanding viral RNA synthesis will allow design of better vaccines and development of antivirals.

Introduction

Mumps virus (MuV) is a human pathogen of the rubulavirus genus of the *Paramyxoviridae* family that causes an acute infection with symptoms ranging from parotitis to mild meningitis and severe encephalitis (1). The nonsegmented, negative-stranded RNA genome of MuV contains 15,384 nucleotides and encodes nine viral proteins (1). The viral RNA is encapsidated by the nucleoprotein (NP) and this helical nucleocapsid (RNP) functions as the template for viral RNA synthesis. Together, the large protein (L) and the phosphoprotein (P) make up the viral RNA-dependent RNA polymerase (vRdRp) (230). The enzymatic activities of the L protein involve initiation, elongation, and termination of RNA synthesis, as well as mRNA capping (4). While P is not known to have intrinsic enzymatic activity, P is an essential cofactor of the polymerase. P oligomerizes by itself and forms complexes with L, NP, and RNP. It is thought that P docks the vRdRP to RNP (231).

The P proteins of paramyxoviruses are modular and consist of N-terminal, oligomerization, and C-terminal domains with flexible linkers between adjoining domains. Self-association of P is observed throughout negative-stranded RNA viruses (NSVs). The oligomerization domain of Sendai virus (SeV) P was the first to be crystallized and revealed a parallel coiled-coil tetramer (139, 142). Self-association of P is required for transcriptional activity, and neighboring this oligomerization region is the binding site for SeV L (139, 155, 157, 158). Tetrameric P structures have also been

observed for other paramyxoviruses with crystallization of the P oligomerization domains for measles virus, human metapneumovirus, and mumps virus (148–154).

The P protein of vesicular stomatitis virus (VSV), a member of the *rhabdoviridae* family, forms a dimer consisting of two parallel α-helices that are held together through hydrophobic interactions (147). Oligomerization of VSV P is also needed for P activity as observed by a VSV minigenome assay (146, 163). The crystal structure of the P dimerization domain of rabies virus, an additional rhabdovirus, reveals that each monomer consists of a helical hairpin between two α-helices that permits interactions between the N-terminal helix of one monomer with the C-terminal helix of the other monomer (164). The N-terminal domain of rabies virus P interacts with the nascent NP and L, whereas the C-terminal domain binds to RNP (165–167). This structural difference may be important for rabies P function since the N-terminal and C-terminal domains of rabies are positioned on the same side, whereas these domains are at opposite ends of the oligomerization domains for VSV and SeV.

A C-terminal nucleocapsid-binding domain is found in numerous paramyxovirus P proteins (159, 161, 162). The last 49 amino acid residues (aa) of MuV P (defined as aa343-391) were found to directly mediate binding to the nuclecocapsid through its interaction with the assembly domain of NP (36). This nucleocapsid-binding domain is conserved, but MuV P is unique in that the N-terminal domain also binds to the nucleocapsid (154). Electron microscopy revealed uncoiling of the helical nucleocapsid by the N-terminal domain of P, which resulted in enhanced viral RNA synthesis in a minigenome system (42). The crystal structure of the oligomerization domain (defined as aa213-277) revealed two pairs of parallel α-helices that are antiparallel to each other,

which positions two N-terminal and two C-terminal domains on each end of the oligomerization domain (154). This antiparallel configuration is unique among P proteins of all nonsegmented negative stranded RNA viruses.

In this study, we have developed a novel minigenome system in which functional domains of P can be studied using trans-complementation. Using this system, we have determined the configuration of the MuV P dimer and tetramer.

Materials and Methods

Molecular cloning. Plasmids used in this work were constructed using standard molecular cloning techniques. Construction details and sequence files of the plasmids are available upon request. MuV NP, P, and L genes of the $MuV^{Iowa/US/06}$ strain were cloned into the pCAGGS expression vector (11). The MuV minigenome plasmid (BH526/ pMG-RLuc), containing Renilla, and a plasmid containing firefly-luciferase (pFF-Luc) were described previously (47). P truncations with Flag epitope tags are defined as P_N (aa1-194-flag), P_O (aa213-277-Flag), P_C (Flag-aa286-391), P_{NO} (aa1-277-Flag), and P_{OC} (Flag-aa213-391). P chimeric truncations with flag epitope tags are defined as N_{MuV}-O_{PIV5} (aa1-212_{MuV}-213-278_{PIV5}-Flag), O_{PIV5}-C_{MuV} (Flag-aa213-278_{PIV5}-278-391_{MuV}), N_{PIV5}-O_{MuV} (aa1-212_{PIV5}213-277_{MuV}-Flag), and O_{MuV}-C_{PIV5} (Flag-aa213-277_{MuV}-279-391_{PIV5}). The MuV L deletion mutant consisting of domains I through III with an HA tag is defined as $L_{dI\text{-}III}$ (aa1-914-HA).

Cell culture and transfections. 293T cells were maintained in Dulbecco's modified Eagle medium (DMEM) with 5% fetal bovine serum (FBS) and 1% penicillin-

streptomycin (P/S) (Mediatech Inc., Manassas, VA). BSRT7 cells were maintained in DMEM supplemented with 10% FBS, 1% P/S, 10% tryptose phosphate broth (TPB), and 400 μg/ml G418 sulfate antibiotic (Mediatech Inc.). All cell lines were incubated at 37°C with 5% CO_2 and passed at an appropriate dilution 1 day prior to use to achieve 80% to 90% confluence upon transfection**.** Cells were transfected using JetPRIME (Polyplus Transfection Inc., New York, NY) following the manufacturer's protocols.

MuV minigenome system and dual-luciferase assay. The MuV minigenome system used in this study was described previously (47). Increasing amounts (0, 10, 20, 40, 80, 160, or 320 ng) of total P or P domain truncations were transfected along with NP (25 ng), L (500 ng), pMG-RLuc (100 ng), and pFF-Luc (1 ng) in BSRT7 cells. Empty pCAGGS vector was used to normalize the amount of transfected DNA per sample. After 48 hours (h), 2/5 of the lysate from each well was used to carry out the dual-luciferase assay according to the manufacturer's protocol (Promega, Madison, WI), and light intensity was detected using a GloMax 96 Microplate Luminometer (Promega). Relative luciferase activity was defined as the ratio of Renilla luciferase (R-Luc) to firefly luciferase (FF-Luc) activity. Six replicates of each sample were used to compare the peak activity of each P mutant to that of wild-type P. Aliquots of the minigenome system cell lysates were used for Western blot analysis. Mouse monoclonal anti-MuV-NP and anti-MuV-P or anti-Flag (M2 clone, Sigma-Aldrich, St. Louis, MO) antibodies were used together to detect expression of NP and P or P truncations.

Cysteine residue replacement and oligomer orientation determination. 293T cells were transfected with 1 ug of P_{NO} or P_{OC} containing cysteine mutations. After 24 h, the cells were lysed with whole-cell extraction buffer (WCEB) (50 mM Tris-HCl [pH 8.0], 280 mM NaCl, 0.5% NP-40, 0.2 mM EDTA, 2 mM EGTA, and 10% glycerol) with a mixture of protease inhibitors as previously described (58). Prior to lysis, iodoacetamide (25 mM) was added to WCEB where specified. Cleared lysates were divided into equal fractions, mixed with one-half volume of 3X SDS loading buffer containing DTT (reducing conditions) or without DTT (nonreducing conditions) and heated at 95°C for 5 min. Samples were resolved in 12.5% SDS-PAGE and transferred to a polyvinylidene difluoride membrane (GE Healthcare, Piscataway, NJ).

Immunoblotting was performed as previously described (47). The membrane was blocked with ECL prime blocking agent (GE Healthcare Life Sciences, Piscataway, NJ) and incubated with mouse anti-Flag (1:1000 dilution), followed by incubation with goat Cy3 labeled anti-mouse IgG secondary antibody (KPL, Gaithersburg, MD, 1:2500 dilution) and scanned using a Typhoon 9700 imager (GE Healthcare Life Sciences).

Coimmunoprecipitation. To determine P domains that interact with L, 6-well plates of 293T cells were transfected with 2 μg of P truncations with 3 μg of $L_{dI\text{-}III}$. At 18 hours post transfection (hpt), the cells were starved with DMEM lacking cysteine-methionine and then labeled with 36.4 μCi/ml ^{35}S-EasyTag Express35S Protein Labeling (Perkin Elmer, Waltham, MA) for 4 h. The cells were then lysed with WCEB, and the lysate was precleared with recombinant protein G-Sepharose 4B conjugate (Invitrogen) for 1 h at 4°C and was then subjected to immunoprecipitation (IP) using recombinant

protein G-Sepharose 4B conjugate and mouse anti-Flag or mouse anti-HA (Sigma-Aldrich). The IP products were washed with WCEB in 12.5% SDS-PAGE. The gels were fixed (20% methanol, 7% acetic acid) and dried, and the proteins were visualized using a Typhoon 9700 imager (GE Healthcare).

Statistical analysis. Statistical analysis was performed using GraphPad Prism version 5.00 for Windows (GraphPad Software, San Diego, CA). Student's *t* test was used to calculate P values.

Results

Functional activity of P domains.

The MuV P protein contains an N-terminal domain (P_N), oligomerization domain (P_O), and a C-terminal domain (P_C) which are connected with flexible linker regions. To determine the roles of these domains, a series of truncations was generated (Fig 3.1). To examine the role of the individual P domains in viral RNA synthesis in the absence of viral infection, these deletion mutants were tested in the MuV minigenome system modified from that as previously described (47). A range of concentrations of the P plasmids was used to obtain the maximal minigenome activity since expression levels varied between the P domains. Previously, we showed that the individual domains do not maintain the P function in the MuV minigenome system (42). P truncations lacking the N-terminal domain or the C-terminal domain also had no activity (Fig. 3.2A). Surprisingly, when P_{NO} and P_{OC} were transfected together in equal amounts, the luciferase activity was detected and significantly greater than that of full-length P (Fig.

3.2A). Expression levels of P and NP were determined using immunoblotting (Fig. 3.2B). These results suggest that all P domains are required for P function. Most interestingly and importantly, P_{NO} and P_{OC} can trans-complement to restore the biological activity of P.

We previously found that addition of P_N with full-length P resulted in enhanced minigenome activity due to the role of the N-terminal domain in inducing uncoiling of the nucleocapsid (42). To determine if trans-complementation requires the oligomerization domain, the N-terminal domain alone was transfected with P_{OC} and tested in the minigenome system. Transfection of P_N with P_{OC} resulted in some activity, however the luciferase activity was significantly less than that of full-length P (Fig. 3.2C). Expression levels of P and NP were determined using immunoblotting (Fig. 3.2D). A lower ratio of P_{OC} was used due to higher expression of this plasmid (Fig. 3.2B). These results suggest that self-oligomerization via P_O is required for functional trans-complementation of P in viral transcription and replication. The fact that P_N and P_C can trans-complement each other indicates they indeed likely form functional domains.

P oligomerizes to form parallel dimers.

Crystal structure analysis of P_O shows formation of a tetramer consisting of two pairs of parallel α-helices that are antiparallel to each other (154). This is unique among known paramyxovirus P proteins. To determine the preferential α-helical orientation during P dimerization, cysteine residues were strategically incorporated into the P protein for disulfide bond crosslinking. However, wild-type P contains one natural cysteine residue in the C-terminal domain at amino acid 356. To avoid potential interference from

this wild-type cysteine residue, a series of C356 mutants were generated in full-length P and P_{OC} and tested in the minigenome system in order to identify a mutation that maintains P function (Fig. 3.3A and 3.3B). P-C356V maintained the highest activity among the cysteine mutants, therefore this modification was incorporated for all remaining P alterations.

P_O is defined as amino acid residues 213 to 277 (154). To determine if P forms parallel dimers, residues Q213 and V273 were changed to cysteine residues based on the crystal structure of the oligomerization domain (Fig. 3.4A). P_{NO} and P_{OC} could be differentiated by their sizes (Fig. 3.4B). 293T cells were transfected with plasmids expressing P_{NO} and P_{OC} that contain no cysteine residues, or $P_{NO\text{-}213C}$ and $P_{OC\text{-}273C}$. Polypeptides were separated by SDS-PAGE analysis under reducing and nonreducing conditions and detected by immunoblotting (Fig. 3.4C). As expected, only monomers were detected for P_{NO} and P_{OC} in all denaturing gels. Transfection with $P_{NO\text{-}213C}$ and $P_{OC\text{-}273C}$ resulted in bands corresponding to monomer and dimer polypeptides. Bands with molecular weights higher than a monomer were eliminated under reducing conditions, suggesting that oligomerization was due to disulfide bond formation (Fig. 3.4C). To confirm that the cysteine mutations maintain P function, $P_{NO\text{-}213C}$ and $P_{OC\text{-}273C}$ were tested in the minigenome system (Fig. 3.4D). Luciferase activity was similar for P_{NO}/P_{OC} and $P_{NO\text{-}213C}/P_{OC\text{-}273C}$, suggesting that addition of 213C and 273C does not disrupt P function. These results suggest that P forms parallel dimers.

Presence of antiparallel P molecules in a tetramer.

In the P tetramer, the two pairs of parallel dimers are antiparallel to each other. The crystal structure of P_O was also utilized to strategically incorporate cysteine residues at possible sites of antiparallel interactions. It is important to note that a kink at G246 is found in only one molecule in the pair of the parallel α-helices, thus distinguishing interacting side chains of each parallel pair (Fig. 3.5A). To determine if there are antiparallel P molecules with a kink or without a kink, cysteine residues were introduced at residues K241 and M248 or L243 and T250, respectively (Fig. 3.5B).

Cells were transfected with plasmids expressing P_{NO} and P_{OC} that contain no cysteine residues, $P_{NO\text{-}213C}$ and $P_{OC\text{-}273C}$ as parallel dimer controls, and $P_{NO\text{-}241C}$, $P_{OC\text{-}248C}$, $P_{NO\text{-}243C}$, and $P_{OC\text{-}250C}$. Polypeptides were separated by SDS-PAGE analysis under reducing and nonreducing conditions and detected by immunoblotting (Fig. 3.5C). Co-transfection with $P_{NO\text{-}243C}$ and $P_{OC\text{-}250C}$ resulted in separation of an additional band corresponding to the size of a P_{NO}-P_{OC} antiparallel dimer. Since each pair of cysteine residues only forms a single disulfide bond, cysteine pairs were incorporated into each set of P truncations and polypeptides were examined to see if a cross-linked tetramer could be detected (Fig. 3.5D). Co-transfection with $P_{NO\text{-}241C,248C}$ and $P_{OC\text{-}241C,248C}$ also resulted in separation of an additional band corresponding to the size of a P_{NO}-P_{OC} antiparallel dimer. Even though the higher molecular weight bands were eliminated in Figures 3.5C and 3.5D under reducing conditions, cell lysates were treated with iodoacetamide to confirm disulfide bond formation between dimers in their native conformation. As seen in Figure 3.5E, only polypeptides corresponding to parallel dimers were observed for $P_{NO\text{-}213C}$ and $P_{OC\text{-}273C}$.

To confirm that the putative antiparallel cysteine mutations maintain P function, these mutants were tested in the minigenome system (Fig. 3.5F). Luciferase activity was reduced for the cysteine mutants, however activity was still observed indicating that incorporation of cysteine residues at these sites may hinder but not eliminate P function. These results suggest that even though the incorporated antiparallel cysteine residues can interact to form disulfide bonds, the P oligomerization domain preferentially polymerizes to form functional parallel dimers before formation of a more dynamic tetramer.

Charged P_O zipper residues critical for P function.

To validate amino acid residues critical for tetramer formation, we examined residues likely to disrupt parallel and antiparallel associations of the P subunits. The crystal structure of P_O revealed that the tetramer is primarily formed with hydrophobic interactions and two zippers of charged side chain interactions formed by D229, E236, and D240 (chain A) and R231 and K238 (chain B) between the parallel pair of helices, and K253 and K260 (chain B) and D229, E236, and D240 (chain B') between the antiparallel pair of helices (154). To examine the roles of these residues in viral RNA synthesis, R231 and K238 were mutated to alanine to disrupt charge interactions between the pair of parallel helices, and K253 and K260 were mutated to alanine to disrupt charge interactions between the pair of antiparallel helices, and tested in the minigenome system. Disrupting the charged zipper interactions resulted in significantly reduced activity and completely abolished activity for K253A (Fig. 3.5A). Expression levels of P and NP were determined using immunoblotting (Fig. 3.5B).

MuV P_C contains putative L binding site.

To determine the putative L binding site within P, P truncations were utilized. In order to investigate L binding within each individual P domain, P chimeras were generated with the corresponding regions of PIV5, the most closely related virus to MuV, to enhance the structural stability of the MuV P domains (Fig. 3.7A). Visualization of full-length MuV L expression is limited therefore L truncations were generated. The N-terminal residues of L of related viruses have been found to be essential for P binding, therefore a sequence alignment of these L proteins with MuV L was analyzed to generate a MuV L truncation consisting of domains I through III ($L_{dI\text{-}III}$, aa 1-914) (data not shown) (115, 120, 124, 126). Interactions between the P chimeras and MuV L were examined using coimmunoprecipitation of transfected 293T cells. The radioactively labeled cell lysates were immunoprecipitated with anti-MuV-P, anti-PIV5-P, anti-Flag, or anti-HA. As shown in Figure 3.7B, only chimeras containing the C-terminal domain of MuV P interact with $L_{dI\text{-}III}$. It is important to note that the coimmunoprecipitation band corresponding to full-length PIV5 P is not above background, suggesting that PIV5 P does not interact with MuV $L_{dI\text{-}III}$. These results demonstrate that the C-terminal domain of MuV P interacts with $L_{dI\text{-}III}$.

Discussion

The P proteins of paramyxoviruses have a modular structure and it is thought that the individual P domains can be modified or deleted without affecting the function of the other P domains (139). The MuV P domains have been systematically mapped and characterized (154). In this study, we generated P truncations to examine the function of

the P domains in viral RNA synthesis. Previously, we found that transfecting additional P_N with full-length P resulted in enhanced activity in the MuV minigenome system due to uncoiling of the nucleocapsid (42). In the present study, we confirmed that all P domains are required for full P function. P multimerization has been found to be essential for viral transcription of Rinderpest virus and VSV (146, 148). Interestingly, when MuV P truncations lacking either the N-terminal domain (P_{OC}) or C-terminal domain (P_{NO}) were transfected together, P activity was restored due to trans-complementation through P_O. Thus, P multimerization via the central oligomerization domain is likely required for MuV P to function in viral RNA synthesis.

The crystal structure of MuV P_O revealed formation of a tetramer consisting of two pairs of parallel α-helices that are antiparallel to each other (154). It is unknown whether MuV P favorably forms parallel or antiparallel dimers during oligomerization. To further characterize the P oligomerization structure during viral RNA synthesis, the preferential α-helical orientation of P dimers was examined using engineered disulfide bond crosslinking. The introduction of cysteine residue pairs for crosslinking analysis is an applicable strategy for examination of protein structures. MuV P residues were strategically mutated to cysteine based on the close proximity of side chains found in either the parallel or antiparallel orientations of the crystal structure (Fig. 3.4 and 3.5). Our studies show that P dimerization is preferentially parallel and these mutants were biologically active in the MuV minigenome system. The selected antiparallel residues did not always crosslink antiparallel molecules and resulted in reduced minigenome activity, possibly because mutation of these residues disrupted the native P structure. However, when multimerization was investigated with the addition of iodoacetamide, the parallel

dimers were observed thus suggesting that disulfide bonds can form readily between the parallel helices. Crosslinking between antiparallel molecules was not clearly observed in several cases, suggesting that the tetramer may be a more dynamic complex or the selection of the cysteine mutations was not appropriate. However, tetramer formation is required for P activity as supported by the mutational studies of the charged zippers (Fig. 3.6A).

A necessity of phosphorylation for oligomerization differs between P proteins. Phosphorylation of P is required for multimerization of the rhabdoviruses VSV and Chandipura, and the more closely related paramyxovirus RSV (149, 163, 172, 232, 233). Oligomerization of unphosphorylated P proteins expressed in bacteria suggest that phosphorylation is not required and has been shown for Rinderpest virus (148). Phosphorylation has also been found to be dispensable for P oligomerization of MuV, SeV, and measles virus (139, 158). We previously screened the serine and threonine (S/T) residues of MuV P to determine phosphorylated residues critical for viral transcription and replication. Unexpectedly, six of the nine identified residues are located in the oligomerization domain (T250, S257, T258, T261, T262, and T265) (47). Analysis of these residues within the crystallized MuV P_O structure revealed that all six side chains are positioned outward to the tetramer, thus it is unlikely that these residues are important for oligomerization and instead are more accessible to interactions with host proteins such as kinases. Further analysis of the phosphorylation of these S/T residues is ongoing.

We found a putative binding site of L to be in the C-terminal domain of P. Alterations of MuV L were required for visualization of protein expression in our assays. The N-terminal 1147 residues of the SeV L protein (dI-IV) were found to bind to SeV P,

however shorter truncations abolished P binding (120). Similarly for PIV5, hPIV3, and measles virus, P binds to the N-terminal portion of L with the shortest truncation of L being from measles virus which included the 408 amino acids through domain I (126–128). A sequence alignment of these L proteins with MuV L was analyzed to generate MuV L truncations consisting of domains I through III (aa1-914), domains II through VI (aa506-2261), and domains IV through VI (aa882-2261) (114, 115). Visualization of L truncation expression was only achieved for $L_{dI\text{-}III}$. Generating truncations of L and P to determine binding sites may cause misfolding of the viral proteins. Additional binding sites within P may be unidentified because failure of P domains to bind to L in our studies may be a result of structural changes rather than the deletion of putative binding sites. It is important to note that the C-terminal domain of MuV P alone was unable to coimmunoprecipiate with $L_{dI\text{-}III}$, therefore sequences of PIV5 P, the most closely related virus to mumps, were utilized to stabilize MuV P domain structures. Further studies are needed to more precisely locate the L binding residues in P_C.

Oligomerization of MuV P results in two parallel dimers that are in an antiparallel orientation to each other during tetramer formation. This unique tetramer alignment likely has functional significance. Both the N-terminal and C-terminal domains of P bind to the nucleocapsid and it has been proposed that P oligomerization brings the terminal regions together in close proximity for effective nucleocapsid binding (154). Our studies reveal that the N-terminal and C-terminal domains of P can trans-complement for functional activity in a minigenome system, likely through oligomerization of the P trunctations. A cartwheel model has been proposed from studies on SeV, where P is thought to simultaneously make and break contacts with the nucleocapsid to ensure polymerase

processivity during viral RNA synthesis (144). This model also proposes that binding of P to the nucleocapsid or L may open the RNP structure so that the polymerase can access the viral template. Recent studies on MuV have shown that the nucleocapsid uncoils to expose the RNA for access to the polymerase through an interaction between the N-terminal domain of P and the nucleocapsid (42). Our studies suggest that MuV P is able to place the polymerase complex on the NP-RNA template via an L-binding site in the C-terminal domain of P.

Acknowledgements

We appreciate the helpful discussion and technical assistance from all members of Dr. Biao He's laboratory. This work was supported by grants (R01AI097368 and R01AI106307) from National Institutes of Health.

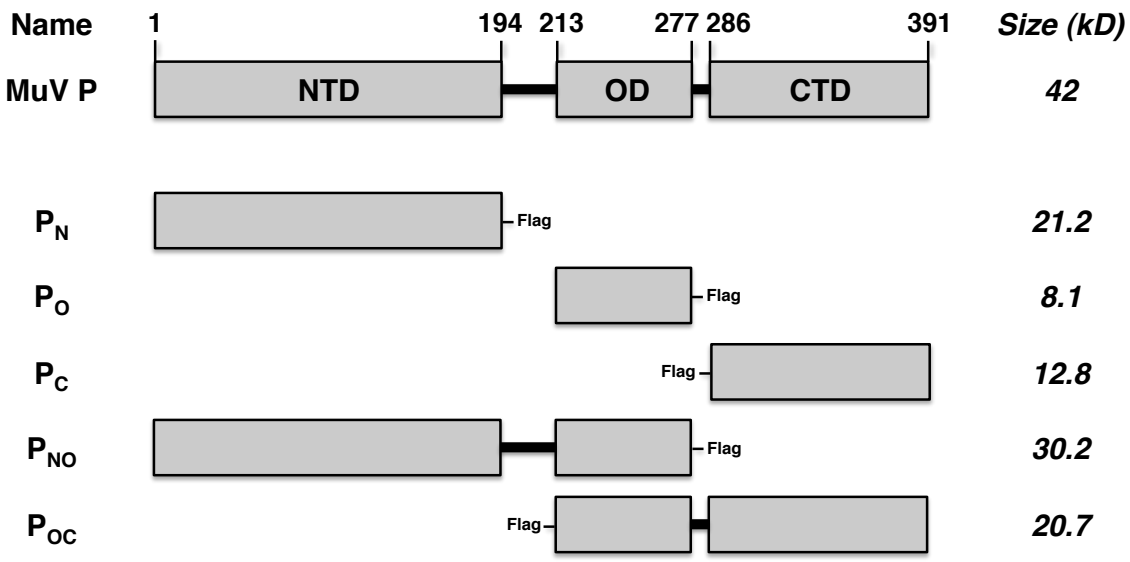

Figure 3.1. Schematic representation showing truncations of MuV P. Amino acid residues for the N-terminal domain (P_N), oligomerization domain (P_O) and C-terminal domain (P_C) are provided. Mutant names correspond to domains included in P truncations and approximate sizes are provided. The terminal Flag tag locations are included for each mutant.

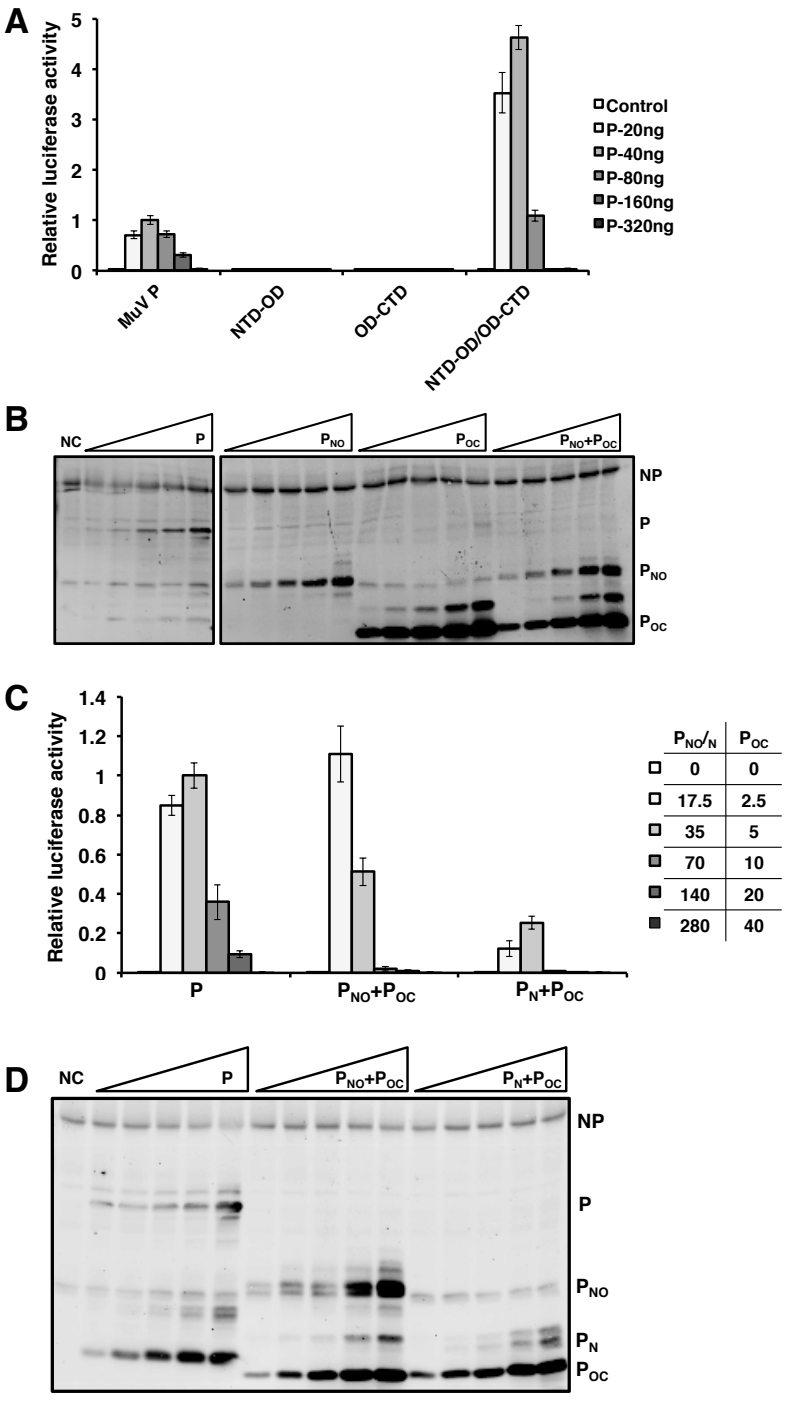

Figure 3.2. Trans-complementation of P in minigenome system. (A) Minigenome activity of P, P_{NO}, and P_{OC}. Increasing amounts of P or P truncations were transfected together with other plasmids as described in Materials and Methods. Transfection amounts of each

P truncation in P_{NO}+P_{OC} were one-half of the total transfected P. *Renilla* luciferase was the reporter gene in the minigenome and Firefly luciferase expression was used as a transfection control. The minigenome activity was measured and normalized as the ratio of *Renilla* luciferase activity to firefly luciferase activity (relative luciferase activity). (C) Minigenome activity of P, P_N, P_{NO}, and P_{OC}. Increasing amounts of P or P truncations are provided in graph. Error bars represent the standard errors of the means (SEM) of data from six replicates. (B and D) Immunoblotting was performed to detect the expression levels of NP, P, and P truncations.

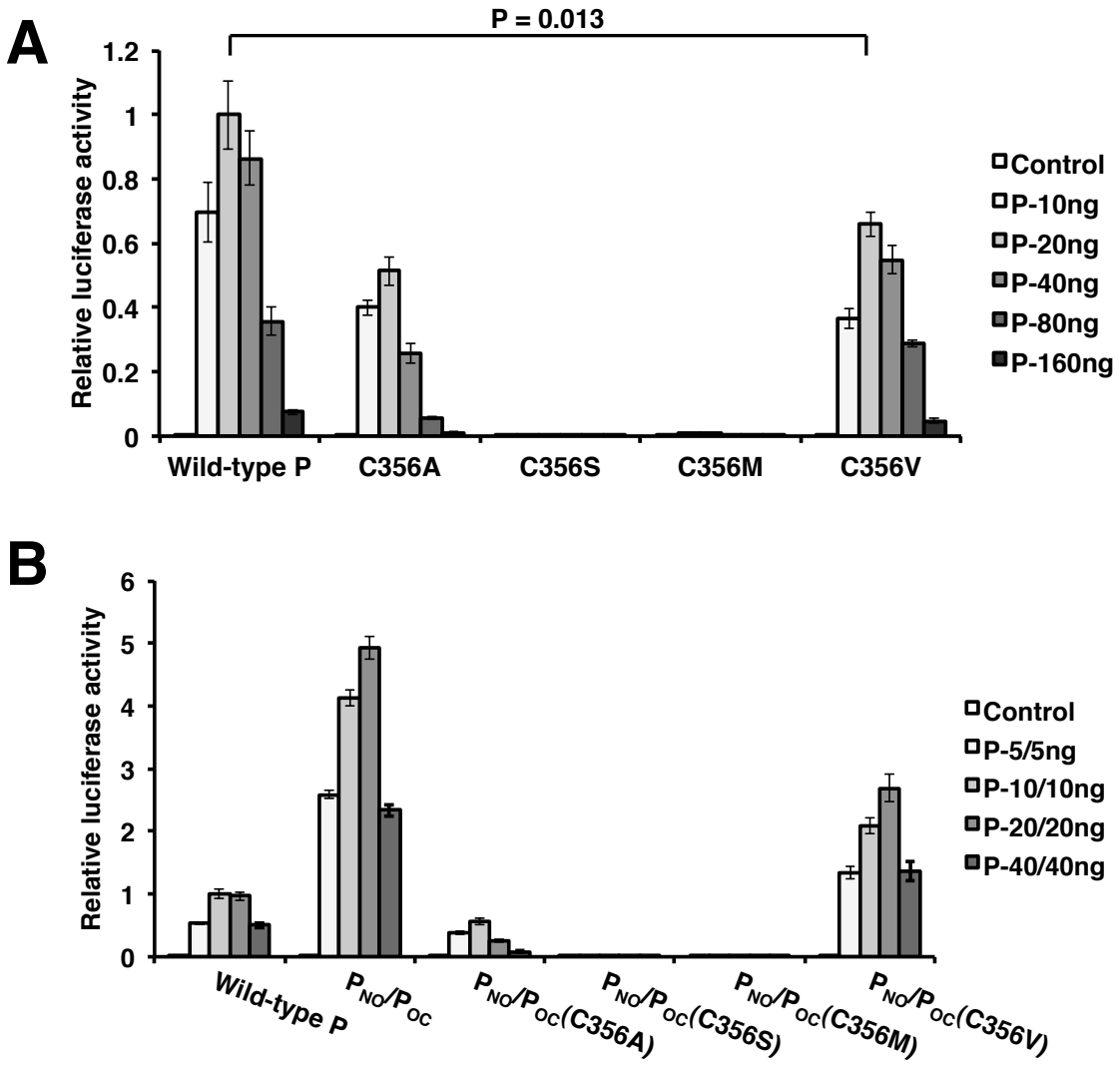

Figure 3.3. Mutation analysis of cysteine residue 356 of P. (A and B) Residue C356 in full-length P and P_{OC} was mutated to alanine, serine, methionine and valine and tested in the minigenome system. Increasing amounts of P or P truncations were transfected together with other plasmids as described in Materials and Methods. Transfection amounts are provided in each graph. *P* values were calculated using student's *t* test. Error bars represent the SEM of data from six replicates.

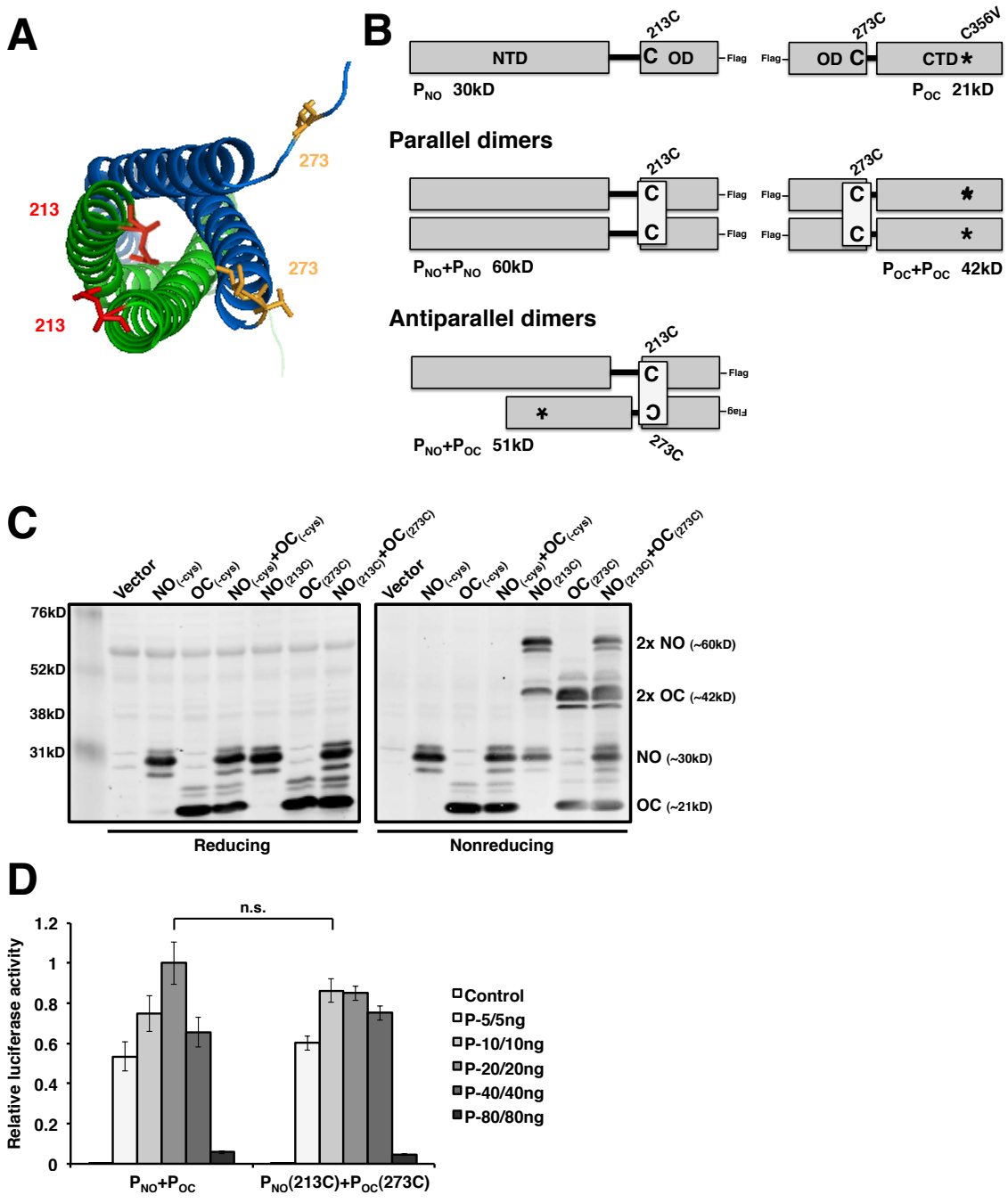

Figure 3.4. P mutants with engineered cysteine residues dimerize in parallel orientation with biological activity. (A) Pairs of parallel chains shown in green or blue. Side chains of mutated amino acid residues 213 (red) and 273 (yellow) are highlighted. The 213 residue not contained in the file was superimposed from the adjacent parallel chain.

Figure generated using Pymol (234). (B) Schematic representation of incorporated cysteine residues for disulfide bond engineering. Parallel and antiparallel oriented dimer sizes are provided. (C) Assessment of the parallel oligomerization status of P truncations containing cysteine residues under reducing and nonreducing conditions. (D) Minigenome activity of engineered P deletion mutants. Increasing amounts of P mutants were transfected with other plasmids as described in Materials and Methods. *P* values were calculated using student's *t* test. Error bars represent the SEM of data from six replicates.

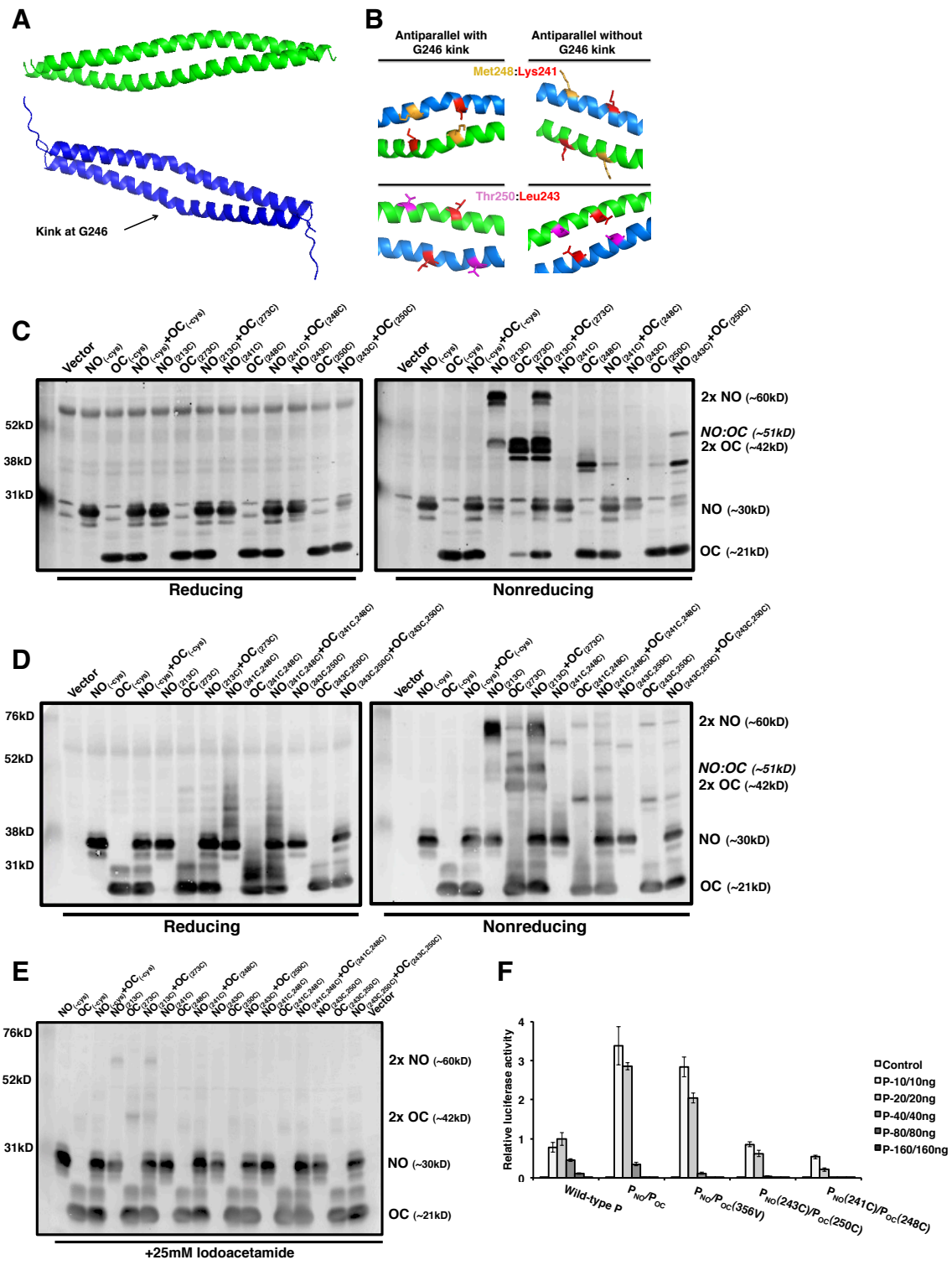

Figure 3.5. P mutants with engineered cysteine residues for crosslinking antiparallel helices. (A and B) Pairs of antiparallel chains are shown in green or blue. The kink at

G246 located on only one pair of helices is highlighted. (B) Residues with side chains in close proximity are highlighted. These residues were mutated to cysteine to engineer disulfide bonds between antiparallel α-helices in chains containing and lacking the G246 kink. Figure generated using Pymol (234). (C and D) Assessment of the antiparallel oligomerization status of P truncations containing single (C) or double (D) cysteine residues under reducing and nonreducing conditions. (E) Iodoacetamide treatment (25mM) for natural dimerization orientation of P mutants with engineered parallel or antiparallel disulfide bonds. (F) Minigenome activity of engineered P mutants. Increasing amounts of P mutants were transfected with other plasmids as described in Material and Methods. Error bars represent the SEM of data from six replicates.

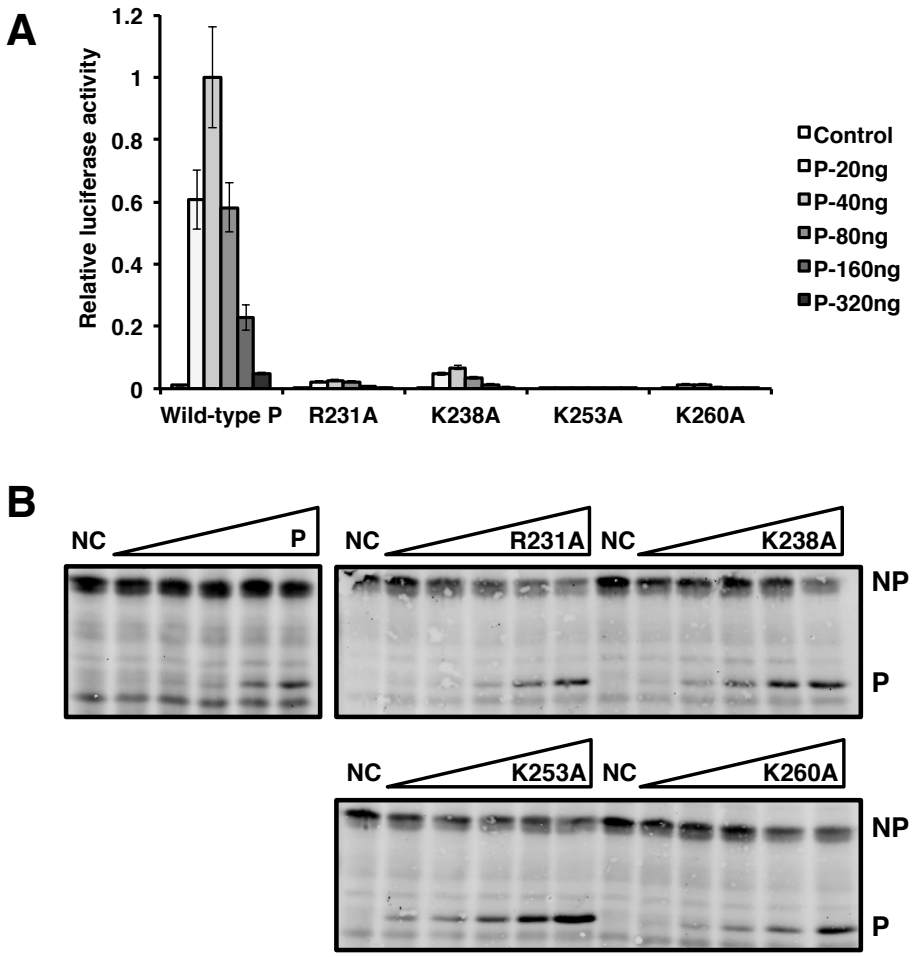

Figure 3.6. Charged residues in P oligomerization domain are critical for P activity in minigenome. (A) Residues found in charged zippers were mutated to alanine and tested in the minigenome system. Increasing amounts of P mutants were transfected with other plasmids as described in Materials and Methods. *P* values were calculated using student's *t* test. Error bars represent the SEM of data from six replicates. (B) Immunoblotting was performed to detect the expression levels of NP, P, and P mutants.

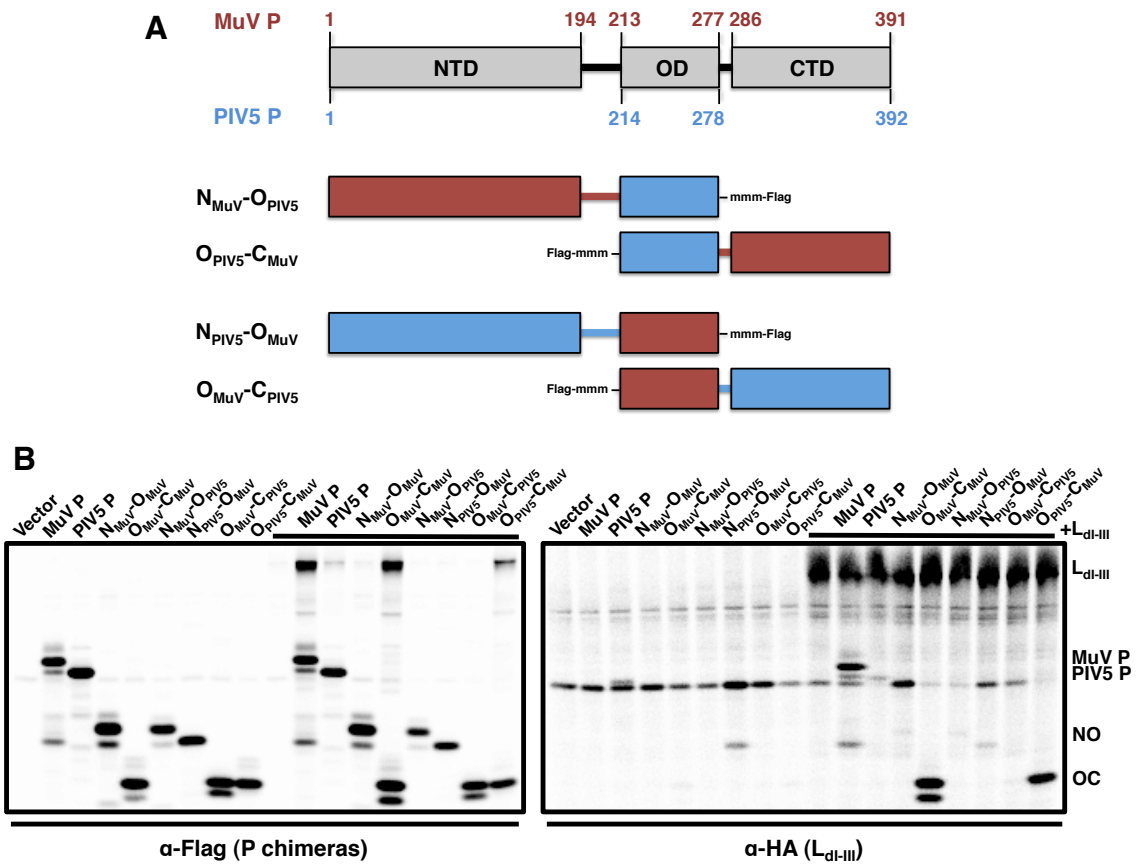

Figure 3.7. The C-terminal domain of P binds to L. (A) Schematic representation of the predicted amino acid residues for the PIV5 P_N, P_O and P_C from sequence analysis with MuV P are provided. Mutant names correspond to domains included in P truncations. The terminal Flag tag locations are included for each mutant as well as additional methionine residues to aid in visualization by ^{35}S-radioactive labeling. (B) Interaction between P domains and $L_{dI\text{-}III}$ in 293T cells. Cells were transfected with full-length P, P chimeras, $L_{dI\text{-}III}$, or cotransfected with P and $L_{dI\text{-}III}$, and labeled with ^{35}S. Cell lysates were precleared with sepharose G beads and coimmunoprecipitated with monoclonal anti-MuV P, anti-PIV5 P, anti-flag, or anti-HA antibody and resolved by 12.5% SDS-PAGE.

CHAPTER 4

THE ROLES OF SERINE AND THREONINE RESIDUES OF MUMPS VIRUS P PROTEIN IN VIRAL TRANSCRIPTION AND REPLICATION[2]

[2] Pickar A., Xu P., Elson A., Li Z., Zengel J., He B. 2014. *Journal of Virology.* 88:4414-4422. Reprinted here with permission of the publisher.

Abstract

Mumps virus (MuV), a paramyxovirus containing a negative-sense nonsegmented RNA genome, is a human pathogen that causes an acute infection with symptoms ranging from parotitis to mild meningitis and severe encephalitis. Vaccination against mumps virus has been effective in reducing mumps cases. However, recently large outbreaks have occurred in vaccinated populations. There is no anti-MuV drug. Understanding replication of MuV may lead to novel antiviral strategies. MuV RNA-dependent RNA polymerase minimally consists of the phosphoprotein (P) and the large protein (L). The P protein is heavily phosphorylated. To investigate the roles of serine (S) and threonine (T) residues of P in viral RNA transcription and replication, P was subjected to mass spectrometry and mutational analysis. P, a 391-amino acid residue (AA) protein, has 64 S and T residues. We have found that mutating nine S/T residues significantly reduced and mutating residue T at 101 to A (T101A) enhanced activity in a minigenome system. A recombinant virus containing the P-T101A mutation (rMuV-P-T101A) was recovered and analyzed. rMuV-P-T101A grew to higher titers and had increased protein expression at early time points. Together, these results suggest that phosphorylation of MuV-P-T101 plays a negative role in viral RNA synthesis. This is the first time that the P protein of a paramyxovirus has been systematically analyzed for S/T residues that are critical for viral RNA synthesis.

Significance

Mumps virus (MuV) is a reemerging paramyxovirus that caused large outbreaks in the United States, where vaccination coverage is very high. There is no anti-MuV drug. In this work, we have systematically analyzed roles of Ser/Thr residues of MuVP in viral RNA synthesis. We have identified S/T residues of P critical for MuV RNA synthesis and phosphorylation sites that are important for viral RNA synthesis. This work leads to a better understanding of viral RNA synthesis as well as to potential novel strategies to control mumps.

Introduction

Mumps virus (MuV) is a human pathogen that causes acute parotitis and is highly neurotropic (1). Invasion of the central nervous system is evident in almost half of all clinical cases, with asceptic meningitis occurring in approximately 10% of cases and encephalitis in less than 1% (1). Even though the mumps vaccine has dramatically reduced disease incidence, large outbreaks have recently occurred in vaccinated populations (2, 3). Over 5,700 mumps cases were reported in a 2006 outbreak that originated at a university in Iowa and spread to 10 other states (2). A mumps outbreak occurred in New York and New Jersey in 2009 to 2010 where 88% of the patients had one dose of mumps vaccine and 75% of patients had two doses (3). There is no antiviral drug for MuV infection. Understanding functions of viral proteins will aid development of antiviral strategies. In this study, a strain of MuV from a recent outbreak in Iowa in 2006 (11), $MuV^{Iowa/US/06}$ (referred to here as MuV), was used to examine the role of phosphorylation of the MuV phosphoprotein (P) in virus transcription and replication.

MuV is a member of the family *Paramyxoviridae* and has a nonsegmented, negative-stranded RNA genome of 15,384 nucleotides (1). The RNA genome of MuV contains a series of tandemly linked genes separated by nontranscribed sequences in the order 3'-NP-V/P-M-F-SH-HN-L-5'. Synthesis of all viral mRNAs initiates at the 3' end sequence, termed the leader sequence, where the viral RNA-dependent RNA polymerase (RNAP) (vRdRp) transcribes the viral RNA genome (vRNA) into mRNAs, containing a 5' cap structure and 3' poly(A) tail, in a sequential manner. To replicate vRNA (the negative-sense viral RNA), an anti-genome sense RNA (cRNA or positive-sense anti-genomic RNA) is first replicated starting at the 3' leader sequence and then the cRNA is replicated into the vRNA by vRdRp starting at the 5' trailer sequence (4). The functional template for viral RNA synthesis (viral mRNA transcription and viral RNA replication) of MuV, like other nonsegmented, negative-sense RNA viruses, is contained in the helical nucleocapsid, i.e., the viral genomic RNA encapsidated by the nucleoprotein (NP) (reviewed in reference 5). The vRdRp of MuV minimally consists of two proteins, the phosphoprotein (P) and the large (L) polymerase protein (230). The L protein has enzymatic activities capable of initiation, elongation, and termination of RNA synthesis, and the L protein adds the 5' cap and 3' poly(A) sequence to transcribed viral mRNA (4). P is an essential cofactor for the polymerase. The P protein does not have intrinsic enzymatic activity, but it has numerous functions in virus transcription and replication (4). It enables binding of the P-L complex to the nucleocapsid template and prohibits self-assembly of nascent NP protein (48).

To study the functions of NP, P, and L of paramyxoviruses in the absence of viral infection, minigenome systems are often used. The system contains NP, P, and L, but

lacks all other viral proteins, and the viral genome is substituted by an RNA with a reporter gene that is flanked by the 3' leader sequence and the 5' trailer sequence (235, 236). In this study, mass spectrometry analysis and a MuV minigenome system were used to screen for S/T amino acid residues of the P protein that are phosphorylated and critical for virus transcription and replication. Furthermore, the putative critical residues were incorporated into a recombinant MuV and analyzed.

Materials and Methods

Plasmids and cells. Plasmids used in this work were constructed using standard molecular cloning techniques. Construction details and sequence files of the plasmids are available upon request. MuV NP, P, and L genes were cloned into the pCAGGS expression vector (237). A plasmid containing firefly-luciferase (pFF-Luc) and the MuV minigenome plasmid (BH526/ pMG-RLuc), containing *Renilla* and driven by the T7 promoter, were used in the MuV minigenome assays. Mutations in the P protein were incorporated into the full-length MuV genome ($MuV^{Iowa/US/06}$) as described before (11).

293T cells were maintained in Dulbecco's modified Eagle medium (DMEM) with 5% fetal bovine serum (FBS) and 1% penicillin-streptomycin (P/S) (Mediatech Inc., Manassas, VA). Vero and HeLa cells were maintained in DMEM supplemented with 10% FBS and 1% P/S. BSRT7 cells were maintained in DMEM supplemented with 10% FBS, 1% P/S, 10% tryptose phosphate broth (TPB), and 400 μg/ml G418 sulfate antibiotic (Mediatech Inc.). All cell lines were incubated at 37°C with 5% CO_2 and passed at an appropriate dilution 1 day prior to use to achieve 80% to 90% confluence upon transfection or infection.

Transfections, infections, and virus rescue. Cells were transfected using JetPRIME (Polyplus Transfection Inc., New York, NY) following the manufacturer's protocols. For virus infections, cells were inoculated with viruses at a multiplicity of infection (MOI) of 0.5, 0.1, or 0.01 in DMEM-1% bovine serum albumin (BSA) and incubated at 37°C with 5% CO_2 for 1 to 2 h. The inocula were then replaced with DMEM supplemented with 2% FBS and 1% P/S.

To rescue an infectious virus, a plasmid containing the full-length genome (5 μg), along with plasmids pCAGGS-L (2 μg), pCAGGS-NP (100ng), and pCAGGS-P (320ng), was transfected into BSRT7 cells. Three days later, transfected BSRT7 cells were mixed with Vero cells at a 1:5 dilution. Four days later, media was transferred to fresh Vero cell monolayers and propagated further. When syncytium formation was observed, media were collected and used for plaque assays in Vero cells as previously described (58). Single plaques were selected and further amplified in Vero cells. The genome of the rescued virus was confirmed by sequencing. Total RNA was extracted from infected cells using an RNeasy minikit (Qiagen, Waltham, MA) and reverse transcribed into cDNA using Super Script III reverse transcriptase (Invitrogen, Frederick, MD) with random primers (Promega, Madison, WI). Synthesized cDNA served as the templates for PCR using MuV genome-specific primers and *Taq* polymerase (Invitrogen). Primers (15 sets) were designed to divide the genome into overlapping fragments, and the primers were used for the subsequent sequencing of the PCR products, as previously described (11). Primer sequences are available upon request.

Mass spectrometry analysis. To determine the phosphorylated residues within the P protein of MuV-infected cells, liquid chromatography-tandem mass spectrometry (LC-MS/MS) was performed as previously described (7). Vero cells in 10-cm-diameter plates were mock or MuV infected at an MOI of 0.5. At 24 h postinfection (hpi), the cells were lysed with whole-cell extraction buffer (WCEB) (50 mM Tris-HCl [pH 8.0], 280 mM NaCl, 0.5% NP-40, 0.2 mM EDTA, 2 mM EGTA, and 10% glycerol) with a mixture of protease inhibitors as previously described (238). Lysates were incubated with monoclonal anti-MuV-P antibody (11) and protein G-Sepharose 4B conjugate (Invitrogen, Grand Island, NY) to precipitate the P protein. After washing, the agarose beads were mixed with one-half volume of 3X SDS loading buffer (188 mM Tris-HCl [pH 6.8], 6% SDS, 30% glycerol, 0.03% [wt/vol] bromophenol blue, and 200 mM dithiothreitol [DTT]), heated at 95°C for 5 min, and resolved using 10% SDS-polyacrylamide gel electrophoresis (PAGE). The gel was stained with Coomassie blue in a solution of 45% methanol and 10% acetic acid. After destaining with a solution containing 45% methanol and 10% acetic acid, the major and minor phosphorylated P bands became visible and were excised separately. The bands were digested with trypsin, enriched using TiO_2, and analyzed by LC-MS/MS (using the Waters Q-Tof Ultima mass spectrometer at the W.M. Keck Foundation Biotechnology Resource Laboratory, Yale University). The MS/MS spectra were searched against the NCBI database using the automated Mascot algorithm to identify peptides with possible phosphorylation residues of tyrosin (Tyr), threonine (Thr), and serine (Ser).

MuV minigenome system and dual-luciferase assay. BSRT7 cells in 24-well plates were transfected with pCAGGS-NP (25 ng), pCAGGS-L (500 ng), pMG-RLuc (100 ng), pFF-Luc (1 ng), and various amounts (0, 20, 40, 80, 160, or 320 ng) of pCAGGS-P or pCAGGS-P mutant. Empty pCAGGS vector was used to normalize the amount of transfected DNA per sample. After 48 h, cells were lysed in 100 μL passive lysis buffer (Promega, Madison, WI) and vigorously mixed for 20 min to permit full lysis. Clear lysate (40 μL) from each well was used to carry out the dual-luciferase assay according to the manufacturer's protocol (Promega), and light intensity was detected using a GloMax 96 Microplate Luminometer (Promega). Relative luciferase activity was defined as the ratio of *Renilla* luciferase (R-Luc) to firefly luciferase (FF-Luc) activity. Six replicates of each sample were used to compare the peak activity of each P mutant to that of wild-type P. Aliquots of the minigenome system cell lysates were used for Western blot analysis to detect NP and P protein expression.

Immunoblotting. Cell lysate aliquots from the dual-luciferase assay were mixed with one-half volume of 3X SDS loading buffer and heated at 95°C for 5 min. Samples were resolved in 10% SDS-PAGE and transferred to a polyvinylidene difluoride membrane (GE Healthcare, Piscataway, NJ). Immunoblotting using monoclonal MuV protein-specific antibodies was performed as previously described (11). The membrane was incubated with mouse anti-MuV-NP antibody (1:2,000 dilution) and mouse anti-MuV-P antibody (1:1,000 dilution), followed by incubation with Cy3-conjugated goat anti-mouse IgG secondary antibody (1:2,500 dilution) (Jackson ImmunoResearch, West

Grove, PA), and scanned using a Typhoon 9700 imager (GE Healthcare Life Sciences, Piscataway, NJ).

To compare the viral protein expression levels in infected cells, Vero cells were mock infected or infected with recombinant MuV (rMuV) or rMuV-P-T101A at an MOI of 0.01. At 12, 24, 48, 72, and 96 h postinfection (hpi), cells were lysed with WCEB and cell debris was removed. Lysates were mixed with 3X SDS loading buffer, heated, and resolved using a 10% SDS-PAGE gel as described above. Immunoblotting was performed with primary antibodies and with mouse anti-MuV-NP and -P antibodies as described above as well as with rabbit anti-actin at a 1:1,000 dilution (Sigma-Aldrich, St. Louis, MO), followed by Cy3-conjugated goat anti-mouse IgG secondary antibody and Cy5-conjugated goat anti-rabbit IgG secondary antibody at 1:2,500 dilutions (Jackson Immuno-Research).

IP. To detect phosphorylation of P, HeLa cells were transfected with 2 μg of pCAGGS-P or pCAGGS-P mutant or infected with MuV or rMuV-P-T101A at an MOI of 0.1. At 18 hpi, the cells were starved with DMEM lacking cysteine-methionine and then labeled with 72.7 μCi/ml ^{35}S-EasyTag Express35S Protein Labeling (Perkin Elmer, Waltham, MA) for 4 h or starved with DMEM lacking sodium phosphate and then labeled with 100 μCi [^{33}P]Radionuclide Orthophosphoric acid (Perkin Elmer, Waltham, MA) and 100 nM okadaic acid (Sigma-Aldrich) for 8 h. The cells were then lysed with WCEB, and the lysate was subjected to immunoprecipitation (IP) using recombinant protein G-Sepharose 4B conjugate and anti-MuV-P antibody. The immunoprecipitated products were washed and resolved as described above. Phosphorylation of the P protein

of 4 individual experiments was calculated by densitometry analysis of the total P $^{33}P/^{35}S$ ratio using ImageQuant TL software (GE Healthcare Life Sciences).

To detect tetramer formation of P and P mutants, Vero cells in 6-cm-diameter plates were mock infected or infected with rMuV or rMuV-P-T101A at an MOI of 0.5. At 24 hpi, the cells were starved with DMEM lacking cysteine-methionine and then labeled with 72.7 μCi/ml ^{35}S-EasyTag Express35S Protein Labeling (Perkin Elmer) for 4 h. The labeled cells were incubated with dimethyl sulfoxide (DMSO) or 1 mM disuccinimidyltartarate (DSP) (Pierce, Rockford, IL) in PBS-0.5% NP-40 to cross-link the disulfide bonds as previously described (239) and incubated for 2 h at 4°C. The cells were lysed with WCEB, and the lysate was subjected to immunoprecipitation (IP) using recombinant protein G-Sepharose 4B conjugate and anti-MuV-P antibody. Samples were washed and then mixed with a half-volume of 3X SDS loading buffer. The immunoprecipitated products were washed with WCEB and resolved using 10% SDS-PAGE. The gel was fixed and dried, and the proteins were visualized using a Typhoon 9700 imager (GE Healthcare).

To study the interaction of NP and L with P and P mutants, Vero cells in 6-cm-diameter plates were mock infected or infected with MuV or rMuV-P-T101A at an MOI of 0.5. At 24 hpi, the cells were starved and labeled as described above. The cells were then lysed with WCEB and the lysate was immunoprecipitated using protein G-sepharose 4B conjugate (Invitrogen) and half of the lysate with anti-MuV-P and half with anti-MuV-NP antibodies. The IP products were washed with WCEB and resolved using 10% SDS-PAGE. The gel was fixed (20% methanol, 7% acetic acid) and dried, and the proteins were visualized using a Typhoon 9700 imager (GE Healthcare).

Multistep growth curve. Vero cells in 6-cm-diameter plates were infected with MuV or rMuV-P-T101A at an MOI of 0.01. Media were collected at 12, 24, 48, 72, and 96 hpi and supplemented with 1% BSA and then stored at -80°C. Virus titers were determined in Vero cells by plaque assays and completed in triplicate as previously described (58).

Flow cytometry. Vero cells in 6-well plates were infected with MuV or rMuV-P-T101A at an MOI of 0.1. Trypsonized cells of 4 individual replicates were harvested and combined with floating cells in the media at 12, 24, 48, and 72hpi, fixed in PBS with 1% formaldehyde, and stored at 4°C. Cells were permeabilized in PBS with 5% FBS and 0.5% saponin and stained with anti-MuV-NP antibody at a 1:200 dilution, followed by R-Phycoerythrin (PE)-labeled goat anti-mouse IgG secondary antibody at a 1:200 dilution (KPL, Gaithersburg, MD). Flow cytometry was completed using a LSRII flow cytometer (BD Biosciences, San Jose, CA) and analyzed using BD FACSDiva v6 software (BD Biosciences). The mean fluorescence intensity of NP was calculated for infected cells.

RT PCR. Vero cells in 6-well plates were infected with MuV or rMuV-P-T101A at an MOI of 0.01. Total RNA was extracted at 0, 2, 4, 8, 12, 16, and 20 hpi using an RNeasy minikit (Qiagen). cDNA was generated using reverse transcription with Super Script III reverse transcriptase (Invitrogen). Oligo$(dT)_{15}$ primers (Promega) were used to synthesize cDNA for viral mRNA, and gene-specific primers flanking the negative-sense genomic MuV-F gene were used for synthesizing cDNA for genomic RNA. Synthesized

cDNAs served as the templates for real-time PCR (RT-PCR) in triplicate using a MuV-F-specific FAM-tagged probe (Applied Biosystems, South San Francisco, CA) and the TaqMan Gene Expression Master Mix (Applied Biosystems), according to the manufacturer's protocol. Real-time PCR was completed using a StepOnePlus RT PCR System (AB Biosciences, Foster City, CA). Threshold cycle (C_T) values were normalized to input RNA (defined as the genomic RNA for the corresponding virus when the inoculum was removed at 0 hpi).

Statistical analysis. Statistical analysis was performed using GraphPad Prism version 5.00 for Windows (GraphPad Software, San Diego, CA). Student's *t* test was used to calculate *P* values.

Results

Mass spectrometry analysis of P.

To determine the phosphorylation status of the P protein of the $MuV^{Iowa/US/06}$ strain (referred to here as MuV), Vero cells were infected with MuV, radioactively labeled with [^{35}S]Met or [^{33}P]phosphate, and then immunoprecipitated with monoclonal anti-MuV-P antibody. The immunoprecipitated products were resolved using SDS-PAGE. Consistent with previous observations, there were two bands distinguished for the P protein in the ^{35}S-labeled lane: a slower-migrating minor band (P_1) and a faster-migrating major band (P_2) (Fig. 4.1A). It had been speculated that the slower-migrating band was P with increased phosphorylation. When the major ^{35}S-labeled P_2 was labeled with ^{33}P, the weaker ^{35}S-labeled P_1 band had stronger ^{33}P labeling, indicating that P_1 was

the major phosphorylated product of P (Fig. 4.1A). To determine phosphorylation sites within the MuV P protein, the P protein from MuV-infected cells was purified using a monoclonal anti-MuV-P antibody (Fig. 4.1B). Both the P_1 and P_2 bands were excised separately from the SDS-PAGE gel and then subjected to trypsin digestion and TiO_2 enrichment and analyzed by LC-MS/MS, as previously described (18). The coverage of the mass spectrometry analysis for the P_1 band was 73.9% with 4 predicted phosphorylated residues (Fig. 4.1C), and the coverage of the mass spectrometry analysis for the P_2 band was 88.5% with 14 predicted phosphorylated residues (Fig. 4.1D). Upon more rigorous statistical analysis (peptides receiving an expectation/ random probability score greater than 5% were excluded), the coverages and putative sites for the P_1 and P_2 bands were reduced to 61.6% and 76.4% with 0 and 2 phosphorylation sites, respectively. Only residues S69 and T165 were considered phosphorylated. A summary of the results is shown in Table 4.1, where the higher-stringency phosphorylation data are provided using two "plus" symbols (++).

Effects of mutating S69 and T165 to alanine in the minigenome system.

To study the role of P in viral transcription and replication, a minigenome system for MuV is desirable. Our lab has previously developed a minigenome system, free of vaccinia virus, for parainfluenza virus 5 (PIV5) (235), which is closely related to MuV. By the use of a similar approach, a plasmid containing a renilla luciferase gene flanked by the MuV leader and trailer sequences under the control of a T7 RNAP promoter, along with plasmids expressing the proteins NP, P, and L, was transfected into BSRT7 cells. To study whether phosphorylation of the P protein affects MuV transcription and/or

replication, the S69 and T165 putative phosphorylated residues that were detected with LC-MS/MS were mutated to alanine and the mutants were then tested in the minigenome system (Fig. 4.2A and B). Because the ratio of NP to P is critical for the minigenome activity, a range of concentrations of the P plasmid was used to obtain the maximal minigenome activity. Expression levels of P and NP were determined using immunoblotting (Fig 3.2C). Mutating T165 and S69 to alanine resulted in peak luciferase activities similar to those seen with wild-type P (Fig. 4.2A and 4.2B), indicating that phosphorylation of these residues did not play a role in MuV transcription and/or replication in the minigenome system.

A systematic mutational analysis of P.

To identify potential serine and threonine phosphorylation sites within P that are critical for viral RNA synthesis, all serine and threonine residues were mutated to alanine and all mutants were tested in the minigenome system. Clusters of mutations that affected the minigenome activity ($P < 0.01$) were then mutated individually and the mutants with a single amino acid change were tested. This screen identified substitutions that reduced minigenome activity (T10A, T250A, S257A, T258A, T261A, T262A, T265A, T350A, and T354A), and one substitution that enhanced minigenome activity (T101A), indicating that these residues were important for transcription and/or replication in the minigenome system. Table 4.1 summarizes the minigenome data for all serine and threonine residues in P, with the critical residues highlighted in boldface. Expression levels of P mutants were determined using immunoblotting and similar expression levels of P were detected in wild-type and mutant P-transfected cells (data not shown), indicating that the

mutations did not affect expression of P. Minigenome results and immunoblotting analysis for T10A, a representative mutation that negatively affected the minigenome activity, and T101A, the mutation that positively affected the minigenome activity, are provided (Fig. 4.3C and 4.3D). Using the ViPR database, sequence comparison of 59 different MuV isolates showed that nine residues (T10, T250, S257, T258, T261, T262, T265 and T350) were conserved (data not shown). The only variance was found at T354 for two mumps isolates (Mumps_Virus_ODATE-3 [Gene accession AB600942] and Mumps_virus_Y213 [Gene accession AB576764)].

Reduced P phosphorylation in rMuV-P-T101A infected cells.

To determine if the S and T residues identified in Table 4.1 were phosphorylated, plasmids expressing mutant T10A and T101A were transfected into HeLa cells and the cells were radioactively labeled with ^{35}S or ^{33}P and then immunoprecipitated with monoclonal anti-MuV-P antibody as described above. Interestingly, the P protein band patterns in transfected cells differed from those in infected cells (Fig. 4.4A). Because of this, we were concerned that using transfected cells for analyzing P phosphorylation might generate misleading results. We decided to incorporate the mutations into the genome of MuV and tried to recover infectious virus with the mutations. We have been successful in incorporating the mutations into the genome of MuV cDNA. Using a reverse genetics system we developed, a recombinant virus containing the P-T101A mutation (rMuV-P-T101A) was recovered and confirmed by sequencing (Fig. 4.4B). We attempted to rescue infectious virus containing P-T10A 11 times. However, we were unsuccessful even though a recombinant MuV that expresses GFP was recovered

alongside 9 of those attempts. We speculate that the rMuV-P-T10A mutation likely causes defects in virus growth.

To determine the impact of the T101A mutation on the phosphorylation status of P, HeLa cells were mock infected or infected with MuV or rMuV-P-T101A at an MOI of 0.01. The infected cells were radioactively labeled with ^{35}S or ^{33}P, and cell lysates were immunoprecipitated with monoclonal anti-MuV-P. As shown in Figure 4.4C, P protein phosphorylation of rMuV-P-T101A was significantly reduced by about 35% compared to MuV phosphorylation (Fig. 4.4D), indicating that T101 was phosphorylated in infected cells. The partial reduction of phosphorylation is consistent with the observation that P has multiple phosphorylation sites.

rMuV-P-T101A grew to higher titers than MuV in tissue culture cells.

To examine growth rates of rMuV-P-T101A in cells, Vero cells were infected with MuV or rMuV-P-T101A at an MOI of 0.01 and media from infected cells were collected at different intervals until 96 hours post infection (hpi). Titers of virus in the media were determined using a plaque assay. rMuV-P-T101A grew to a higher titer than MuV at 24 hpi and maintained its higher titer at all time points (Fig. 4.5A). Similar results were obtained in HeLa cells (Fig. 4.5B).

Viral protein expression levels in rMuV-P-T101A-infected cells.

To examine viral protein expression levels in rMuV-P-T101A-infected cells, Vero cells were infected. Lysates from infected cells were collected at various time points and subjected to immunoblotting with monoclonal anti-MuV-NP. At 24 hpi, the band

intensity of NP from rMuV-P-T101A-infected cells was greater than that from rMuV-infected cells (Fig. 4.6A). However, no significant difference in band intensity was observed at later time points (Fig. 4.6A).

Enhanced viral protein expression in rMuV-P-T101A-infected cells shortly after infection was confirmed by flow cytometry. At 24 hpi, rMuV-P-T101A-infected cells had a greater mean fluorescence intensity (MFI) than MuV-infected cells (Fig. 4.6C) and no significant difference was observed at later time points, consistent with the results from immunoblotting (Fig. 4.6B). The findings that mutating P-T101 to A resulted in a mutant with increased minigenome activity and in a recombinant virus with enhanced growth at early stages after infection indicate that phosphorylation of T101 negatively regulates viral RNA transcription and replication.

rMuV-P-T101A had a higher level of viral RNA transcription than wild-type MuV.

To further investigate the mechanism of accelerated viral protein expression in rMuV-P-T101A-infected cells, real-time PCR was used to compare the levels of viral mRNA and viral genomic RNA in Vero cells. The cells were infected with MuV or rMuV-P-T101A at an MOI of 0.01, and total RNA was purified from infected cells at 2, 4, 8, 12,16 and 20 hpi. Interestingly, more viral mRNAs were detected in rMuV-P-T101A-infected cells at earlier time points (4 and 8 hpi) (Fig. 4.7A) whereas significantly more viral genomes were produced by MuV at 8 and 16 hpi (Fig. 4.7B). Overall, there was an increased viral mRNA-to-genome ratio in rMuV-P-T101A-infected cells compared to MuV-infected cells (Fig. 4.7C). This indicates that the T101A mutation

enhanced viral mRNA transcription, suggesting that phosphorylation at this residue negatively regulates viral mRNA transcription in infected cells.

Mutation of a critical P residue did not affect P oligomerization or NP-P-L complex interactions.

P is known to form homo-oligomers and to interact with NP and L. To investigate the mechanism for the effect of T101-to-A mutation, the ability of P-T101A to form homo-oligomers was examined using dithiobis succinimidyl propionate (DSP), a cross-linking agent. The mutant P protein of rMuV-P-T101A-infected Vero cells formed dimers and tetramers similar to those formed by the wild-type P protein of rMuV in infected cells (Fig. 4.8A), suggesting that the mutation did not affect oligomerization of P.

NP-P-L complex interactions were examined using coimmunoprecipitation of infected Vero cells. The P, NP, and L interactions seen with MuV-infected cells and rMuV-P-T101A-infected cells were similar (Fig. 4.8B), suggesting that the P-T101 residue did not play a role in NP and L interaction.

Discussion

In this study, we performed mass spectrometry, as well as a systematic mutational analysis, to identify S and T residues of the P protein that are critical for MuV transcription and replication. To the best of our knowledge, this is the most comprehensive study that has been performed for a paramyxovirus protein to investigate the roles of S/T residues and their potential phosphorylation in viral RNA synthesis.

Interestingly, there is little overlap between MS-identified S/T phosphorylation sites and the S/T residues identified by mutational analysis. While MS can directly detect phosphorylation of S/T resides, this method is limited by many factors, such as the amount of sample available for analysis, time of sample collection (phosphorylation of a site can be temporally regulated), and percentage of total protein that is phosphorylated at the time of sample collection (only a small percentage of a given S/T residue may be phosphorylated at the time of sample collection). Mutational analysis can overcome these issues. However, the results generated through mutational analysis are circumstantial to determine whether these S/T residues are phosphorylated. Thus, mutational analysis using a minigenome system is likely to identify critical S/T residues for viral RNA synthesis, but whether they are indeed phosphorylated and whether their phosphorylation plays a critical role in viral RNA synthesis need further investigation. Using a reverse genetics system, we incorporated a P-T101A mutation into the MuV genome and analyzed the mutant virus. The facts that (i) mutating T101 of the P protein to A resulted in a virus that resembled the phenotype of T101A in the minigenome and (ii) the phosphorylation level of P of the mutant virus was reduced compared to the wild-type P level indicate that T101 is likely phosphorylated and that its phosphorylation is important for regulating viral RNA synthesis. The observation that 9 of 10 S/T residues identified by the mutational analysis are conserved among 59 different isolates of MuV indicates these residues play a critical role in the functionalities of P. Further analysis of these S/T residues using a similar approach with a reverse genetics system is underway.

To investigate the mechanism for the enhanced viral protein expression in rMuV-P-T101A-infected cells at an early stage after initial infection, viral mRNA synthesis and

genome replication were examined. It was found that the T101A mutation led to higher transcription levels of viral mRNA. The NP, P, and L proteins are packaged in the virion of negative-sense RNA viruses. Upon infection, these proteins transcribe viral genome to generate the viral mRNAs to produce more viral proteins. Accumulation of the soluble NP-P complex is thought to trigger the switch from RNA transcription to genome replication (44–46). However, the fact that P and mutant T101A interacted with NP at similar levels indicates that the mutant did not exert its impact on viral mRNA synthesis through its interaction with NP. That the ability of the mutant P to oligomerize as well as to interact with L in infected cells remained the same as that of wild-type P suggests that the mutation at T101 likely acts through a host factor. Identification of this host factor will lead to a better understanding of the mechanism of T101A's regulation of viral mRNA synthesis.

While mumps vaccines have been effective in reducing cases of mumps, recent outbreaks in vaccinated populations raise concerns about vaccination programs. The current mumps vaccine was developed based on a genotype A strain in the 1960s and has been used ever since. A new mumps vaccine that matches circulating strains (for instance, genotype G in the U.S. outbreaks) may be ideal. We have used a reverse genetics system to develop novel mumps vaccine candidates based on genotype G by introducing specific mutations in the genome of MuV, such as deletion of SH and V (11, 58). One challenge for generating a vaccine is to obtain a virus that grows well in tissue culture cells for vaccine production purposes and is also attenuated *in vivo*. Incorporating the mutation at P-T101 into vaccine candidates may increase vaccine yields during production.

The importance of P protein phosphorylation in paramyxovirus transcription and replication has been studied in many paramyxoviruses, and it has been shown to play a role in regulating viral mRNA synthesis (44–46, 176, 239). It is commonly believed that phosphorylation of the P proteins is carried out by host kinases (176). The host kinases, CKII, protein kinase C-ζ (PKC-ζ), AKT, and PLK1 have been identified so far as the main host kinases that phosphorylate paramyxovirus P proteins. CKII is thought to phosphorylate the P proteins of respiratory syncytial virus (RSV) (171, 177) and measles virus (178). PKC-ζ is reported to phosphorylate the P proteins of human parainfluenza virus 3 (HPIV3) (179) and Sendai virus (180). The P protein of canine distemper virus is phosphorylated by both PKC-ζ and CKII (181). AKT phosphorylates the P protein of PIV5 to upregulate its gene expression whereas PLK1's phosphorylation of P of PIV5 downregulates its gene expression. It has been proposed to target host kinases that are critical for viral RNA synthesis as an antiviral strategy for theses paramyxoviruses (182). The identification of S/T residues and phosphorylation sites within MuV P will aid in the identification of host kinases that are important for MuV replication, which will lead to novel targets for anti-MuV drug development.

Acknowledgements

We appreciate the helpful discussion and technical assistance from all members of Biao He's laboratory.

This work was supported by grants (R01AI097368 and R01AI106307) from the National Institutes of Health.

Mutation	MS Detected Sites P_1	MS Detected Sites P_2	Relative peak luciferase activity	P Value
Wild-type P			1	
T10A		+	0.449 ± 0.037	< 0.001
T16A		+	1.013 ± 0.107	0.943
S26A			1.009 ± 0.114	0.966
T32A			0.813 ± 0.107	0.309
S36A/**T39A**		+	0.813 ± 0.056	0.093
T61A/S63A			1.057 ± 0.079	0.625
S67A/**S69A**		++	0.940 ± 0.049	0.621
S73A/S74A			1.016 ± 0.063	0.873
S82A/S83A/S84A			0.925 ± 0.058	0.553
T88A/**T91A**		+	0.932 ± 0.204	0.796
T101A			1.377 ± 0.059	< 0.001
T106A/T108A/T109A			1.031 ± 0.073	0.712
T115A/T119A			1.157 ± 0.070	0.084
S121A/S124A			0.973 ± 0.073	0.869
T145A/S146A/**T147A/T150A**	+	+	0.801 ± 0.071	0.229
T165A	+	++	1.169 ± 0.183	0.183
S177A/S180A			1.087 ± 0.069	0.278
S184A/S186A			1.020 ± 0.035	0.702
S188A/T191A	+	+	1.001 ± 0.172	0.996
S197A			0.823 ± 0.103	0.242
S203A/T204A			0.910 ± 0.093	0.479
S214A/S217A			1.063 ± 0.164	0.751
S247A			0.940 ± 0.114	0.730
T250A		+	0.706 ± 0.035	< 0.001
S257A		+	0.261 ± 0.008	< 0.001
T258A		+	0.007 ± 0.001	< 0.001
T261A			0.760 ± 0.011	< 0.001
T262A			0.197 ± 0.013	< 0.001
T265A	+		0.057 ± 0.001	< 0.001
T272A			0.930 ± 0.052	0.543
T282A		+	0.920 ± 0.042	0.469
S292A/S294A			1.090 ± 0.113	0.626
T298A/S301A			0.948 ± 0.039	0.618
S307A			1.026 ± 0.053	0.774
S309A/S310A/S311A			1.194 ± 0.092	0.181
T315A			0.890 ± 0.049	0.482
T350A			0.733 ± 0.046	< 0.001
T354A			0.759 ± 0.052	0.001
S374A/T375A		+	1.169 ± 0.038	0.183
S389A			0.938 ± 0.037	0.466

Table 4.1. Summary of minigenome activity of MuV P protein mutants. All serine and threonine residues of the MuV P protein were mutated to alanine. The effects of the mutations were examined in the MuV minigenome system. Peak luciferase activities of P protein mutants relative to wild-type P were calculated and are shown. Clusters of

significant residues were individually mutated and tested again. Standard errors of the means (SEM) of data from 6 replicates are provided. *P* values were calculated using Student's *t* test and critical residues are highlighted in boldface. MS-detected phosphorylated residues are symbolized by +, and residues in peptides receiving an expectation/random probability score of less than 5% are symbolized by ++.

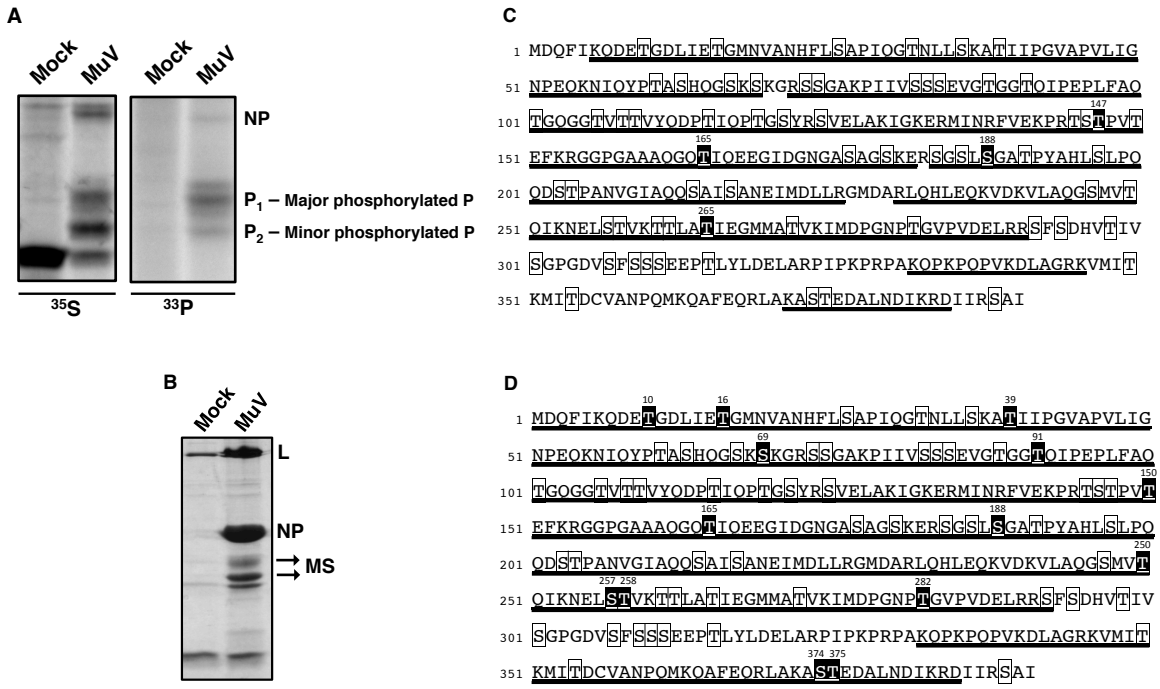

Figure 4.1. Mass spectrometry analysis of MuV P protein products. (A) Phosphorylation of P in infected cells. Vero cells were infected with MuV and then labeled with [^{35}S]Met or [^{33}P]phosphate. The cells were lysed and immunoprecipitated with monoclonal anti-MuV-P antibody. The immunoprecipitated products were resolved in SDS-PAGE. (B) Purification of P from MuV-infected cells. Vero cells were infected with MuV. The cells were lysed and then immunoprecipitated with monoclonal anti-MuV-P antibody. The products were resolved in SDS-PAGE and stained with Commassie blue. Both the major (P_1) and minor (P_2) phosphorylated P bands were excised and processed for mass spectrometry analysis. The excised proteins were digested with trypsin, enriched using TiO_2, and analyzed by LC-MS/MS. (C) Schematic of LC-MS/MS coverage of the major phosphorylated MuV P protein (P_1). All serine and threonine residues are boxed, and underlined residues represent the detected peptides. MS achieved 73.9% of P coverage. S/T residues highlighted in black represent detected phosphorylated residues, which

include T147, T165, S188, and T265. (D) Schematic of LC-MS/MS coverage of the minor phosphorylated MuV P protein (P_2). MS achieved 88.5% of P was coverage. S/T residues highlighted in black represent detected phosphorylated residues, which included T10, T16, T39, S69, T91, T150, T165, S188, T250, S257, T258, T282, S374, and T375.

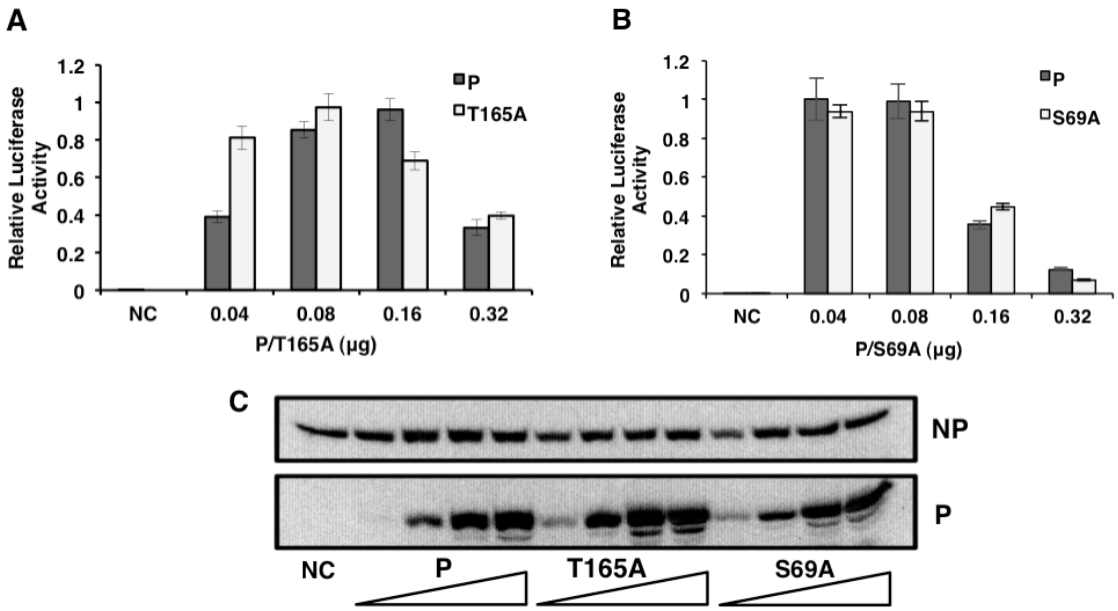

Figure 4.2. Mutation of phosphorylated residues identified by MS resulted in similar levels of minigenome activity. (A) Minigenome activity of P-T165A. Increasing amounts of P or P-T165A were transfected together with other plasmids as described in Materials and Methods. The negative control (NC) contained no transfected P. *Renilla* luciferase was the reporter gene in the minigenome, and Firefly luciferase expression was used as a transfection control. The minigenome activity was measured and normalized as the ratio of *Renilla* luciferase activity to firefly luciferase activity (relative luciferase activity). (B) Minigenome activity of P-S69A. *P* values were calculated using Student's *t* test. Error bars represent the standard errors of the means (SEM) of data from 6 replicates. *, $P<0.001$. (C) Immunoblotting was performed to detect the expression levels of NP and P, P-T165A, or P-S69A.

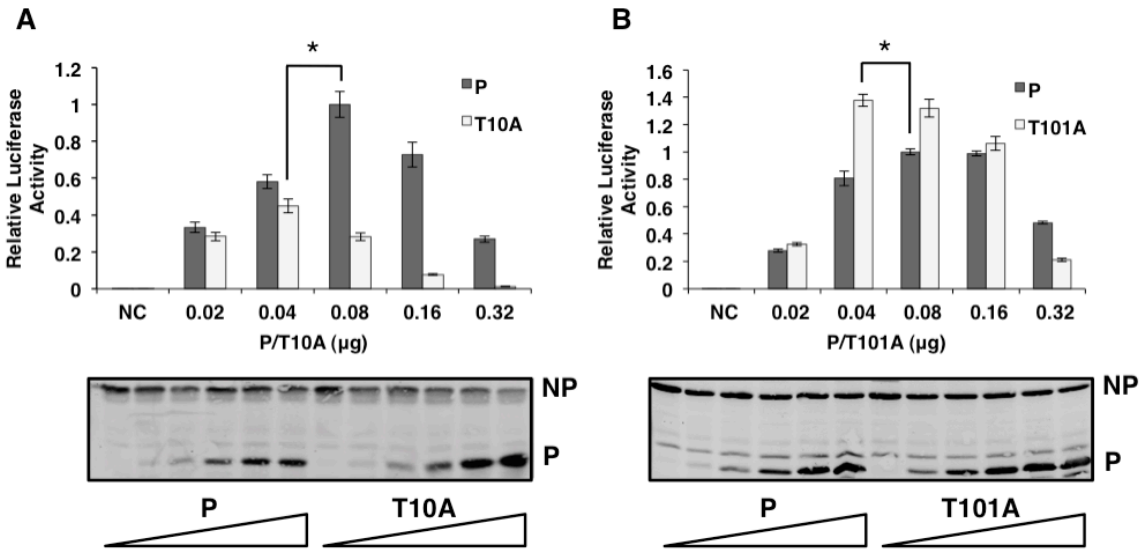

Figure 4.3. Identification of the S/T residues that were critical for RNA synthesis using the MuV minigenome system. Minigenome activity of P-T10A (A) and P-T101A (B) is shown. *P* values were calculated using Student's *t* test. Error bars represent the SEM of data from 6 replicates. *,$P<0.001$. Western blotting was performed to detect the expression levels of NP and P, P-T10A, and P-T101A.

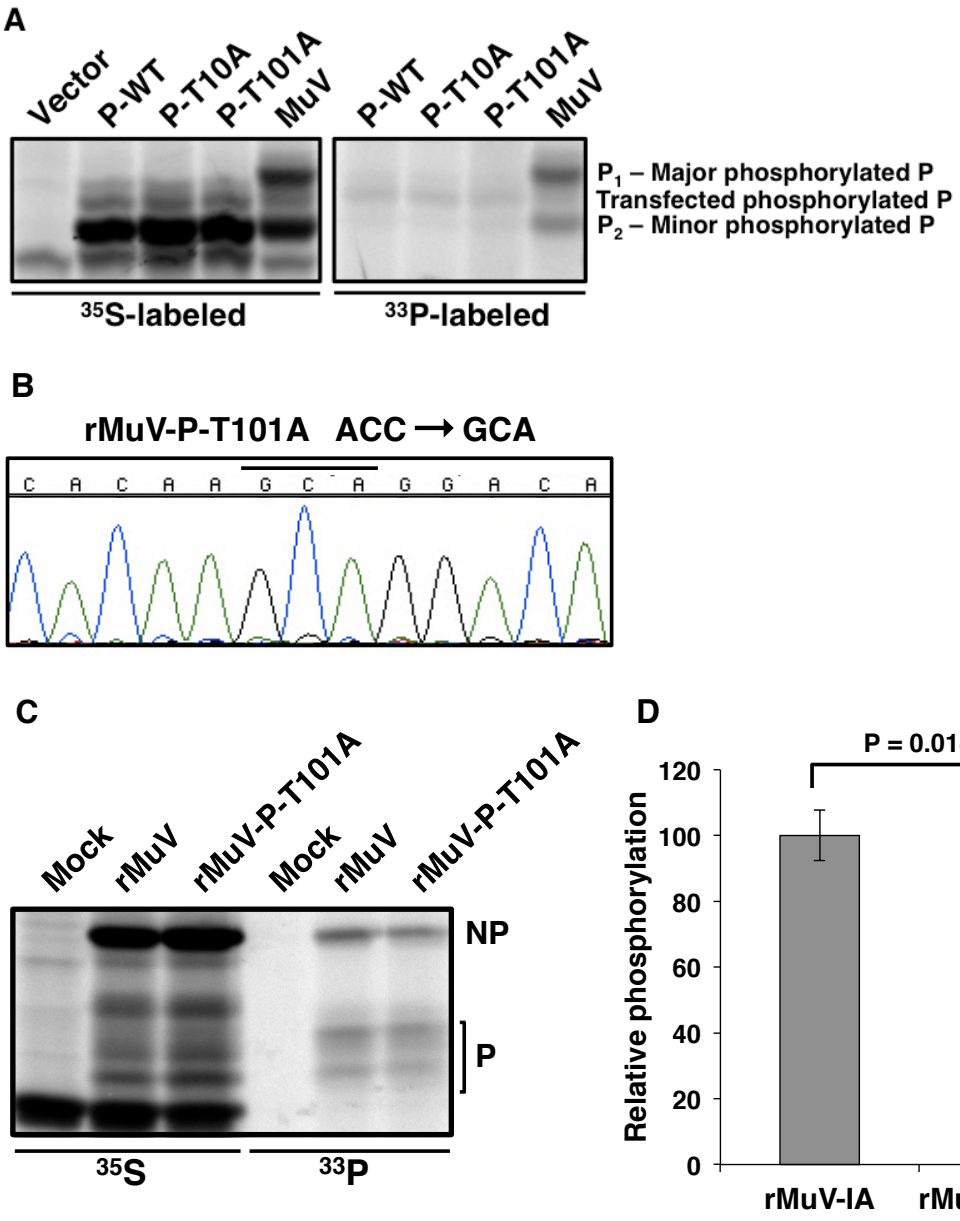

Figure 4.4. Reduced phosphorylation of P in rMuV-P-T101A-infected cells. (A) MuV P protein band patterns of transfected and infected cells. HeLa cells were transfected with pCAGGS-P or pCAGGs-P-mutants or infected with MuV and labeled with ^{35}S or ^{33}P. Cell lysates were immunoprecipitated with monoclonal anti-MuV-P antibody and resolved on a 10% SDS-PAGE gel. (B) Sequence confirmation of rMuV-P-T101A. The genome of rMuV-P-T101A was sequenced, and the region that contained the mutation is

shown. (C) Phosphorylation of P in rMuV-P-T101A-infected cells. Mock-, MuV-, and rMuV-P-T101A-infected Hela cells were labeled with ^{35}S or ^{33}P. Cell lysates were immunoprecipitated with monoclonal anti-MuV-P and resolved on a 10% SDS-PAGE gel. (D) Relative phosphorylation level of P in infected cells. The relative level was calculated as the ratio of phosphorylated protein (^{33}P-labeled P) to total protein (^{35}S-labeled P) and standardized to that of MuV. *P* values were calculated using Student's *t* test. Error bars represent the SEM of data from 4 individual experiments.

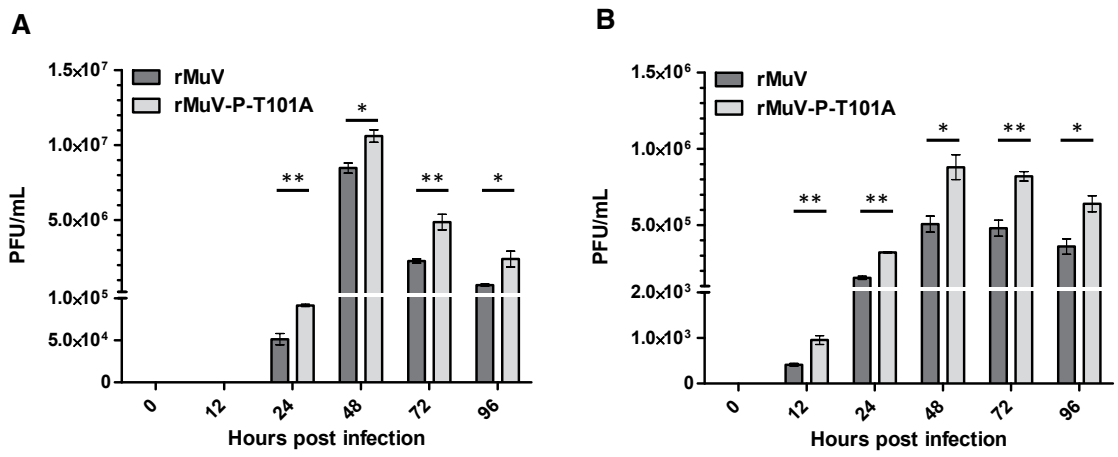

Figure 4.5. Growth rates of rMuV-P-T101A in cells. (A) Growth rates of MuV and rMuV-P-T101A in Vero cells at an MOI of 0.01. (B) Growth rates of MuV and rMuV-P-T101A in HeLa cells at an MOI of 0.01. *P* values were calculated using Student's *t* test. *,$P<0.05$; **,$P<0.01$. Error bars represent the SEM of data from 3 replicates.

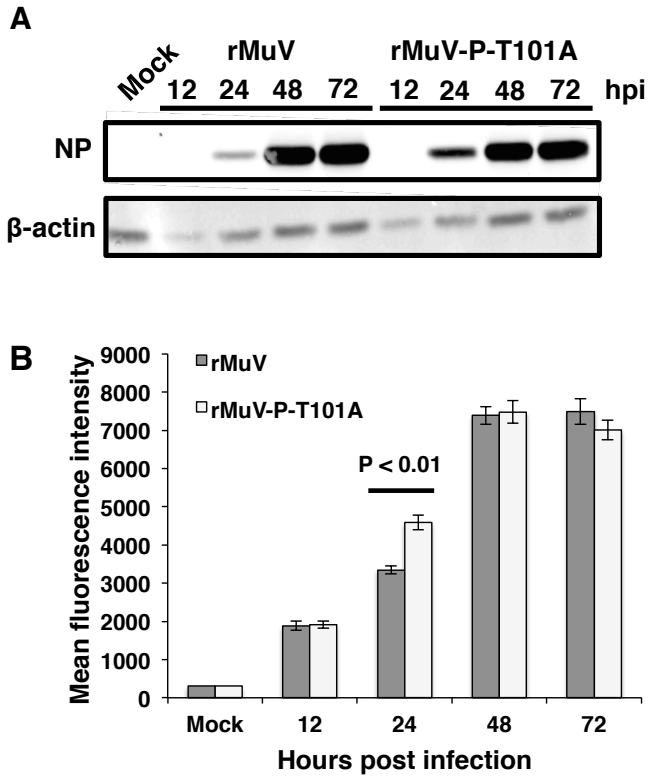

Figure 4.6. Viral protein expression was initially enhanced in rMuV-P-T101A-infected cells. (A) Detection of viral protein expression using immunoblotting. Vero cells were mock, MuV, or rMuV-P-T101A infected at an MOI of 0.01. Cell lysates were collected at 12, 24, 48, and 72 hpi and monoclonal anti-MuV-NP antibody was used for NP protein expression. β-Actin expression is provided as a control to show Vero cell growth. (B) Detection of viral protein expression using flow cytometry. MuV- or rMuV-P-T101A-infected Vero cells (MOI of 0.1) were collected at 12, 24, 48, and 72 hpi and processed for flow cytometry. The mean fluorescent intensity of infected cells (for MuV NP protein) was used to show viral protein expression levels. Error bars represent the SEM from 4 replicates.

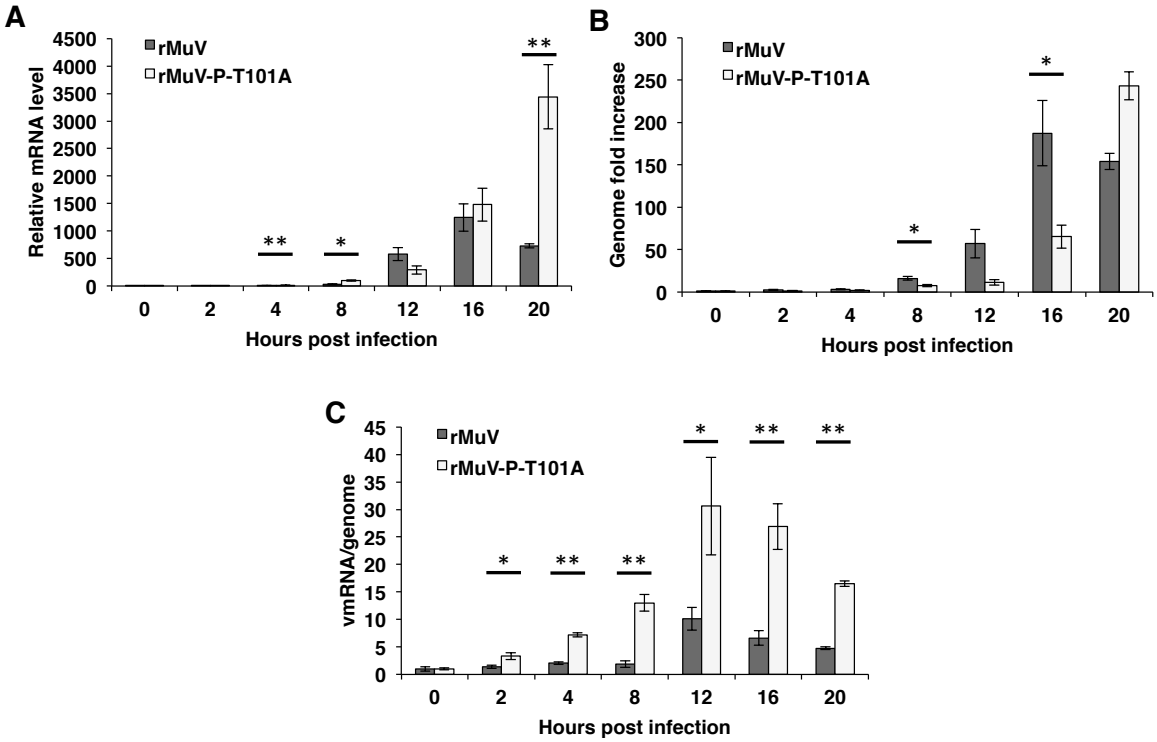

Figure 4.7. Viral RNA synthesis in rMuV-P-T101A-infected cells. (A) Viral mRNA levels. Vero cells were infected with MuV or rMuV-P-T101A at an MOI of 0.01. Total RNA was extracted at 0, 2, 4, 8, 12, 16, and 20 hpi. To measure viral mRNA levels, oligo(dT) primers and a MuV-F-specific 6-carboxyfluorescein (FAM)-tagged probe were used for real-time PCR. Genome levels of MuV or rMuV-P-T101A at 0 hpi were used as the baseline for normalization. (B) Genome replication of MuV and rMuV-P-T101A in Vero cells at an MOI of 0.01. To measure genomic RNA levels, gene-specific primers flanking the MuV-F gene and a MuV-F-specific FAM-tagged probe were used for real-time PCR. Genome levels at 0 hpi for each virus were used as a baseline for normalization. (C) Relative viral mRNA levels per genome at each time point were calculated for MuV- or rMuV-P-T101A-infected Vero cells at an MOI of 0.01. *P* values

were calculated using Student's *t* test. *,$P<0.05$; **,$P<0.01$. Error bars represent the SEM of data from 3 replicates.

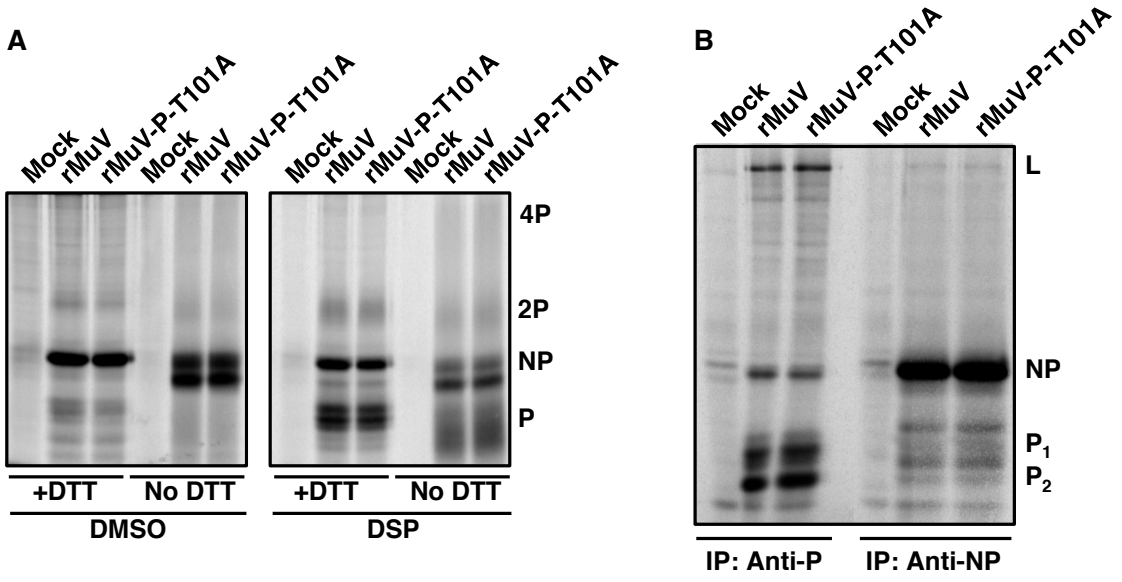

Figure 4.8. Interactions of P with itself, NP and L. (A) Oligomerization of P-T101A. Mock-, MuV-, or rMuV-P-T101A-infected Vero cells were labeled with ^{35}S. DSP (DMSO as a negative control) was used for cross-linking. The cross-linked products were immunoprecipitated using monoclonal anti-MuV-P antibody. Half of the products were mixed with the loading buffer without DTT, and the other half were mixed with the loading buffer with DTT. (B) Interaction between P-T101A and NP and L. Vero cells were mock infected or infected with MuV or rMuV-P-T101A and labeled with [^{35}S]Met. Cell lysates were inmmunoprecipitated with monoclonal anti-MuV-NP.

CHAPTER 5

MUMPS VIRUS NUCLEOPROTEIN ENHANCES PHOSPHORYLATION OF THE PHOSPHOPROTEIN BY POLO-LIKE KINASE 1[3]

[3] Pickar A.*, Zengel, J.*, Xu P., Li Z., He B. To be submitted to *PLOS Pathogens*.
*Authors contributed equally

Abstract

The RNA-dependent RNA polymerases (vRdRP) of non-segmented, negative-sense viruses (NNSV) consist of the enzymatic large protein (L) and the phosphoprotein (P). P is heavily phosphorylated and its phosphorylation plays a critical role in viral RNA synthesis. Since NNSVs do not encode kinases, P is phosphorylated by host kinases. In this study, we investigate the roles that viral proteins play in the phosphorylation of P. Using mumps virus (MuV) as a model, we found that NP enhances the phosphorylation of P. We have identified the serine/threonine kinase polo-like kinase 1 (PLK1) as a host kinase that phosphorylates P and that phosphorylation of P by PLK1 is enhanced by NP. The PLK1 binding site in MuV P was mapped to residues 146-148 within the S(pS/T)P motif and the phosphorylation site was identified as residues S292 and S294. In addition to MuV, we also show that NP enhances phosphorylation of P of parainfluenza virus 5 (PIV5) and J paramyxovirus (JPV).

Significance

It has previously been shown that P acts as a chaperone for NP, which encapsidates viral genomic RNA to form the NP-RNA complex, the functional template for viral RNA synthesis. Thus, it is assumed that phosphorylation of P may regulate NP's ability to form the NP-RNA complex, thereby regulating viral RNA synthesis. Our work demonstrates that NP affects phosphorylation of P, suggesting that NP can regulate viral RNA synthesis by regulating phosphorylation of P.

Introduction

Many human and animal pathogens such as mumps virus (MuV), Sendai virus (SeV), human respiratory syncytial virus (RSV), the parainfluenza viruses, Measles virus (MeV), J paramyxovirus (JPV), Hendra virus (HeV), and Nipah virus (NiV) are in the *Paramyxoviridae* family of the *Mononegavirales* (4). The non-segmented, negative-stranded RNA genome of these viruses is encapsidated by the nucleoprotein (NP) to produce the helical nucleocapsid that functions as the template for viral RNA synthesis. The viral RNA dependent RNA polymerase (vRdRp), which minimally consists of the phosphoprotein (P) and the large protein (L), functions for both transcription and replication of the viral RNA genome. The enzymatic activities of the L protein are responsible for initiation, elongation, and termination of RNA synthesis, and the L protein functions to add the 5' cap and 3' poly(A) sequences to transcribed viral mRNA (4). P protein interacts with NP to dock the vRdRp to the NP-RNA template.

The P proteins of paramyxoviruses are highly phosphorylated and phosphorylation of these proteins has been shown to play critical roles in regulating viral mRNA synthesis (6–10, 47). Phosphorylation of residues within the P protein of PIV5, a prototypical paramyxovirus, plays both negative and positive roles in mRNA synthesis (7–9). A phosphorylation site at S157 was found in the P protein of PIV5-infected cells (7). Further studies found that polo-like kinase 1 (PLK1) associates with S157 and phosphorylates the PIV5 P protein at S308 (7, 8). Phosphorylation of both of these residues reduces viral gene expression and prevents cytokine induction and cell death. This report found that P phosphorylation negatively regulates viral gene expression, suggesting that PIV5 limits its gene expression to avoid induction of innate immune

responses (8). Further studies of the PIV5 P protein by mass spectrometry have identified T286 as a phosphorylation site and mutation of this residue reduces minigenome activity (9). A recombinant virus containing the T286 mutation grows slower than wild-type PIV5 and has delayed viral mRNA synthesis and protein expression, demonstrating that phosphorylation at T286 plays a positive role in virus growth and viral gene expression by up-regulating viral mRNA transcription (9). These studies suggest a role of P phosphorylation in viral mRNA synthesis.

It is commonly believed that phosphorylation of the P proteins is carried out by host kinases (176). The main host kinases that have been identified so far to phosphorylate paramyxovirus P proteins are casein kinase II (CKII), protein kinase c isoform zeta (PKC-ζ), protein kinase B (AKT) and PLK1. The P proteins of RSV and measles virus are thought to be phosphorylated by CKII (171, 177, 178). The P proteins of HPIV3 and Sendai virus are reported to be phosphorylated by PKC-ζ (179, 180) The P protein of canine distemper virus is phosphorylated by both PKC-ζ and CKII (181). Phosphorylation of the PIV5 P protein results in up regulation of viral gene expression whereas phosphorylation by PLK1 results in down regulation. It has been proposed to target host kinases that are critical for viral RNA synthesis as an anti-viral strategy for these paramyxoviruses (182).

MuV is a human pathogen of the *Rubulavirus* genus of the family *Paramyxovidae*. MuV infection causes acute parotitis and it is a neurotropic agent with symptoms ranging from mild meningitis to severe encephalitis. Phosphorylation of MuV P was found to play a role in viral RNA synthesis (47). A systematic mutational analysis using a minigenome system identified residue P-T101 as important in viral RNA

synthesis. A recombinant MuV containing this mutation (rMuV-P-T101A) was generated. Analysis of this virus revealed that phosphorylation at P-T101 plays a negative role in viral transcription (47). Host kinases that are important for MuV phosphorylation remain to be identified.

In this work, we examined the role of viral proteins in phosphorylation of P of MuV and we identified a host kinase that binds P and mapped the phosphorylation site within P.

Materials and Methods

Plasmids and cells. A plasmid containing the human PLK1 gene was obtained from Open Biosystems (AL, USA). A Flag tag was added to the N-terminus of PLK1 and cloned into pCAGGS vector. Kinase-deficient PLK1 (Flag-PLK1-K82M) was constructed using Flag-PLK1 as the template as previously described (8). MuV NP, P, and L genes of the $MuV^{Iowa/US/06}$ strain were cloned into the pCAGGS expression vector (11). Plasmids expressing P mutants were constructed using standard molecular cloning techniques. Plasmids containing the full-length genome for rMuV-P-T147A, rMuV-P-T204A, rMuV-P-S292A/S294A, rMuV-P-T147A/T204A, and rMuV-P-T147A/S292A/S294A viruses were made similarly to that of rMuV-P-T101A as described before (47). The MuV minigenome plasmid (BH526/ pMG-RLuc), containing *Renilla*, and a plasmid containing firefly-luciferase (pFF-Luc) were described previously (47). Construction details and sequence files of the plasmids are available upon request.

293T cells were maintained in Dulbecco's modified Eagle medium (DMEM) with 5% fetal bovine serum (FBS) and 1% penicillin-streptomycin (P/S) (Mediatech Inc.,

Manassas, VA). Vero and HeLa cells were maintained in DMEM supplemented with 10% FBS and 1% P/S. BSR-T7 cells were maintained in DMEM supplemented with 10% FBS, 1% P/S, 10% tryptose phosphate broth (TPB), and 400 μg/ml G418 sulfate antibiotic (Mediatech Inc.). All cell lines were incubated at 37°C with 5% CO_2 and passed at an appropriate dilution one day prior to use, to achieve 80 to 90% confluence upon transfection or infection.

Transfections, infections, and virus rescue. Cells were transfected using JetPRIME® (Polyplus-transfection Inc., New York, NY) following the manufacturer's protocols. For virus infections, cells were inoculated with viruses at a multiplicity of infection (MOI) of 0.1 or 3 in DMEM plus 1% bovine serum albumin (BSA) and incubated at 37°C with 5% CO_2 for 1-2 hours. The inocula were then replaced with DMEM supplemented with 2% FBS and 1% P/S.

rMuV-P-T147A, rMuV-P-T204A, rMuV-P-S292A/S294A, rMuV-P-T147A/T204A, and rMuV-P-T147A/S292A/S294A were rescued from the plasmids containing their respective full-length genome as described before (47). A plasmid containing the full-length genome (5 μg), along with plasmids pCAGGS-L (2 μg), pCAGGS-NP (100ng), and pCAGGS-P (320ng), were transfected into BSR-T7 cells. Three days later, transfected BSR-T7 cells were mixed with Vero cells at a 1:5 dilution. Four days later, media was transferred to fresh Vero cell monolayers and propagated further. When syncytia formation was observed, media was collected and used for plaque assays in Vero cells as previously described (5). Single plaques were isolated 6-7 days later and cultured in fresh Vero cells to produce passage 1 (P1). After titer determination,

P1 was passaged again at an MOI of 0.01 to produce P2. After 72 hrs, virus was collected, sucrose-phosphate-glutamate SPG (2.18 M sucrose, 37.6 mM potassium phosphate monobasic, 71 mM potassium phosphate dibasic, and 49 mM potassium glutamate) was added to 1% final concentration, and aliquots were stored at -80°C. Titers were determined by plaque assay. Viral genomes were sequenced as previously described (240). Viral RNA was isolated using QIAamp Viral RNA Mini Kit (Qiagen, Valencia, CA) followed by synthesis of DNA templates using SuperScript III One-Step RT-PCR System with Platinum Taq (Life Technologies, Grand Island, NY) and 5 sets of primers to amplify the entire genome. Fragments were sent to Genewiz (South Plainfield, NJ) for sequencing using 6-10 primers per fragment. Only viruses matching the full-length plasmid sequence were used for further experiments. Primer sequences are available upon request.

Phosphorylation of P. To examine phosphorylation of P, HeLa cells or 293T cells in 6-well plates were transfected with 1 μg of pCAGGS-P or pCAGGS-P mutants, 1 μg of pCAGGS-NP, and 1 μg of Flag-PLK1 or Flag-PLK1-K82M, or infected with MuV or a recombinant mutant MuV at an MOI of 0.1. After 18 hpt, the cells were starved with DMEM lacking cysteine-methionine and then labeled with 72.7 μCi/ml ^{35}S-EasyTagTM Express35S Protein Labeling (Perkin Elmer, Waltham, MA) for 3-8 hours (h) or starved with DMEM lacking sodium phosphate and then labeled with 100 μCi ^{33}P-Radionuclide Orthophosphoric acid (Perkin Elmer, Waltham) for 8 h. The cells were then lysed with whole-cell extraction buffer (WCEB) (50mM Tris-HCl [pH 8.0], 280 mM NaCl, 0.5% NP-40, 0.2 mM EDTA, 2 mM EGTA, and 10% glycerol) with a mixture of protease

inhibitors as previously described (7).The lysate was immunoprecipitated using rec-protein G-sepharose 4B conjugate and mouse monoclonal anti-MuV-P, mouse monoclonal anti-MuV-NP, or mouse anti-Flag (M2 clone, Sigma-Aldrich, St. Louis, MO) antibodies. After washing 3x with WCEB, the agarose beads were mixed with 3x SDS loading buffer (188 mM Tris-HCl [pH 6.8], 6% SDS, 30% glycerol, 0.03% w/v bromophenol blue, and 200 mM dithiothreitol [DTT]), heated at 95°C for 5 min, and resolved by 10% SDS-polyacrylamide gel electrophoresis (PAGE). Phosphorylation of the P protein of 4 individual experiments was calculated by densitometry analysis of the $^{33}P/^{35}S$ ratio using ImageQuant TL software (GE Healthcare Life Sciences).

PLK1 inhibitor. The highly selective PLK1 inhibitor, BI 2536, was purchased from Selleck Chemicals (Houston, TX). The compound was dissolved in ethanol. To study the effect of the PLK1 inhibitor on P phosphorylation in infected cells, Vero cells were infected with MuV at an MOI of 0.1 and incubated with 1 uM BI 2536. To study the effect of the PLK1 inhibitor on P phosphorylation in transfected cells, 293T cells were transfected with 1 μg of P or P mutants, 1 μg of NP, and 1 μg of Flag-PLK1. At 18 hours post infection (hpi) or transfection, cells were starved with DMEM lacking cysteine-methionine and then labeled with 72.7 μCi/ml ^{35}S-EasyTagTM Express35S Protein Labeling (Perkin Elmer) in the presence of 1 uM BI 2536 for 3 h. The cells were then lysed with WCEB and immunoprecipitated as described above.

To study the effect of PLK1 inhibitor on viral protein expression, Vero cells were infected with a recombinant virus expressing a *Renilla* luciferase protein (rMuV-Rluc) at an MOI of 0.01 and incubated with BI 2536 at various concentrations. After 24 hpi cells

were lysed with *Renilla* luciferase assay lysis buffer (Promega) and vigorously mixed for 20 min to permit full lysis. *Renilla* luciferase activity was measured according to manufacturer's protocol (Promega) and light intensity was detected by a GloMax® 96 Microplate Luminometer (Promega). Aliquots of the cell lysates were used for Western blot analysis to detect P protein expression.

MuV minigenome system and dual-luciferase assay. The MuV minigenome system used in this study was described previously (47). BSR-T7 cells in 24-well plates were transfected with pCAGGS-P (80ng) pCAGGS-NP (25 ng), pCAGGS-L (500 ng), pMG-RLuc (100 ng), pFF-Luc (1 ng), and various amounts of Flag-PLK1 or Flag-PLK1 (K82M) (0, 16, 32, or 64 ng). Empty pCAGGS vector was used to normalize the amount of transfected DNA per sample. After 48 hpt, 2/5 of the lysate from each well was used to carry out the dual-luciferase assay according to the manufacturer's protocol (Promega, Madison, WI), and light intensity was detected using a GloMax 96 Microplate Luminometer (Promega). Relative luciferase activity was defined as the ratio of *Renilla* luciferase (R-Luc) to firefly luciferase (FF-Luc) activity. Six replicates of each sample were measured. Cell lysate aliquots from the dual luciferase assay were mixed with one-half volume of 3x SDS loading buffer and heated at 95°C for 5 min. Samples were resolved by 10% SDS-PAGE and transferred to a polyvinylidene difluoride membrane (GE Healthcare, Piscataway, NJ). The membrane was incubated with mouse anti-MuV-NP antibody (1:2000 dilution) or mouse anti-Flag (M2 clone, Sigma, 1:1000 dilution), followed by incubation with Cy3 conjugated goat anti-mouse IgG secondary antibody

(1:2500 dilution) (Jackson ImmunoResearch, West Grove, PA) and scanned using a Typhoon 9700 imager (GE Healthcare Life Sciences, Piscataway, NJ).

Pulse-chase labeling. To examine the stability of P, 293T cells were transfected with 1 μg of P, 1 μg of NP, and 1 μg of Flag-PLK1. Empty pCAGGS vector was used to normalize the amount of transfected DNA per sample. After 18 hpt, the cells were starved with DMEM lacking cysteine-methionine and then labeled with 72.7 μCi/ml ^{35}S-EasyTagTM Express35S Protein Labeling for 30 min. The cells were then washed with PBS and the media was replaced with DMEM supplemented with 2% FBS and 1% P/S. After replacing the media (0 h) and after 4, 8, and 12 h, cells were lysed with WCEB and the lysate was immunoprecipitated using rec-protein G-sepharose 4B conjugate and mouse anti-MuV-P as described above. The P half-life of 4 individual experiments was calculated by normalization of P expression at 0 h using ImageQuant TL software (GE Healthcare Life Sciences).

Single-step growth curve. Vero cells in 10-cm dishes were infected with MuV, rMuV-P-T147A, rMuV-P-T204A, rMuV-P-S292A/S294A, rMuV-P-T147A/T204A, or rMuV-P-T147A/S292A/S294A at a MOI of 3 in triplicate. Media was collected at 0, 8, 16, 24, 48, 72 hpi and supplemented with 1% SPG, then stored at -80°C. Virus titers were determined in Vero cells by plaque assays, and completed in triplicate as previously described (5).

Phosphorylation of P in related viruses. Plasmids encoding NP and P for parainfluenza virus 5 (PIV5, W3A), J paramyxovirus (JPV, JPV-BH), and respiratory syncytial virus (RSV, A2) were previously produced or cloned into pCAGGS vector for this study. Plasmids were transfected along with PLK1 or PLK1 (K82M) in different combinations. After 24 h, radioactive labeling was performed as described above. Immunoprecipitation was performed using monoclonal antibodies specific to P (PIV5: anti-P/V, JPV: rabbit anti-P, RSV: clone C1). Samples were resolved by SDS-PAGE.

Statistical analysis. Statistical analysis was performed using GraphPad Prism version 5.00 for Windows (GraphPad Software, San Diego, CA). Student's *t* test was used to calculate *P* values when comparing two groups. When performing multiple comparisons, the Holm-Sidak method with alpha = 5% was used to determine statistical significance.

Results

Phosphorylation of MuV P is greater in virus-infected cells compared to cells transfected with P.

Previous research shows that there is a difference in the phosphorylation of MuV P in MuV-infected cells versus cells transfected with plasmid encoding MuV P (47). To confirm these results, HeLa cells were transfected with plasmids encoding MuV P or infected with MuV. The cells were radioactively labeled with either ^{35}S-Cys/Met or ^{33}P-orthophosphate and lysates were immunoprecipitated with a monoclonal anti-MuV-P antibody to determine the amount of phosphorylation (Fig. 5.1A). P phosphorylation was

lower during transfection compared to virus infection. Most interestingly, there was a difference in the patterns of P bands associated with the P protein in infected cells versus transfected cells. This higher band was also the major phosphorylated species in infected cells. The major phosphorylated P species, the slower migrating band, was detected in MuV-infected cells but not in transfected cells.

To understand the discrepancy in phosphorylation of P in transfected cells versus infected cells, we examined phosphorylation of P in cells containing the minigenome system components. The minigenome system has been used to examine MuV RNA synthesis (7). Plasmids encoding P, L, and NP were transfected along with a plasmid encoding the MuV minigenome under a T7 promoter. When the minigenome plasmid is transcribed by T7 RNAP, a negative-sense minigenome RNA is produced, consisting of the leader and trailer of MuV flanking the negative sense coding sequence for Renilla luciferase. Since this system is able to model the transcriptional activity observed during infection, we reasoned that phosphorylation of P in this system should reflect that of P in infection. BSR-T7 cells are typically used for minigenome experiments due to their stable expression of T7 RNAP. However, the expression level of transfected plasmids in BSR-T7 cells was not sufficient to examine phosphorylation using radioactive labeling. Instead, 293T cells were used and a plasmid encoding the T7 RNAP was added to the minigenome transfection mixture. P was transfected alone, with the individual minigenome components, or with all of the components together. Radioactive labeling and P immunoprecipitation was performed as before and samples were resolved by SDS-PAGE (Fig. 5.1B). The phosphorylation of MuV P was enhanced in the presence of MuV NP, while the other minigenome components had no effect. The phosphorylation of

transfected P was closer to that of P during infection when NP was co-transfected. Most importantly, the pattern of phosphorylated P looked similar between P+NP and MuV-infected samples.

MuV NP and PLK1 are both required for high levels of MuV P phosphorylation.

To understand the mechanism of the enhanced phosphorylation of P by NP, it will be important to identify the host kinase that phosphorylates P during viral infection. It has been shown that PLK1 is responsible for the phosphorylation of P for the closely related virus parainfluenza virus 5 (PIV5) (8). PLK1 is a serine/threonine kinase that functions as the critical regulator in progression through mitosis (241). PLK1 contains a polo-box domain (PBD) and a kinase activity domain. The PBD domain of PLK1 interacts with its target through the consensus binding motif (S p(S/T) P), where the second amino acid residue is phosphorylated for optimal binding (242). Upon binding of PLK1 to its target within the STP motif, PLK1 phosphorylates the target itself or a protein associated with the target (243). To determine if PLK1 was responsible for MuV P phosphorylation in infected cells, we treated MuV-infected cells with a PLK1 inhibitor (BI 2536) during radioactive labeling. Treatment of infected cells with BI 2536 resulted in an 80% reduction in P phosphorylation (Fig. 5.2A and 5.2B). The P_1 band (the major phosphorylated P species) was no longer visible in the BI 2536-treated sample. These results suggest that PLK1 phosphorylates P in infected cells.

To determine the role of PLK1 in phosphorylation of P in transfected cells, plasmids encoding P, NP and Flag-PLK1 were transfected in different combinations (Fig. 5.3A). As seen previously, the addition of NP resulted in greater P phosphorylation.

There was also an increase in P phosphorylation when P and PLK1 were co-expressed. When all three plasmids were transfected together, there was a large increase in the amount of P phosphorylation and a shift to a dominant P_1 band. The increase was greater than the additive effect when adding NP or PLK1 alone, suggesting that the coordination of NP, P, and PLK1 results in synergistic enhancement of P phosphorylation.

PLK1 kinase activity is required for increased phosphorylation of MuV P.

To confirm that PLK1 kinase activity was required for phosphorylation of MuV P, we used a plasmid encoding a PLK1 kinase deficient mutant (PLK1-K82M). The PLK1 kinase deficient mutant has a point mutation in the ATP binding motif (K82M) and lacks all kinase activity (244). We found that the enhanced phosphorylation phenotype and dominant P_1 band for the P+NP+PLK1 sample was absent when PLK1 was replaced with the kinase deficient mutant (Fig. 5.3B). This suggests that PLK1 kinase activity is required for enhanced P phosphorylation.

We further confirmed that PLK1 activity is required for P phosphorylation by treating transfected samples with BI 2536 during radioactive labeling (Fig 5.3C). A band shift from P_1 to P_2 was observed in the inhibitor-treated sample. This band shift was consistent with a loss of phosphorylation observed in earlier experiments and suggests that BI 2536 prevents P phosphorylation during transfection. There was also an increase in the amount of PLK1 that co-immunoprecipitated with P in the inhibitor-treated samples. PLK1 may dissociate from the transient P-PLK1 complex following phosphorylation, therefore inhibiting PLK1 activity may result in retention of the P-PLK1 interaction.

Stability of MuV P in the presence of NP and PLK1.

It is possible that NP increases stability of P, not phosphorylation of P. To examine stability of P in the presence of NP, P was transfected with NP, PLK1 or both NP and PLK1. After 18 hours post transfection (hpt), cells were pulsed with radioactive isotope, and the amount of P was determined over time (Fig. 5.4A). The half-life of P in transfected cells was determined for each condition (Fig. 5.4B). The half-life of P was similar when NP and PLK1 were also transfected. There was a significant decrease in the half-life of P when PLK1 was present (P=0.031). These results suggest increased phosphorylation of P in the presence of NP or PLK1 was not due to protein stability. Although there was no difference between half-lives of the total amount of P, the P_1 band appeared to be more stable than the P_2 band when P, NP, and PLK1 were co-transfected (data not shown).

PLK1 inhibits MuV viral protein production.

To understand the role of P phosphorylation by PLK1 in the MuV life cycle, we assessed the role of PLK1 inhibition using recombinant MuV expressing *Renilla* luciferase (rMuV-Rluc) (11). When Vero cells infected (MOI=0.01) with rMuV-Rluc were treated with BI 2536, there was an increase in reporter expression (Fig. 5.5A). Similar increases were observed in HeLa cells and with a high MOI (data not shown). Increased luciferase activity as also observed using a different PLK1 inhibitor (GW 843682X, Tocris Bioscience) (data not shown). Viral protein levels were also increased after treatment with BI 2536, corroborating the results observed using the Renilla reporter (Fig. 5.5B).

To determine if treatment with PLK1 inhibitor had a direct effect on viral RNA synthesis, we examined the effects of the inhibitor on the MuV minigenome system. BSR-T7 cells were transfected with plasmids required for optimal minigenome activity followed by treatment with BI 2536. After 48 hpt, minigenome activity was measured (Fig. 5.5C). There was an increase in minigenome activity at all concentrations of BI 2536 ≥ 50nM. This result suggests that phosphorylation of P by PLK1 decreases MuV transcription and replication.

To determine if overexpression of PLK1 would have the converse effect, PLK1 or PLK1-K82M were transfected along with the minigenome components. The addition of PLK1 resulted in a decrease in minigenome activity in a dose dependent manner, while there was no significant difference in the minigenome activity when the kinase deficient PLK1-K82M plasmid was added (Fig. 5.5D). This result confirms the role of PLK1 as a negative regulator of MuV transcription and replication.

Determining the critical residues in MuV P required for phosphorylation by PLK1.

PLK1 has been shown to interact with its target through a highly conserved binding site motif (S-pS/pT-P), where the second amino acid residue, S or T, is phosphorylated for optimal binding and subsequent kinase activity (242, 245). MuV P contains two possible PLK1 binding sites: residues 146-148 (STP) and 203-205 (STP). The second residue of each binding motif was mutated to alanine (A) to produce plasmids encoding P-T147A and P-T204A, as well as a double mutant P-T147A/T204A. The P mutants were co-transfected with NP and PLK1 to determine if there was still enhanced phosphorylation of P, characterized by the presence of a strong P_1 band (Fig. 5.6). Cells

transfected with NP, PLK1 and P showed the characteristic P_1 band, as did the P-T204A mutant. When NP and PLK1 were co-transfected with P-T147A or P-T147A/T204A, the P_1 band was lost. When BI 2536 was included during labeling, P_1 was lost for all treated samples. As seen previously (Fig. 5.3C), a greater amount of PLK1 co-immunoprecipitated with P when treated with BI 2536. The amount of PLK1 co-immunoprecipitated was reduced for both mutants containing the T147A mutation. This data shows that PLK1 binding and subsequent phosphorylation of P is dependent on the motif at positions 146-148.

To determine the sites in P that are phosphorylated by PLK1 after PLK1 binding, a library of P mutants containing each serine or threonine residue mutated to alanine was screened. Each P mutant was transfected with NP and PLK1, and P phosphorylation was determined based on the presence of the P_1 band (Fig. 5.7A). There were three mutants that had decreased P_1 band intensity: P-T147A, P-T145A/S146A/T150A, and P-T292A/S294A. To determine critical residues, the two clusters were separated into single site mutats and tested (Fig. 5.7B). As expected, P-T147A had decreased phosphorylation. While P-S292A/S294A had a very low level of phosphorylation, the individual mutations had little difference in phosphorylation. It is likely that these residues are a target for PLK1 phosphorylation and that both residues are compensating each other. The P-T145A/S146A/T150A mutant also had decreased phosphorylation. When split into individual mutations, P-T145A and P-T150A both had low levels of phosphorylation, while P-S146A was similar to wild-type P. Since these sites are close to the PLK1 binding site, it is possible that mutating these sites disrupted the PLK1 binding site, similar to the P-T147A mutation.

Determining the effects of point mutations in P of rMuV.

To determine the effects of the mutations at two possible PLK1 binding sites (P-T147A and P-T204A) and the target site (P-S292A/S294A), viruses were rescued (rMuV-P-T147A, rMuV-P-T204A, rMuV-P-S292A/S294A, rMuV-P-T147A/T204A, and rMuV-P-T147A/S292A/S294A). Following rescue, Vero cells were infected and P phosphorylation was determined (Fig. 5.8A). Relative P phosphorylation was decreased by approximately 60% for the mutants containing the T147A mutation, while there was a slight increase in phosphorylation for rMuV-P-T204A (Fig. 5.8B). While total phosphorylated levels of rMuV-P-S292A/S294A were similar to wild-type, the slower moving phosphorylated P was no longer detected.

Growth of rMuV P mutants in cell culture.

To determine the effects of these mutations on viral growth, single-step growth curves were performed in Vero cells. Viral titers were determined up to 72 hours post-infection (hpi) (Fig. 5.9A). Each of the P mutations had a significant effect on the growth kinetics of MuV (Fig. 5.9B). rMuV-P-T147A, rMuV-P-T147A/T204A, and rMuV-P-T147A/S292A/S294A had increased titers at multiple time points, while rMuV-P-T204A growth was greatly attenuated with significantly reduced titers at 16 hpi or later. rMuV-P-T204A had about a two log reduction in titer at each of these time points compared to MuV. Mutations that decreased phosphorylation in the transfection experiments had a positive effect on viral growth, while the P-T204A mutation had a dramatic negative effect. This data suggests that P phosphorylation by PLK1 has a negative effect on viral growth.

The role of NP and PLK1 in the phosphorylation of P for related viruses.

Since NP played an important role in the phosphorylation of MuV P, we thought that it may also play a role in related viruses. We tested this hypothesis for PIV5, J paramyxovirus (JPV), and respiratory syncytial virus (RSV). For each virus, the effects of NP and PLK1 on P phosphorylation were assessed. PIV5 had a similar phenotype to MuV, with P phosphorylation greatly increasing with the addition of both NP and PLK1 (Fig. 5.10A). The phosphorylation of JPV P was dependent on the presence of NP, but it was not dependent on PLK1 (Fig. 5.10B). For JPV, there was little or no P phosphorylation when NP was not present. For RSV (Fig. 5.10C), P was highly phosphorylated when transfected alone and NP or PLK1 had no effect. These results suggest that NP plays a role in the phosphorylation and function of the P protein in viruses other than MuV.

Discussion

In a previous publication, we observed that the banding pattern and the phosphorylation of MuV P differed in MuV-infected cells compared with transfected cells expressing MuV P alone (47). We suspected that there were other viral proteins playing a role in the phosphorylation of P. Previous research on the closely related virus PIV5 shows that phosphorylation of PIV5 P is dependent on AKT1 and PIV5 L protein (182, 238). However, phosphorylation of P was not shown to be directly dependent on interaction with L. In our current study, we showed an increase in phosphorylation of P when NP and PLK1 were co-transfected with P for both MuV and PIV5. The degree of phosphorylation and the banding pattern of P in co-transfected samples were similar in

infected cells in contrast to when P was transfected alone. It is important to consider that there may be important interactions that are excluded in the simplified system when a single viral protein is expressed.

The major role of the NP-P interaction is to enable the vRdRP to dock the replication complex onto RNA encapsidated by NP. NP structure, solubility, and RNA binding, are all affected by NP interaction with P. Specifically, P keeps nascent NP soluble until it is ready to bind viral RNA genome (156, 174, 246). Thus, P is thought of as a regulator of NP function. In this work, we have shown that NP can regulated P structure and function. MuV NP is required for enhanced and appropriate phosphorylation of MuV P. This work suggests that NP regulates the phosphorylation status of P, which in turn regulates the functions of P, since the phosphorylation state of P has a clear effect on the transcriptional and replicative activity of the MuV vRdRp complex in both the minigenome system and during viral infection. The discovery that NP plays a role in determining the phosphorylation state of P adds complexity to the NP-P interaction.

We examined the mechanism behind the enhanced and appropriate phosphorylation phenotype, by determining the role that PLK1 plays in P phosphorylation and virus growth. It's know that PIV5 P is phosphorylated by PLK1 and that this phosphorylation down-regulates gene expression (8). The same phenotype was observed in our experiments with MuV. When we inhibited phosphorylation of MuV P by PLK1, we saw an increase in gene expression, protein production, and viral growth. Inhibition of PLK1 using BI 2536 increased reporter readout during infection and in the minigenome system. Over-expression of the kinase deficient mutant of PLK1 (K82M)

did not inhibit minigenome activity, while wild-type PLK1 did. Together, this data shows that PLK1 is a negative regulator of viral RNA synthesis of MuV through its binding and phosphorylation of the P protein.

The discovery that NP enhanced P phosphorylation and induced the P_2 to P_1 band shift was instrumental in identifying PLK1 phosphorylation sites on P. We used this band shift to find mutations in P that reduced phosphorylation. We found the PLK1 binding site in P was at 146-S(pT)P-148 and the target site was at residues S292 and S294. Mutating these sites resulted in increased viral growth, as expected. Surprisingly, when the second potential PLK1 binding site at residues 203-205 was mutated as a control, viral growth was greatly attenuated in Vero cells. Two residues in V are changed (H203R/S204T) in rMuV-P-T204A, which may result in dysfunction of V. This is less likely, as MuV that does not express the V protein (rMuVΔV) does not have a growth defect in Vero cells (58). It is also interesting to note that the double mutant, rMuV-P-T147A/T204A, had increased growth, suggesting that the P-T147A mutation is a dominant mutation. Our finding that rMuV-P-S204A has reduced growth illustrates the limitations of the minigenome system. When a mutant including the S204A was tested in the MuV minigenome system, the activity was comparable to wild-type P (47). The minigenome system is critical for determining the roles of viral proteins in viral RNA synthesis if rescuing virus is not feasible, but there may be additional roles for P that cannot be assessed in this system.

In this work, we demonstrated NP plays a role in P phosphorylation for other paramyxoviruses. PIV5 shows a similar phenotype to MuV, with NP and PLK1 increasing phosphorylation of P and producing a slower migrating P band. We found that

JPV, a currently unclassified paramyxovirus, required NP for enhanced P phosphorylation, but did not require PLK1. JPV P does not possess the PLK1 binding motif found in MuV and PIV5 P, so this result is not surprising. RSV had highly phosphorylated P proteins, even when transfected alone, suggesting that the requirement for NP varies between viruses.

Acknowledgements

We appreciate the helpful discussion and technical assistance from all members of Dr. Biao He's laboratory. This work was supported by grants (R01AI097368 and R01AI106307) from National Institutes of Health.

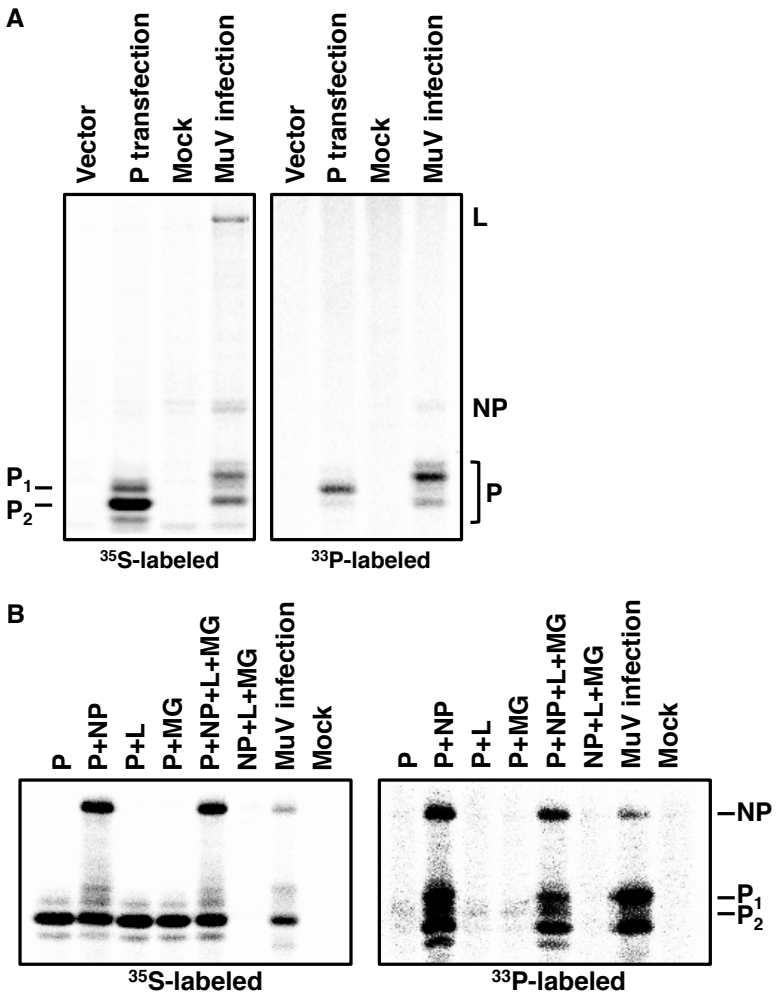

Figure 5.1. Banding pattern of phosphorylated MuV P in transfected and infected cells. (A) P phosphorylation in P-transfected cells. HeLa cells were transfected with empty vector or P or infected with MuV and radioactively labeled with [^{35}S]Met or [^{33}P]phosphate. The cells were lysed and immunoprecipitated with monoclonal anti-MuV-P antibody. The immunoprecipitated products were resolved by SDS-PAGE. The major (P_1) and minor (P_2) phosphorylated products are defined. (B) P phosphorylation in minigenome-component-transfected 293T cells were transfected with P, NP, L, and MG-RLuc (MG) in various combinations and radioactively labeled with ^{35}S or ^{33}P. The cells were lysed, immunoprecipitated with anti-MuV-P, and resolved by SDS-PAGE.

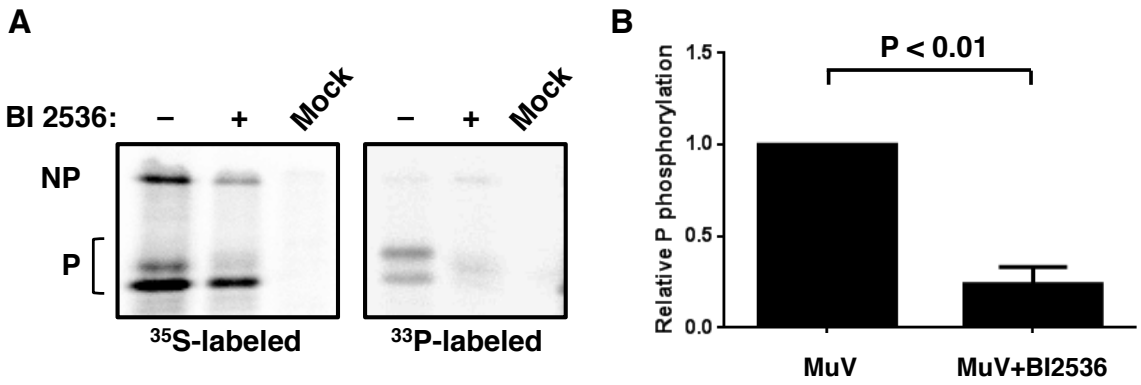

Figure 5.2. Effects of BI 2536 on P phosphorylation. (A) Effects of PLK1 inhibitor on P phosphorylation. Vero cells were mock infected or infected with MuV. At 18 hpi, the cells were radioactively labeled with ^{35}S or ^{33}P in the presence of 1 uM BI 2536. The cells were lysed and immunoprecipitated with anti-MuV-P. (B) Quantification of effects of BI 2536 on P phosphorylation. The relative level of P phosphorylation was calculated as the ratio of phosphorylated protein (^{33}P-labeled P) to total protein (^{35}S-labeled P) and standardized to that of MuV-infected without inhibitor. *P* value was calculated using Student's *t* test. Error bars represent the standard error of the mean (SEM) of 3 individual experiments.

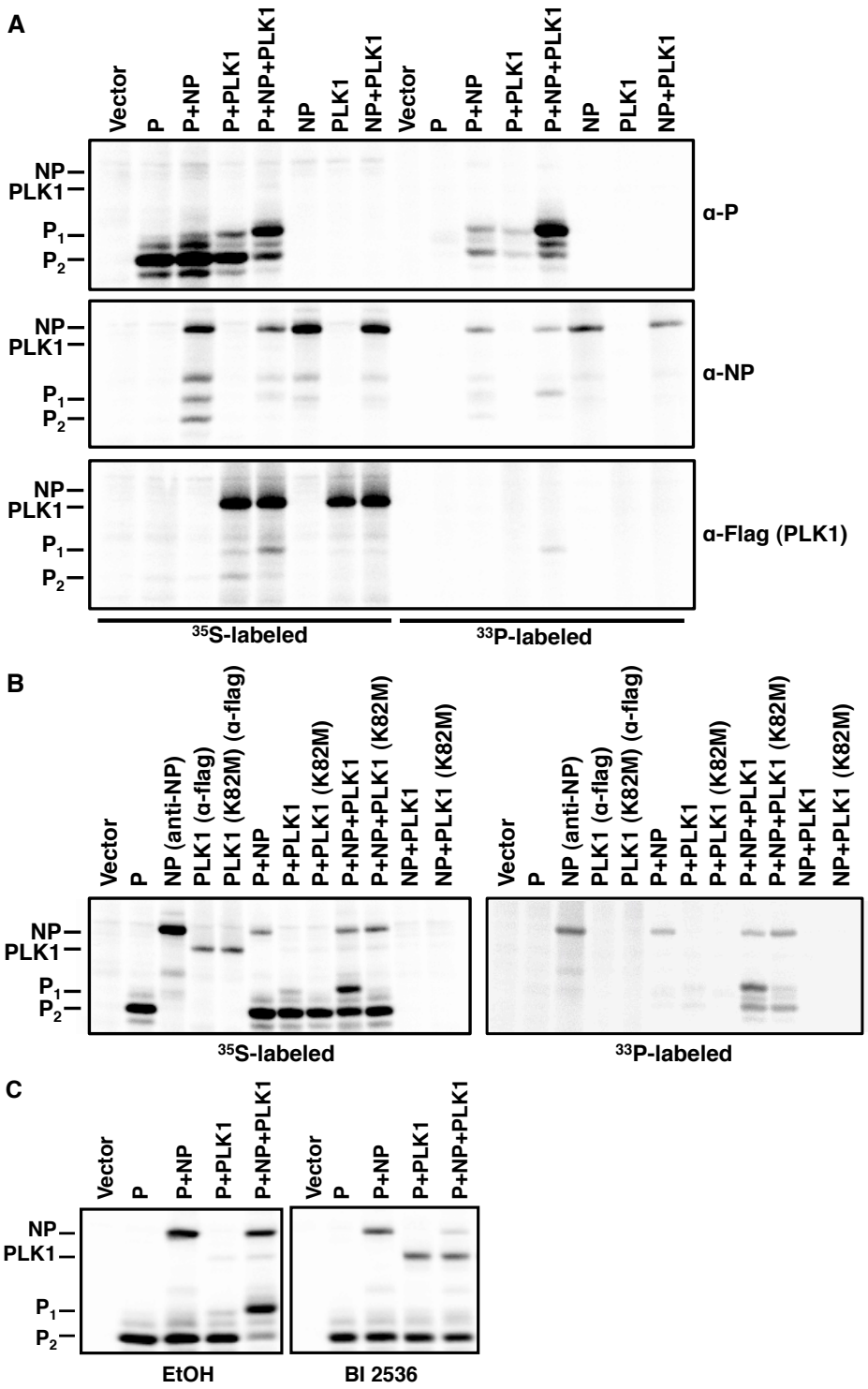

Figure 5.3. PLK1 phosphorylates P. (A) PLK1 enhances P phosphorylation. 293T cells were transfected with P, NP and Flag-PLK1 in various combinations and radioactively

labeled with ^{35}S or ^{33}P. The cells were lysed and immunoprecipitated with monoclonal anti-MuV-P, monoclonal anti-MuV-NP, or monoclonal anti-Flag antibodies. The immunoprecipitated products were resolved by SDS-PAGE. (B) PLK1 kinase activity required for P phosphorylation. 293T cells were transfected with P, NP, Flag-PLK1, and Flag-PLK1(K82M) in various combinations and radioactively labeled with ^{35}S or ^{33}P. The cells were lysed and immunoprecipitated with anti-MuV-P. (C) PLK1 inhibitor prevents P phosphorylation in transfected cells. 293T cells were transfected with P, NP and Flag-PLK1 in various combinations and radioactively labeled with ^{35}S in the presence of 1 uM BI 2536. The cells were lysed and immunoprecipitated with anti-MuV-P.

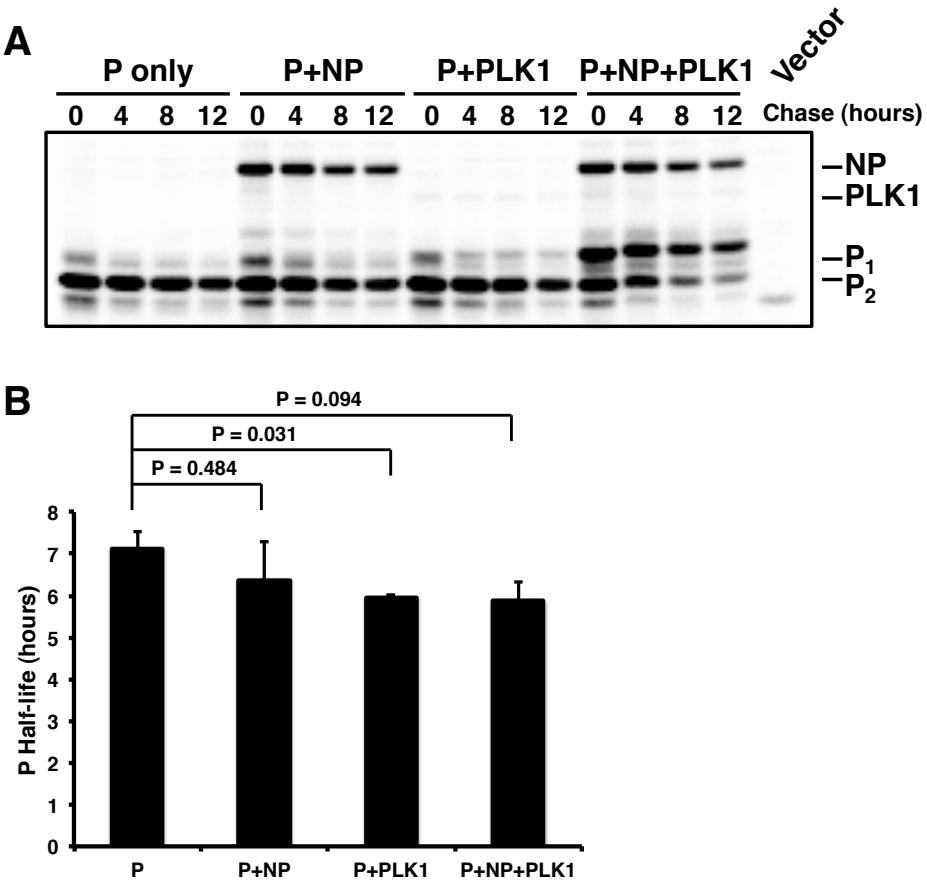

Figure 5.4. Pulse-chase analysis of P stability in the presence of NP and PLK1. (A) Stability of P in the presence of NP and PLK1. 293T cells were transfected with P, NP and Flag-PLK1 in various combinations. Cells were pulsed with ^{35}S for 30 min followed by chase incubations in culture media. At 0, 4, 8, and 12 hours post chase (hpc), cells were lysed and immunoprecipitated with anti-MuV-P and resolved by SDS-PAGE. (B) Quantification of P half-life. The relative level of P was measured and standardized to that of 0 hpc for each group. The half-life of P was calculated based on exponential trend lines for four individual experiments. *P* values were calculated using Student's *t* test.

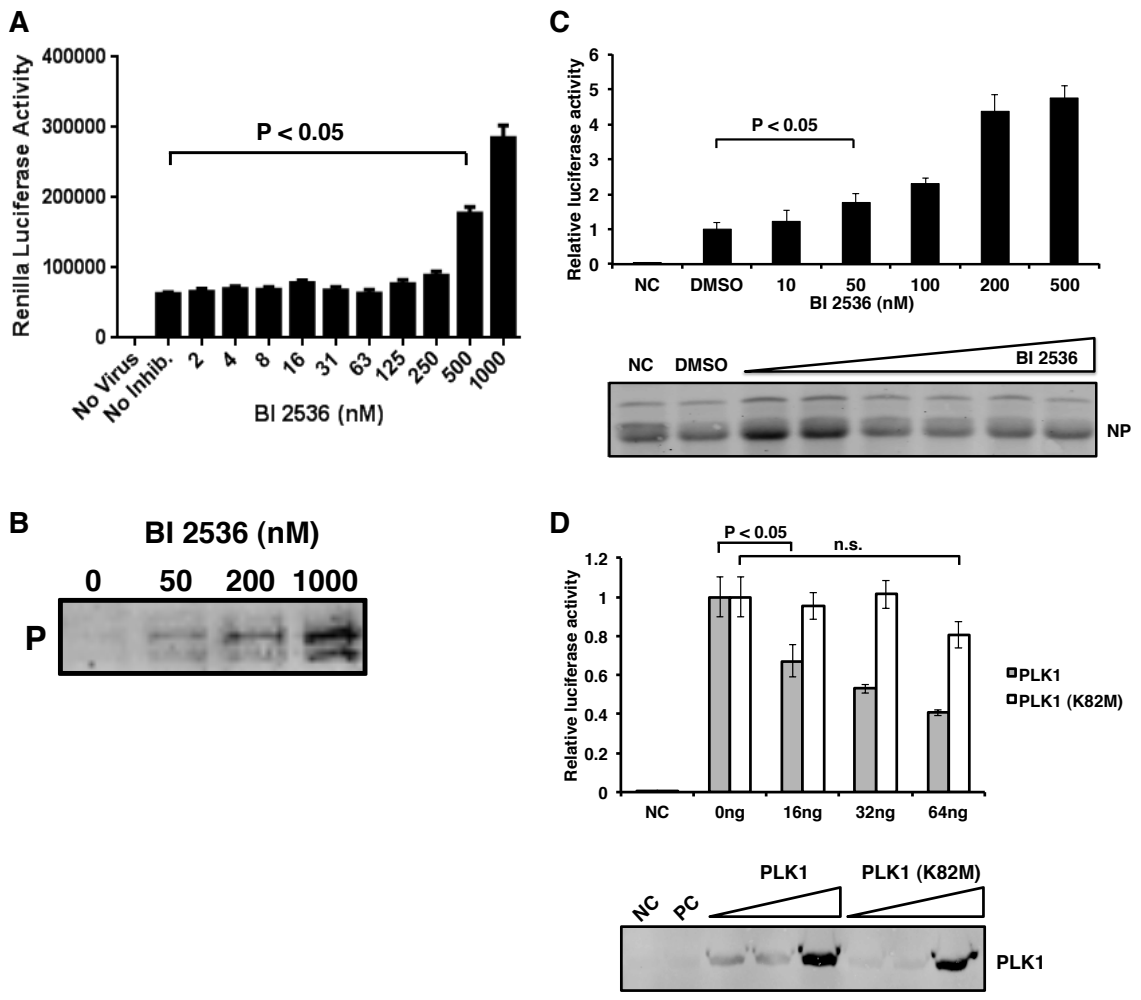

Figure 5.5. PLK1 inhibits viral protein production. (A and B) Effect of BI 2536 on recombinant MuV expressing *Renilla* luciferase (rMuV-Rluc). (A) Vero cells in 96-well plates were infected with rMuV-Rluc at an MOI of 0.01 and incubated with BI 2536 at various concentrations. *Renilla* luciferase activity was measured at 24 hpi. Error bars represent the SEM of data from 4 replicates. (B) Immunoblotting of cell lysates was performed to detect the expression levels of P. (C) Effect of BI 2536 on MuV minigenome activity. BSR-T7 cells in 24-well plates were transfected with P (80ng), NP (25 ng), L (500 ng), pMG-RLuc (100 ng), pFF-Luc (1 ng), and incubated with BI 2636 at various concentrations. Activity was measured at 48 hpt as described in Materials and

Methods. *Renilla* luciferase was the reporter gene in the minigenome and Firefly luciferase expression was used as a transfection control. The minigenome activity was measured and normalized as the ratio of *Renilla* luciferase activity to firefly luciferase activity (relative luciferase activity). Immunoblotting of minigenome cell lysates was performed to detect the expression levels of NP. (D) Effect of PLK1 and PLK1 (K82M) overexpression on minigenome activity. BSR-T7 cells were transfected as described in (C) along with various amounts of Flag-PLK1 or Flag-PLK1 (K82M) (0, 16, 32, or 64 ng). Activity was measured at 48 hpt as described in Materials and Methods. *P* values were calculated using Student's *t* test. Error bars represent the SEM of data from six replicates. Immunoblotting of minigenome cell lysates was performed to detect the expression levels of PLK1 and PLK1 (K82M).

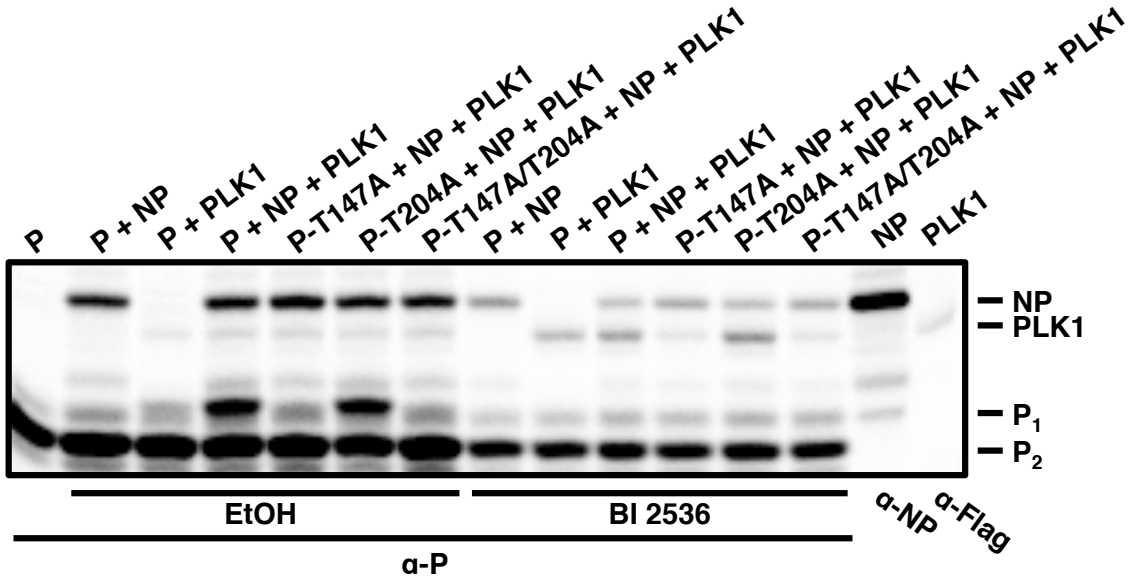

Figure 5.6. Interaction between PLK1 and P at P146-148 binding motif. 293T cells were transfected with P, P mutants, NP and Flag-PLK1 in various combinations and radioactively labeled with ^{35}S in the presence of solvent or 1 uM BI 2536. The cells were lysed and immunoprecipitated with anti-MuV-P, anti-MuV-NP, or anti-Flag antibodies and resolved by SDS-PAGE.

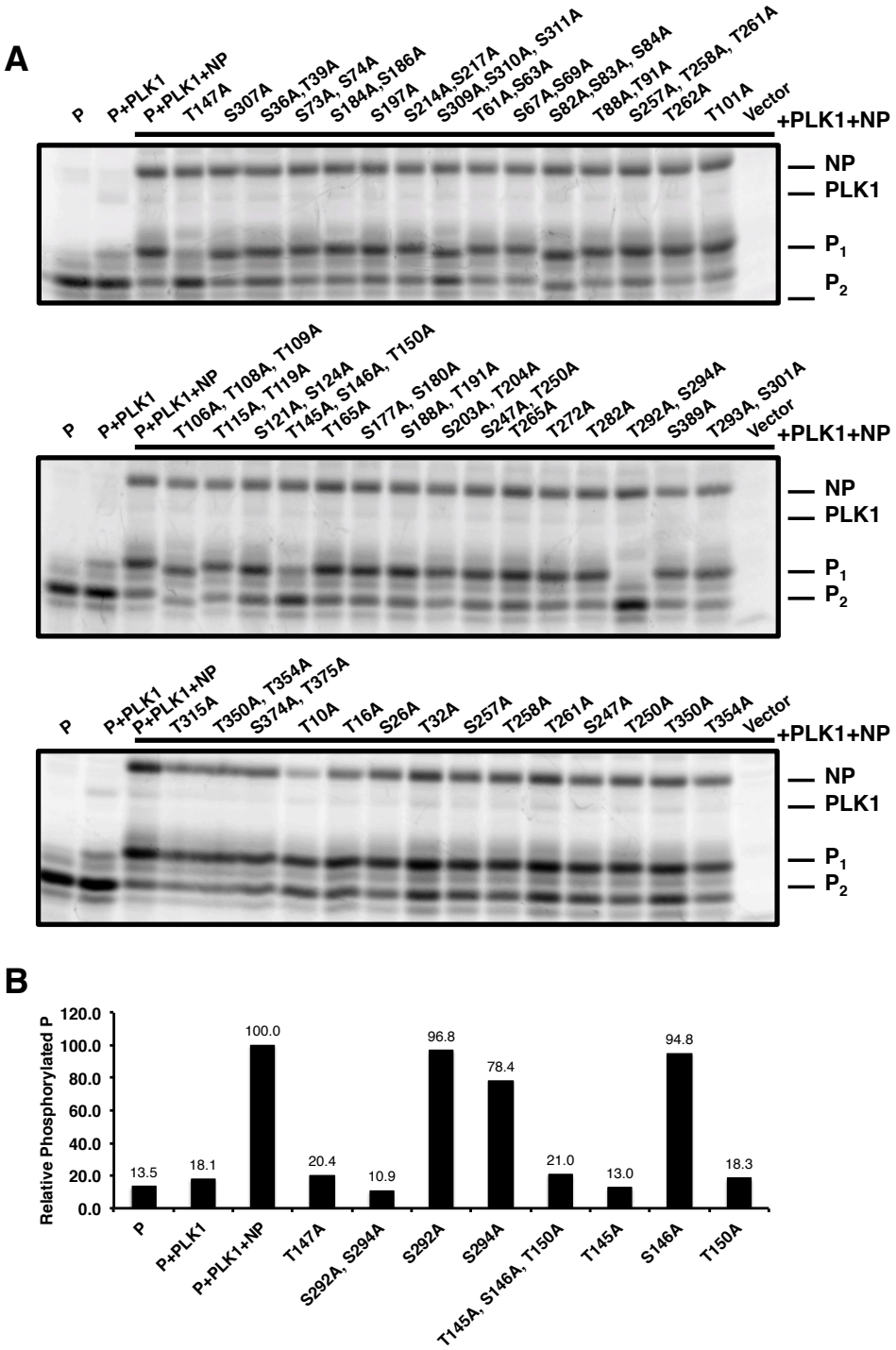

Figure 5.7. PLK1 phosphorylation site in MuV P. (A) Identification of critical residues for P phosphorylation by PLK1. 293T cells were transfected with P, P mutants, NP and

Flag-PLK1 and radioactively labeled with ^{35}S. The cells were lysed and immunoprecipitated with anti-MuV-P. (B) Quantification of P phosphorylation. The relative level of P phosphorylation was calculated as the ratio of phosphorylated protein (P_1) to total protein (P_1+P_2) and standardized to that of wild-type P-transfected with PLK1 and NP.

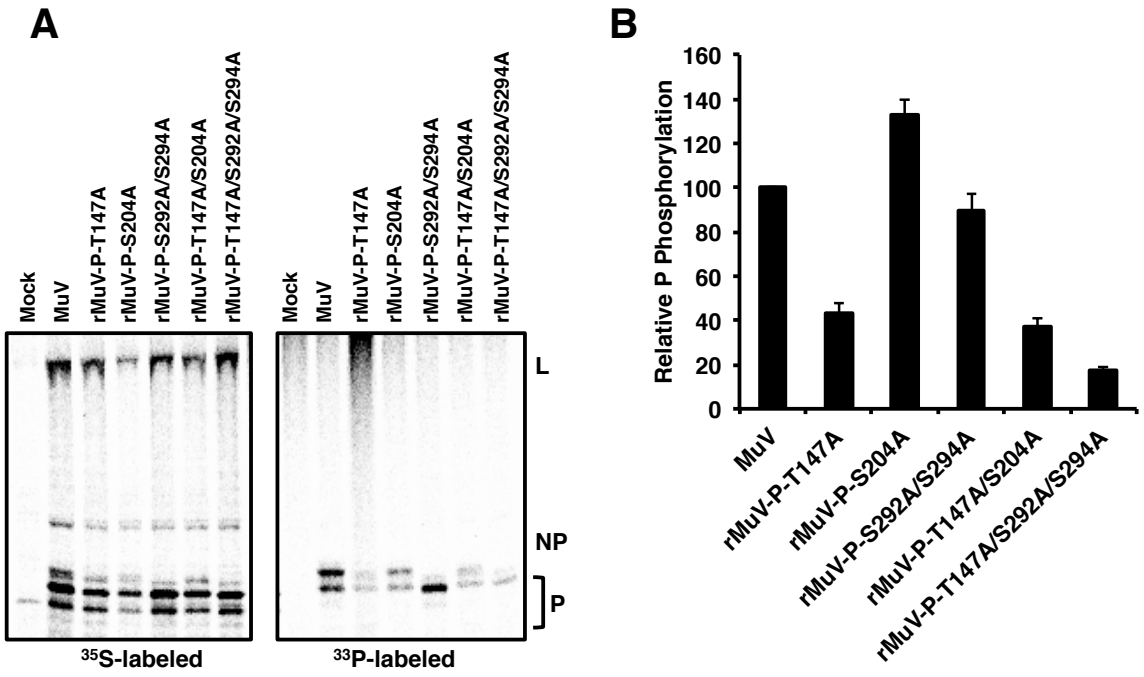

Figure 5.8. P phosphorylation in recombinant viruses. (A) P phosphorylation in infected cells. Vero cells were mock infected or infected with MuV, rMuV-P-T147A, rMuV-P-T204A, rMuV-P-S292A/S294A, rMuV-P-T147A/T204A, or rMuV-P-T147A/S292A/S294A at an MOI of 0.1 and radioactively labeled with ^{35}S or ^{33}P. The cells were lysed and immunoprecipitated with anti-MuV-P. (B) Quantification of P phosphorylation. The relative level of P phosphorylation was calculated as the ratio of phosphorylated protein (^{33}P-labeled P) to total protein (^{35}S-labeled P) and standardized to that of MuV-infected. *P* values were calculated using Student's *t* test. Error bars represent the standard error of the mean (SEM) of 4 individual experiments. *, $P<0.01$.

A

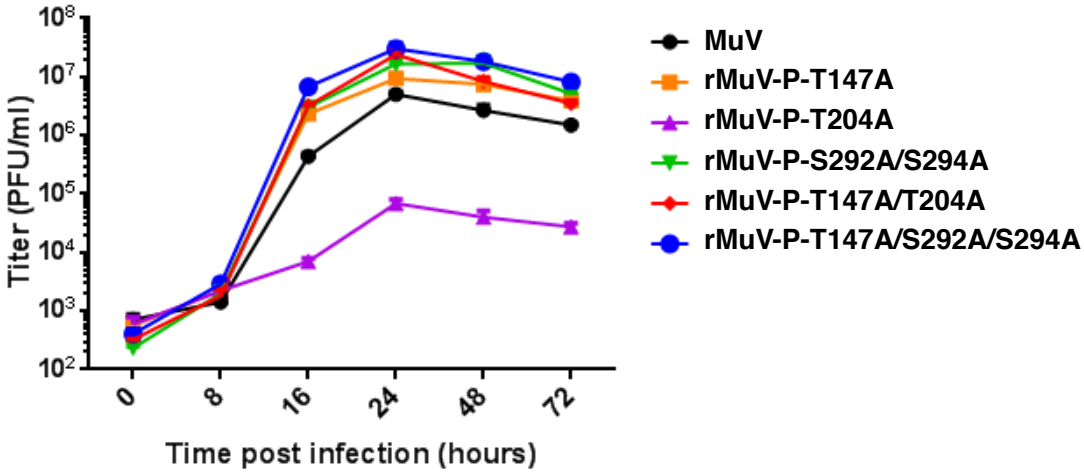

B

	Hours Post Infection					
Virus	0	8	16	24	48	72
MuV-P-T147A	0.4029	0.0450	0.0188	**0.0067**	**0.0022**	0.0415
MuV-P-T204A	0.6478	0.0734	**0.0029**	**0.0016**	**0.0127**	**0.0002**
MuV-P-S292A/S294A	0.0366	0.4818	**0.0001**	**0.0004**	0.0515	**0.0005**
MuV-P-T147A/T204A	0.0666	0.5436	**< 0.0001**	**0.0108**	0.0193	**0.0077**
MuV-P-T147A/S292A/S294A	0.1586	0.0753	**< 0.0001**	0.0303	0.0147	**< 0.0001**

Figure 5.9. Growth kinetics of MuV mutants. (A) Single-step growth curve of recombinant viruses. In each experiment, cells were infected with MuV, rMuV-P-T147A, rMuV-P-T204A, rMuV-P-S292A/S294A, rMuV-P-T147A/T204A, or rMuV-P-T147A/S292A/S294A at an MOI of 3. Media was collected at various time points. The titer of virus in the media was determined by plaque assay using Vero cells. (B) Each mutant virus was compared to wild-type MuV and statistical significance was determined using the Holm-Sidak method with alpha = 5%. The *P* values are provided with significant values in bold.

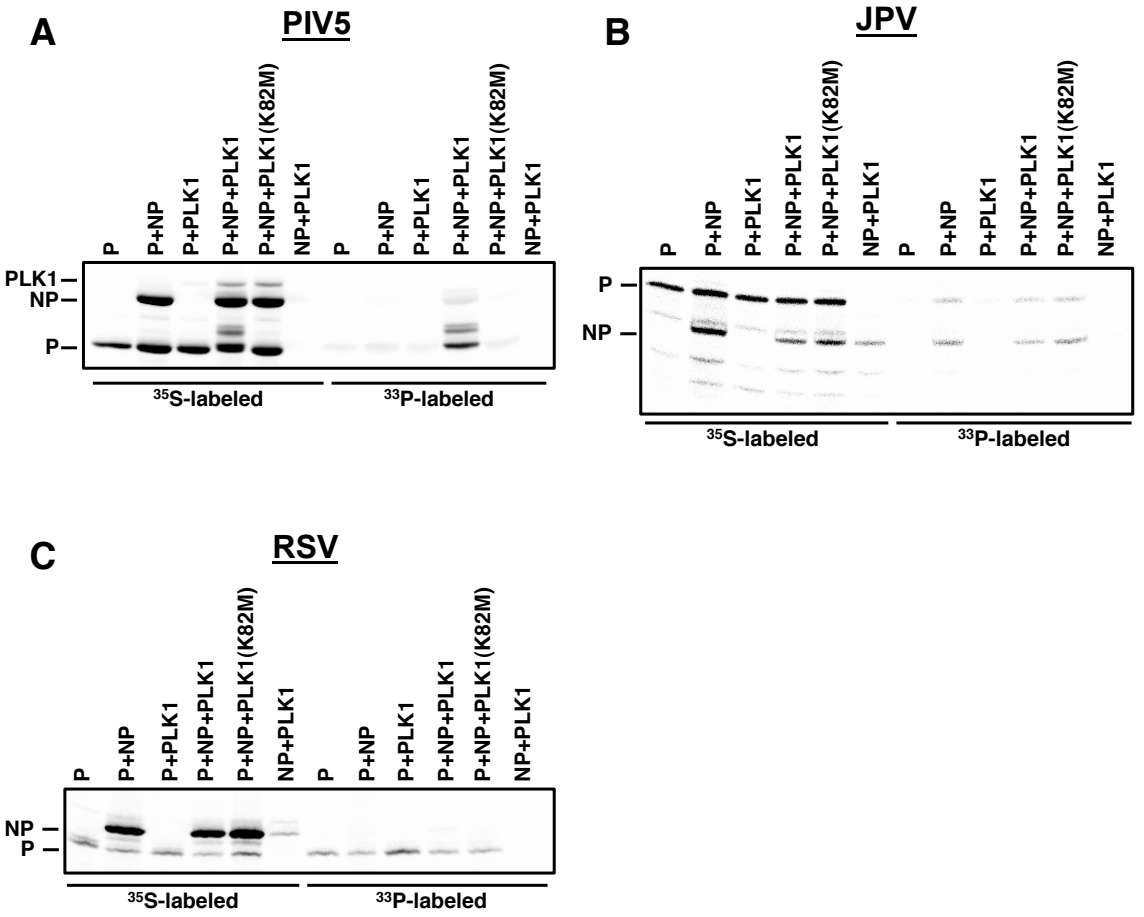

Figure 5.10. Effects of NP and PLK1 on phosphorylation of P in related viruses. P phosphorylation was assessed in transfected cells for PIV5 (A), JPV (B), and RSV (C). Plasmid encoding P of each virus was transfected along with various combinations of NP, PLK1, and PLK1 (K82M) and radioactively labeled with ^{35}S or ^{33}P. The cells were lysed and immunoprecipitated with viral specific anti-P antibodies to determine phosphorylation of P for each transfection condition.

CHAPTER 6

CONCLUSIONS

MuV is a human pathogen that causes acute parotitis and is highly neurotropic, with infection of the central nervous system evident in almost half of all clinical cases (1). Recent MuV outbreaks reported on college campuses act as a reminder that mumps infections remain a concern for global healthcare. Even though the mumps vaccine has dramatically reduced disease incidence, continued research is needed for the development of MuV therapeutics and better vaccines. Viral RNA synthesis is a potential process to be exploited and consequently, understanding the viral and host proteins involved is a vital approach in the elucidation of potential antiviral strategies. The P proteins of MuV and other paramyxoviruses play numerous roles in viral transcription and replication. The importance of P phosphorylation in paramyxovirus transcription and replication has been studied in numerous viruses, and it has been shown to play a role in regulating viral RNA synthesis. The central hypothesis of these studies is that phosphorylation of MuV P plays roles in viral transcription and replication. The specific aims addressed included:

Specific Aim 1. To determine the roles of the MuV P domains in viral RNA synthesis. The working hypothesis is that the MuV P domains are biologically active by trans-complementation through the oligomerization domain. The results in Chapter 3 show that

all MuV P domains are required for full P function. In these studies, mutational analysis and a novel minigenome system were used to show that when P truncations lacking either the N-terminal domain or C-terminal domain were transfected together, P activity was restored due to trans-complementation through the oligomerization domain. Using this trans-complement system, we examined the oligomerization status of P and have found that P forms parallel dimers (P_N to P_N and P_C to P_C). Furthermore, we found that residues R231, K238, K253 and K260 in the oligomerization domain were critical for P's functions. Additionally, we identified the C-terminal domain as the region that interacts with L. This study provides structure-function insights into the role of MuV P domains during viral transcription and replication.

Specific Aim 2. To determine the phosphorylated residues of MuV P that are critical for viral transcription and replication. To investigate the roles of serine (S) and threonine (T) residues of P in viral RNA transcription and replication, P was subjected to mass spectrometry and mutational analysis. P, a 391-amino acid residue (AA) protein, has 64 S and T residues. The data from Chapter 4 show that mutating nine S/T residues significantly reduced and mutating residue T at 101 to A (T101A) enhanced activity in a minigenome system. The working hypothesis is that phosphorylation of these 10 residues is critical for viral RNA synthesis. A recombinant virus containing the P-T101A mutation (rMuV-P-T101A) was recovered and analyzed. rMuV-P-T101A grew to higher titers and had increased protein expression at early time points. Together, these results suggest that phosphorylation of MuV-P-T101 plays a negative role in viral RNA synthesis. This study

shows that MuV P contains phosphorylated residues that are critical for virus transcription and replication.

Specific Aim 3. To determine the role of host kinases in MuV P phosphorylation. The working hypothesis is that MuV P is phosphorylated by host kinases. MuV P contains a PLK1 STP binding motif at residues 146-148. The results from Chapter 5 show that MuV P interacts with PLK1 through this motif and the targeted P phosphorylation sites were determined to be residues S292 and S294. Unexpectedly, P phosphorylation by PLK1 was strengthened with the addition of NP, thus suggesting that NP plays a role in enhancing P phosphorylation by host kinases. Furthermore, MuV gene expression, protein production, and growth kinetics were enhanced with the addition of the PLK1 inhibitor, BI 2536. This study shows that MuV P is phosphorylated by the host kinase, PLK1, this phosphorylation is enhanced in the presence of NP, and the phosphorylation negatively regulates viral transcription. This is the first report that function of P can be regulated by NP through phosphorylation of P.

Taken together, this research shows a role for phosphorylation of MuV P in viral pathogenesis. Elucidating the mechanisms of viral transcription and replication regulation by phosphorylation of P may lead to novel antiviral strategies.

Identification of phosphorylated residues that are important for viral transcription and replication may be useful for vaccine development. A recombinant MuV lacking expression of both the SH and V proteins (rMuVΔSHΔV) is a possible vaccine candidate. rMuVΔSHΔV has been shown to induce a neutralizing antibody titer against

$MuV^{Iowa/US/06}$ that is higher than that induced by the current JL vaccine stain (219). Furthermore, rMuVΔSHΔV vaccination stimulated T cell responses in BALB/c mice, although the role of cell-mediated immunity in mumps disease protection remains to be determined. Incorporation of mutations at phosphorylated residues that resulted in enhanced viral replication, such as P-T101A and P-T147A, into vaccine candidates such as rMuVΔSHΔV, may facilitate vaccine development by increasing vaccine yields during production. Enhanced replication of vaccine candidates in the host may also aid in increasing humoral and cellular immune responses that are required to generate protection against MuV infection. An additional strategy to increase vaccine production is to generate modified cell lines that knock out host regulatory factors that play a negative role in viral replication. Specifically, targets like PLK1 that negatively regulate viral RNA synthesis by phosphorylation of MuV P can be knocked out, although PLK1 itself is an unlikely target due to its essential role in the cell cycle.

The minigenome system has been a vital tool to study viral RNA synthesis. However, results using this system to study roles of phosphorylation of paramyxovirus P proteins in viral RNA synthesis have been mixed. It has been reported before that mutations of P reduce phosphorylation and also result in reduced viral RNA synthesis (175, 247–249). Incorporation of these mutations into recombinant viruses does not re-capitulate the phenotype observed using a minigenome system, demonstrating the limitation of the minigenome system in the studies of P phosphorylation. In this work, we found that mutation of MuV P-T204 to A had no impact on MuV minigenome activity. However, a recombinant virus with the P-T204A mutation had a severe defect in growth,

suggesting that P-T204 may play roles beyond viral RNA synthesis, or the minigenome system screen may still miss critical residues.

The development of MuV therapeutics, more effective vaccines, and/or review of current vaccination policies are needed to prevent future outbreaks. Biological characterization of future vaccine candidates must be considered for standardization and safety testing. The JL vaccine strain was originally isolated from a mumps patient in 1963 and was then attenuated through continuous passages in hen eggs and chick-embryo cell cultures (198). A better-defined vaccine with the use of a MuV reverse engineering system will also help distinguish the live attenuated vaccine strain from virulent strains. Attenuation directed through genetic modification of an outbreak strain will be ideal for genotype matching circulating mumps strains, and elicit more specific protective immune responses (219). These studies provide insight into the role of phosphorylation of MuV P in viral pathogenesis that may provide possible anti-viral targets as well as recombinant viruses that will aid in vaccine development strategies against mumps infection.

REFERENCES

1. **Carbone KM, Wolinsky JS**. 2001. Mumps virus, p. 1381–1441. *In* Knipe, DM, Howley, PM (eds.), Fields Virology 4th Ed. Lippincott Williams and Wilkins, New York.

2. **Marin M, Quinlisk P, Shimabukuro T, Sawhney C, Brown C, Lebaron CW**. 2008. Mumps vaccination coverage and vaccine effectiveness in a large outbreak among college students--Iowa, 2006. Vaccine **26**:3601–7.

3. **Centers for Disease Control and Prevention**. 2010. Mumps Outbreak — New York and New Jersey, June 2009 – January 2010. MMWR **59**:125–129.

4. **Lamb RA, Kolakofsky D**. 2001. Paramyxoviridae: The viruses and their replication, p. 1305–1340. *In* Knipe, DM, Howley, PM, Griffin, DE, Lamb, RA, Martin, MA, Roizman, B, Straus, SE (eds.), Fields Virology 4th Ed. Lippincott Williams and Wilkins, Philadelphia.

5. **Chen M, Ogino T, Banerjee AK**. 2007. Interaction of vesicular stomatitis virus P and N proteins: identification of two overlapping domains at the N terminus of P that are involved in N0-P complex formation and encapsidation of viral genome RNA. J. Virol. **81**:13478–85.

6. **Asenjo A, Calvo E, Villanueva N**. 2006. Phosphorylation of human respiratory syncytial virus P protein at threonine 108 controls its interaction with the M2-1 protein in the viral RNA polymerase complex. J. Gen. Virol. **87**:3637–42.

7. **Timani KA, Sun D, Sun M, Keim C, Lin Y, Schmitt PT, Schmitt AP, He B**. 2008. A single amino acid residue change in the P protein of parainfluenza virus 5 elevates viral gene expression. J. Virol. **82**:9123–33.

8. **Sun D, Luthra P, Li Z, He B**. 2009. PLK1 down-regulates parainfluenza virus 5 gene expression. PLoS Pathog. **5**:e1000525.

9. **Sun D, Luthra P, Xu P, Yoon H, He B**. 2011. Identification of a phosphorylation site within the P protein important for mRNA transcription and growth of parainfluenza virus 5. J. Virol. **85**:8376–8385.

10. **Sugai A, Sato H, Yoneda M, Kai C**. 2012. Phosphorylation of measles virus phosphoprotein at S86 and/or S151 downregulates viral transcriptional activity. FEBS Lett. **586**:3900–3907.

11. **Xu P, Li Z, Sun D, Lin Y, Wu J, Rota PA, He B**. 2011. Rescue of wild-type mumps virus from a strain associated with recent outbreaks helps to define the role of the SH ORF in the pathogenesis of mumps virus. Virology **417**:126–136.

12. **Xu P, Huang Z, Gao X, Michel FJ, Hirsch G, Hogan RJ, Sakamoto K, Ho W, Wu J, He B**. 2013. Infection of mice, ferrets, and rhesus macaques with a clinical mumps virus isolate. J. Virol. **87**:8158–8168.

13. **Jr. TEC**. 1967. Hippocrates describes mumps followed by orchitis. Pediatrics **40**:420.

14. **Hamilton R**. 1790. IX. An account of a distemper, by the common people in England vulgarly called the mumps. Earth Environ. Sci. Trans. R. Soc. Edinburgh **2**:59–72.

15. **Johnson CD**. 1934. An investigation of the etiology of mumps. J. Exp. Med. **59**:1–19.

16. **Habel K**. 1945. Cultivation of mumps virus in the developing chick embryo and its application to studies of immunity to mumps in man. Public Heal. Reports **60**:201–212.

17. **Enders JF**. 1946. Mumps; techniques of laboratory diagnosis, tests for susceptibility, and experiments on specific prophylaxis. J. Pediatr. **29**:129–142.

18. **Henle G, Deinhardt F**. 1955. Propagation and primary isolation of mumps virus in tissue culture. Proc. Soc. Exp. Biol. Med. **89**:556–560.

19. **Smorodintsev AA, Klyatchko NS**. 1958. Live anti-mumps vaccine. I. Results of tests of the immunogenic properties of live vaccine when administered intradermally to susceptible children. Acta Virol. **2**:137–144.

20. **Klyatchko NS, Smorodintsev AA**. 1958. Live anti-mumps vaccine. II. Epidemiological effectiveness of the immunization of children with a single intradermal injection of live anti-mumps vaccine. Acta Virol. **2**:145–151.

21. **Centers for Disease Control and Prevention**. 1983. Mumps-United States, 1980-1983. MMWR **32**:545–547.

22. **Duc-Nguyen H, Rosenblum EN**. 1967. Immuno-electron microscopy of the morphogenesis of mumps virus,. J. Virol. **1**:415–429.

23. **Horne R, Waterson A, Wildy P, Farn-Ham A**. 1960. The structure and composition of the myxoviruses. I. Electron microscope studies of the structure of myxovirus particles by negative staining techniques. Virology **11**:79–98.

24. **Hosaka Y, Shimizu K**. 1968. Lengths of the nucleocapsids of Newcastle disease and mumps viruses. J. Mol. Biol. **35**:369–373.

25. **Horne R, Waterson A**. 1960. A helical structure in mumps, Newcastle disease and Sendai viruses. J. Mol. Biol. London.

26. **McCarthy M, Lazzarini RA**. 1982. Intracellular nucleocapsid RNA of mumps virus. J. Gen. Virol. **58 (Pt 1)**:205–209.

27. **Cox R, Green TJ, Qiu S, Kang J, Tsao J, Prevelige PE, He B, Luo M**. 2009. Characterization of a mumps virus nucleocapsidlike particle. J. Virol. **83**:11402–11406.

28. **Calain P, Roux L**. 1993. The rule of six, a basic feature for efficient replication of Sendai virus defective interfering RNA. J. Virol. **67**:4822–4830.

29. **Peeters BP, Gruijthuijsen YK, de Leeuw OS, Gielkens AL**. 2000. Genome replication of Newcastle disease virus: involvement of the rule-of-six. Arch. Virol. **145**:1829–1845.

30. **Weik M, Enterlein S, Schlenz K, Mühlberger E**. 2005. The Ebola virus genomic replication promoter is bipartite and follows the rule of six. J. Virol. **79**:10660–10671.

31. **Elango N, Varsanyi T, Kovamees J, Norrby E**. 1988. Molecular cloning and characterization of six genes, determination of gene order and intergenic sequences and leader sequence of mumps virus. J. Gen. Virol **69 (Pt 11)**:2893–900.

32. **Saito H, Takahashi Y, Harata S, Tanaka K, Sano T, Suto T, Yamada A, Yamazaki S, Morito M**. 1996. Isolation and characterization of mumps virus strains in a mumps outbreak with a high incidence of aseptic meningitis. Microbiol Immuol **40**:271–275.

33. **Okazaki K, Tanabayashi K, Takeuchi K, Hishiyama M, Yamada A**. 1992. Molecular cloning and sequence analysis of the mumps virus gene encoding the L protein and the trailer sequence. Virology **188**:926–930.

34. **Tanabayashi K, Takeuchi K, Hishiyama M, Yamada A, Tsurudome M, Ito Y, Sugiura A**. 1990. Nucleotide sequence of the leader and nucleocapsid protein gene of mumps virus and epitope mapping with the in vitro expressed nucleocapsid protein. Virology **177**:124–130.

35. **McCarthy M, Johnson RT**. 1980. A comparison of the structural polypeptides of five strains of mumps virus. J. Gen. Virol. **46**:15–27.

36. **Kingston RL, Baase WA, Gay LS**. 2004. Characterization of nucleocapsid binding by the measles virus and mumps virus phosphoproteins characterization of nucleocapsid binding by the measles virus and mumps virus phosphoproteins. J. Virol. **78**:8630–8640.

37. **Kingston RL, Gay LS, Baase WS, Matthews BW**. 2008. Structure of the nucleocapsid-binding domain from the mumps virus polymerase; an example of protein folding induced by crystallization. J. Mol. Biol. **379**:719–731.

38. **Kingston RL, Hamel DJ, Gay LS, Dahlquist FW, Matthews BW**. 2004. Structural basis for the attachment of a paramyxoviral polymerase to its template. Proc. Natl. Acad. Sci. U. S. A. **101**:8301.

39. **Buchholz CJ, Retzler C, Homann HE, Neubert WJ**. 1994. The carboxy-terminal domain of Sendai virus nucleocapsid protein is involved in complex formation between phosphoprotein and nucleocapsid-like particles. Virology **204**:770.

40. **Bourhis J-M, Johansson K, Receveur-Bréchot V, Oldfield CJ, Dunker KA, Canard B, Longhi S**. 2004. The C-terminal domain of measles virus nucleoprotein belongs to the class of intrinsically disordered proteins that fold upon binding to their physiological partner. Virus Res. **99**:157–167.

41. **Iseni F, Baudin F, Garcin D, Marq J-B, Ruigrok RWH, Kolakofsky D**. 2002. Chemical modification of nucleotide bases and mRNA editing depend on hexamer or nucleoprotein phase in Sendai virus nucleocapsids. RNA **8**:1056–1067.

42. **Cox R, Pickar A, Qiu S, Tsao J, Rodenburg C, Dokland T, Elson A, He B, Luo M**. 2014. Structural studies on the authentic mumps virus nucleocapsid showing uncoiling by the phosphoprotein. Proc. Natl. Acad. Sci. U. S. A. **111**:15208–15213.

43. **Precious B, Young DF, Bermingham A, Fearns R, Ryan M, Randall RE**. 1995. Inducible expression of the P, V, and NP genes of the paramyxovirus simian virus 5 in cell lines and an examination of NP-P and NP-V interactions. J. Virol. **69**:8001.

44. **Howard M, Wertz G**. 1989. Vesicular stomatitis virus RNA replication: a role for the NS protein. J. Gen. Virol. **70**:2683–2694.

45. **Masters PS, Banerjee AK**. 1988. Complex formation with vesicular stomatitis virus phosphoprotein NS prevents binding of nucleocapsid protein N to nonspecific RNA. J. Virol. **62**:2658–2664.

46. **Peluso RW, Moyer SA**. 1988. Viral proteins required for the in vitro replication of vesicular stomatitis virus defective interfering particle genome RNA. Virology **162**:369–376.

47. **Pickar A, Xu P, Elson A, Li Z, Zengel J, He B**. 2014. Roles of serine and threonine residues of mumps virus P protein in viral transcription and replication. J. Virol. **88**:4414–22.

48. **Chen MZ, Ogino T, Banerjee AK**. 2007. Interaction of vesicular stomatitis virus P and N proteins: identification of two overlapping domains at the N terminus of P that are involved in N0-P complex formation and encapsidation of viral genome RNA. J. Virol. **81**:13478–13485.

49. **Paterson RG, Lamb RA**. 1990. RNA editing by G-nucleotide insertion in mumps virus P-gene mRNA transcripts. J. Virol. **64**:4137–4145.

50. **Parisien J-P, Bamming D, Komuro A, Ramachandran A, Rodriguez JJ, Barber G, Wojahn RD, Horvath CM**. 2009. A shared interface mediates paramyxovirus interference with antiviral RNA helicases MDA5 and LGP2. J. Virol. **83**:7252–7260.

51. **Andrejeva J, Childs KS, Young DF, Carlos TS, Stock N, Goodbourn S, Randall RE, Lamb RA**. 2004. The V proteins of paramyxoviruses bind the IFN-inducible RNA helicase, mda-5, and inhibit its activation of the IFN-β promoter. Proc. Natl. Acad. Sci. U. S. A. **101**:17264–17269.

52. **Ramachandran A, Horvath CM**. 2010. Dissociation of paramyxovirus interferon evasion activities: universal and virus-specific requirements for conserved V protein amino acids in MDA5 interference. J. Virol. **84**:11152–11163.

53. **Kubota T, Yokosawa N, Yokota S, Fujii N**. 2002. Association of mumps virus V protein with RACK1 results in dissociation of STAT-1 from the alpha interferon receptor complex. J. Virol. **76**:12676–12682.

54. **Kubota T, Yokosawa N, Yokota SI, Fujii N**. 2001. C terminal cys-rich region of mumps virus structural V protein correlates with block of interferon alpha and gamma signal transduction pathway through decrease of STAT 1-alpha. Biochem. Biophys. Res. Commun. **283**:255–259.

55. **Nishio M, Garcin D, Simonet V, Kolakofsky D**. 2002. The carboxyl segment of the mumps virus V protein associates with stat proteins in vitro via a tryptophan-rich motif. Virology **300**:92–99.

56. **Rosas-Murrieta NH, Herrera-Camacho I, Palma-Ocampo H, Santos-López G, Reyes-Leyva J**. 2010. Interaction of mumps virus V protein variants with STAT1-STAT2 heterodimer: experimental and theoretical studies. Virol. J. **7**:263.

57. **Ulane CM, Rodriguez JJ, Parisien J-P, Horvath CM**. 2003. STAT3 ubiquitylation and degradation by mumps virus suppress cytokine and oncogene signaling. J. Virol. **77**:6385–6393.

58. **Xu P, Luthra P, Li Z, Fuentes S, D'Andrea JA, Wu J, Rubin S, Rota PA, He B**. 2012. The V protein of mumps virus plays a critical role in pathogenesis. J. Virol. **86**:1768–1776.

59. **Paterson RG, Leser GP, Shaughnessy MA, Lamb RA**. 1995. The paramyxovirus SV5 V protein binds two atoms of zinc and is a structural component of virions. Virology **208**:121–131.

60. **Takeuchi K, Tanabayashi K, Hishiyama M, Yamada YK, Yamada A, Sugiura A**. 1990. Detection and characterization of mumps virus V protein. Virology **178**:247–253.

61. **Elango N**. 1989. Complete nucleotide sequence of the matrix protein mRNA of mumps virus. Virology **168**:426–428.

62. **Mottet-Osman G, Miazza V, Vidalain P-O, Roux L**. 2014. Patchwork structure-function analysis of the Sendai virus matrix protein. Virology **464-465**:330–340.

63. **Udem SA, Cook KA**. 1984. Isolation and characterization of measles virus intracellular nucleocapsid RNA. J. Virol. **49**:57–65.

64. **Takimoto T, Bousse T, Coronel EC, Scroggs RA, Portner A**. 1998. Cytoplasmic domain of Sendai virus HN protein contains a specific sequence required for its incorporation into virions. J. Virol. **72**:9747–9754.

65. **Naim HY, Ehler E, Billeter MA**. 2000. Measles virus matrix protein specifies apical virus release and glycoprotein sorting in epithelial cells. EMBO J. **19**:3576–3585.

66. **Ghildyal R, Li D, Peroulis I, Shields B, Bardin PG, Teng MN, Collins PL, Meanger J, Mills J**. 2005. Interaction between the respiratory syncytial virus G glycoprotein cytoplasmic domain and the matrix protein. J. Gen. Virol. **86**:1879–1884.

67. **Schmitt AP, Leser GP, Morita E, Sundquist WI, Lamb RA**. 2005. Evidence for a new viral late-domain core sequence, FPIV, necessary for budding of a paramyxovirus. J. Virol. **79**:2988–2997.

68. **Li M, Schmitt PT, Li Z, McCrory TS, He B, Schmitt AP**. 2009. Mumps virus matrix, fusion, and nucleocapsid proteins cooperate for efficient production of virus-like particles. J. Virol. **83**:7261–7272.

69. **Pei Z, Bai Y, Schmitt AP**. 2010. PIV5 M protein interaction with host protein angiomotin-like 1. Virology **397**:155–166.

70. **Pei Z, Harrison MS, Schmitt AP**. 2011. Parainfluenza virus 5 m protein interaction with host protein 14-3-3 negatively affects virus particle formation. J. Virol. **85**:2050–2059.

71. **Waxham MN, Wolinsky JS**. 1986. A fusing mumps virus variant selected from a nonfusing parent with the neuraminidase inhibitor 2-deoxy-2,3-dehydro-N-acetylneuraminic acid. Virology **151**:286–295.

72. **Herrler G, Compans RW**. 1982. Synthesis of mumps virus polypeptides in infected vero cells. Virology **119**:430–438.

73. **Merz DC, Server a. C, Waxham MN, Wolinsky JS**. 1983. Biosynthesis of mumps virus F glycoprotein: Non-fusing strains efficiently cleave the F glycoprotein precursor. J. Gen. Virol. **64**:1457–1467.

74. **Naruse H, Nagai Y, Yoshida T, Hamaguchi M, Matsumoto T, Isomura S, Suzuki S**. 1981. The polypeptides of mumps virus and their synthesis in infected chick embryo cells. Virology **112**:119–130.

75. **Chang A, Dutch RE**. 2012. Paramyxovirus fusion and entry: Multiple paths to a common end. Viruses **4**:613–636.

76. **Liu Y, Xu Y, Lou Z, Zhu J, Hu X, Gao GF, Qiu B, Rao Z, Tien P**. 2006. Structural characterization of Mumps virus fusion protein core. Biochem. Biophys. Res. Commun. **348**:916–922.

77. **Liu Y, Zhu J, Feng M-G, Tien P, Gao GF**. 2004. Six-helix bundle assembly and analysis of the central core of mumps virus fusion protein. Arch. Biochem. Biophys. **421**:143–148.

78. **Liu Y, Xu Y, Zhu J, Qiu B, Rao Z, Gao GF, Tien P**. 2005. Crystallization and preliminary X-ray diffraction analysis of central structure domains from mumps virus F protein. Struct. Biol. Cryst. Commun. **61**:855–857.

79. **Lamb RA, Paterson RG, Jardetzky TS**. 2006. Paramyxovirus membrane fusion: Lessons from the F and HN atomic structures. Virology **344**:30–37.

80. **Bose S, Heath CM, Shah PA, Alayyoubi M, Jardetzky TS, Lamb RA**. 2013. Mutations in the parainfluenza virus 5 fusion protein reveal domains important for fusion triggering and metastability. J. Virol. **87**:13520–13531.

81. **Elango N, Kövamees J, Varsanyi TM, Norrby E**. 1989. mRNA sequence and deduced amino acid sequence of the mumps virus small hydrophobic protein gene. J. Virol. **63**:1413–1415.

82. **Takeuchi K, Tanabayashi K, Hishiyama M, Yamada a**. 1996. The mumps virus SH protein is a membrane protein and not essential for virus growth. Virology **225**:156–162.

83. **Hiebert SW, Richardson CD, Lamb RA**. 1988. Cell surface expression and orientation in membranes of the 44-amino-acid SH protein of simian virus 5. J. Virol. **62**:2347–2357.

84. **Künkel U, Driesel G, Henning U, Gerike E, Willers H, Schreier E**. 1995. Differentiation of vaccine and wild mumps viruses by polymerase chain reaction and nucleotide sequencing of the SH gene: brief report. J. Med. Virol. **45**:121–126.

85. **Takeuchi K, Tanabayashi K, Hishiyama M, Yamada A, Sugiura A**. 1991. Variations of nucleotide sequences and transcription of the SH gene among mumps virus strains. Virology **181**:364–366.

86. **Yeo RP, Afzal MA, Forsey T, Rima BK**. 1993. Identification of a new mumps virus lineage by nucleotide sequence analysis of the SH gene of ten different strains. Arch. Virol. **128**:371–377.

87. **Wilson RL, Fuentes SM, Wang P, Taddeo EC, Klatt A, Henderson AJ, He B**. 2006. Function of small hydrophobic proteins of paramyxovirus. J. Virol. **80**:1700–1709.

88. **Woznik M, Rödner C, Lemon K, Rima B, Mankertz A, Finsterbusch T**. 2010. Mumps virus small hydrophobic protein targets ataxin-1 ubiquitin-like interacting protein (ubiquilin 4). J. Gen. Virol. **91**:2773–2781.

89. **Hiebert SW, Paterson RG, Lamb RA**. 1985. Hemagglutinin-neuraminidase protein of the paramyxovirus simian virus 5: nucleotide sequence of the mRNA predicts an N-terminal membrane anchor. J. Virol. **54**:1–6.

90. **Colman PM, Hoyne PA, Lawrence MC**. 1993. Sequence and structure alignment of paramyxovirus hemagglutinin-neuraminidase with influenza virus neuraminidase. J. Virol. **67**:2972–2980.

91. **McGinnes L, Sergel T, Morrison T**. 1993. Mutations in the transmembrane domain of the HN protein of Newcastle disease virus affect the structure and activity of the protein. Virology **196**:101–110.

92. **Crennell S, Takimoto T, Portner a, Taylor G**. 2000. Crystal structure of the multifunctional paramyxovirus hemagglutinin-neuraminidase. Nat. Struct. Biol. **7**:1068–1074.

93. **Lawrence MC, Borg NA, Streltsov VA, Pilling PA, Epa VC, Varghese JN, McKimm-Breschkin JL, Colman PM**. 2004. Structure of the haemagglutinin-neuraminidase from human parainfluenza virus type III. J. Mol. Biol. **335**:1343–1357.

94. **Porotto M, Murrell M, Greengard O, Lawrence MC, McKimm-Breschkin JL, Moscona A**. 2004. Inhibition of parainfluenza virus type 3 and Newcastle disease virus hemagglutinin-neuraminidase receptor binding: effect of receptor avidity and steric hindrance at the inhibitor binding sites. J. Virol. **78**:13911–13919.

95. **Kovamees J, Norrby E, Elango N**. 1989. Complete nucleotide sequence of the matrix protein mRNA of mumps virus. Virology **168**:426–428.

96. **Choppin PW, Scheid A**. 1980. The role of viral glycoproteins in adsorption, penetration, and pathogenicity of viruses. Rev. Infect. Dis. **2**:40–61.

97. **Yuan P, Thompson TB, Wurzburg BA, Paterson RG, Lamb RA, Jardetzky TS**. 2005. Structural studies of the parainfluenza virus 5 hemagglutinin-neuraminidase tetramer in complex with its receptor, sialyllactose. Structure **13**:803–815.

98. **Herrera E, Barcenas P, Hernández R, Méndez A, Pérez-Ishiwara G, Barrón B**. 2010. A 176 amino acid polypeptide derived from the mumps virus HN ectodomain shows immunological and biological properties similar to the HN protein. Virol. J. **7**:195.

99. **Reyes-Leyva J, Baños R, Borraz-Argüello M, Santos-López G, Rosas N, Alvarado G, Herrera I, Vallejo V, Tapia-Ramírez J**. 2007. Amino acid change 335 E to K affects the sialic-acid-binding and neuraminidase activities of Urabe AM9 mumps virus hemagglutinin-neuraminidase glycoprotein. Microbes Infect. **9**:234–240.

100. **Santos-López G, Scior T, Borraz-Argüello MDT, Vallejo-Ruiz V, Herrera-Camacho I, Tapia-Ramírez J, Reyes-Leyva J**. 2009. Structure-function analysis of two variants of mumps virus hemagglutinin-neuraminidase protein. Braz. J. Infect. Dis. **13**:24–34.

101. **Merz DC, Wolinsky JS**. 1983. Conversion of nonfusing mumps virus infections to fusing infections by selective proteolysis of the HN glycoprotein. Virology **131**:328–340.

102. **Dowling PC, Blumberg BM, Kolakofsky D, Cook P, Jotkowitz A, Prineas JW, Cook SD**. 1986. Measles virus nucleic acid sequences in human brain. Virus Res. **5**:97–107.

103. **Grdzelishvili VZ, Smallwood S, Tower D, Hall RL, Hunt DM, Moyer SA**. 2005. A single amino acid change in the L-polymerase protein of vesicular stomatitis virus completely abolishes viral mRNA cap methylation. **79**:7327–7337.

104. **Hercyk N, Horikami SM, Moyer SA**. 1988. The vesicular stomatitis virus L protein possesses the mRNA methyltransferase activities. Virology **163**:222–225.

105. **Einberger H, Mertz R, Hofschneider PH, Neubert WJ**. 1990. Purification, renaturation, and reconstituted protein kinase activity of the Sendai virus large (L) protein: L protein phosphorylates the NP and P proteins in vitro. J. Virol. **64**:4274–4280.

106. **Ogino T, Kobayashi M, Iwama M, Mizumoto K**. 2005. Sendai virus RNA-dependent RNA polymerase L protein catalyzes cap methylation of virus-specific mRNA. J. Biol. Chem. **280**:4429–4435.

107. **Rhodes DP, Abraham G, Banerjee AK**. 1975. The 5'-terminal structure of methylated mRNA synthesized in vitro by vesicular stomatitis virus. Abstr. Annu. Meet. Am. Soc. Microbiol. **75**:252.

108. **Hunt DM, Smith EF, Buckley DW**. 1984. Aberrant polyadenylation by a vesicular stomatitis virus mutant is due to an altered L protein. J. Virol. **52**:515–521.

109. **Hunt DM, Mehta R, Hutchinson KL**. 1988. The L protein of vesicular stomatitis virus modulates the response of the polyadenylic acid polymerase to S-adenosylhomocysteine. J. Gen. Virol. **69**:2555–2561.

110. **Testa D, Banerjee AK**. 1977. Two methyltransferase activities in the purified virions of vesicular stomatitis virus. J. Virol. **24**:786–793.

111. **Isle HD, Emerson SU**. 1982. Use of a hybrid infectivity assay to analyze primary transcription of temperature-sensitive mutants of the New Jersey serotype of vesicular stomatitis virus. J. Virol. **43**:37–40.

112. **Collins PL, Hightower LE, Ball LA**. 1980. Transcriptional map for Newcastle disease virus. J. Virol. **35**:682–693.

113. **Poch O, Sauvaget I, Delarue M, Tordo N**. 1989. Identification of four conserved motifs among the RNA-dependent polymerase encoding elements. EMBO J. **8**:3867–3874.

114. **Poch O, Blumberg BM, Bougueleret L, Tordo N**. 1990. Sequence comparison of five polymerases (L proteins) of unsegmented negative-strand RNA viruses: theoretical assignment of functional domains. J. Gen. Virol. **71**:1153–1162.

115. **Sidhu MS, Menonna JP, Cook SD, Dowling PC, Udem SA**. 1993. Canine distemper virus L gene: sequence and comparison with related viruses. Virology **193**:50–65.

116. **Jablonski SA, Luo M, Morrow CD**. 1991. Enzymatic activity of poliovirus RNA polymerase mutants with single amino acid changes in the conserved YGDD amino acid motif. J. Virol. **65**:4565–4572.

117. **Muller R, Poch O, Delarue M, Bishop DHL, Bouloy M**. 1994. Rift valley fever virus L segment: Correction of the sequence and possible functional role of newly identified regions conserved in RNA-dependent polymerases. J. Gen. Virol. **75**:1345–1352.

118. **Li J, Rahmeh A, Morelli M, Whelan SPJ**. 2008. A conserved motif in region v of the large polymerase proteins of nonsegmented negative-sense RNA viruses that is essential for mRNA capping. J. Virol. **82**:775–784.

119. **Feller JA, Smallwood S, Horikami SM, Moyer SA**. 2000. Mutations in conserved domains IV and VI of the large (L) subunit of the Sendai virus RNA polymerase give a spectrum of defective RNA synthesis phenotypes. Virology **269**:426–439.

120. **Chandrika R, Horikami SM, Smallwood S, Moyer SA**. 1995. Mutations in conserved domain I of the Sendai virus L polymerase protein uncouple transcription and replication. Virology **213**:352–363.

121. **Smallwood S, Cevik B, Moyer SA**. 2002. Intragenic complementation and oligomerization of the L subunit of the Sendai virus RNA polymerase. Virology **304**:235–245.

122. **Çevik B, Smallwood S, Moyer SA**. 2003. The L-L oligomerization domain resides at the very N-terminus of the Sendai virus L RNA polymerase protein. Virology **313**:525–536.

123. **Smallwood S, Moyer SA**. 2004. The L polymerase protein of parainfluenza virus 3 forms an oligomer and can interact with the heterologous Sendai virus L, P and C proteins. Virology **318**:439–50.

124. **Cevik B, Holmes DE, Vrotsos E, Feller JA, Smallwood S, Moyer SA**. 2004. The phosphoprotein (P) and L binding sites reside in the N-terminus of the L subunit of the measles virus RNA polymerase. Virology **327**:297–306.

125. **Horikami SM, Hector RE, Smallwood S, Moyer SA**. 1997. The Sendai virus C protein binds the L polymerase protein to inhibit viral RNA synthesis. Virology **235**:261–270.

126. **Parks GD**. 1994. Mapping of a region of the paramyxovirus L protein required for the formation of a stable complex with the viral phosphoprotein P. J. Virol. **68**:4862–4872.

127. **Malur AG, Choudhary SK, De BP, Banerjee AK**. 2002. Role of a highly conserved NH(2)-terminal domain of the human parainfluenza virus type 3 RNA polymerase. J. Virol. **76**:8101–8109.

128. **Horikami SM, Smallwood S, Bankamp B, Moyer SA**. 1994. An amino-proximal domain of the L protein binds to the P protein in the measles virus RNA polymerase complex. Virology **205**:540–545.

129. **Holmes DE, Moyer SA**. 2002. The phosphoprotein (P) binding site resides in the N terminus of the L polymerase subunit of Sendai virus. J. Virol. **76**:3078–3083.

130. **Nishio M, Ohtsuka J, Tsurudome M, Nosaka T, Kolakofsky D**. 2008. Human parainfluenza virus type 2 V protein inhibits genome replication by binding to the L protein: possible role in promoting viral fitness. J. Virol. **82**:6130–6138.

131. **Yamada A, Tsurudome M, Hishiyama M, Ito Y**. 1984. Abortive infection of mumps virus in murine cell lines. J. Gen. Virol. **65 (Pt 5)**:973–980.

132. **Gresser I, Enders JF**. 1961. Cytopathogenicity of mumps virus in cultures of chick embryo and human amnion cells. Proc. Soc. Exp. Biol. Med. **107**:804–807.

133. **McCarthy M, Johnson RT**. 1980. Morphological heterogeneity in relation to structural and functional properties of mumps virus. J. Gen. Virol. **48**:395–399.

134. **Afzal MA, Dussupt V, Minor PD, Pipkin PA, Fleck R, Hockley DJ, Stacey GN**. 2005. Assessment of mumps virus growth on various continuous cell lines by virological, immunological, molecular and morphological investigations. J. Virol. Methods **126**:149–156.

135. **Conzelmann KK**. 1998. Nonsegmented negative-strand RNA viruses: Genetics and manipulation of viral genomes. Annu. Rev. Genet. **32**:123–162.

136. **Thomas SM, Lamb RA, Paterson RG**. 1988. Two mRNAs that differ by two nontemplated nucleotides encode the amino coterminal proteins P and V of the paramyxovirus SV5. Cell **54**:891–902.

137. **Murphy SK, Parks GD**. 1999. RNA replication for the paramyxovirus simian virus 5 requires an internal repeated (CGNNNN) sequence motif. J. Virol. **73**:805–809.

138. **Schmitt AP, Lamb RA**. 2004. Escaping from the cell: assembly and budding of negative-strand RNA viruses. Curr. Top. Microbiol. Immunol. **283**:145–196.

139. **Curran J, Boeck R, Lin-Marq N, Lupas A, Kolakofsky D**. 1995. Paramyxovirus phosphoproteins form homotrimers as determined by an epitope dilution assay, via predicted coiled coils. Virology **214**:139–149.

140. **Harbury PB, Kim PS**. 1994. Crystal structure of an isoleucine-zipper trimer. Nature **371**:80.

141. **Markwell MA, Fox CF**. 1980. Protein-protein interactions within paramyxoviruses identified by native disulfide bonding or reversible chemical cross-linking. J. Virol. **33**:152–166.

142. **Tarbouriech N, Curran J, Ruigrok RWH, Burmeister WP**. 2000. Tetrameric coiled coil domain of Sendai virus phosphoprotein. Nat. Struct. Biol.

143. **Curran J**. 1996. Reexamination of the Sendai virus P protein domains required for RNA synthesis: A possible supplemental role for the P protein. Virology **221**:130–140.

144. **Curran J**. 1998. A role for the Sendai virus P protein trimer in RNA synthesis. J. Virol. **72**:4274–4280.

145. **Choudhary SK, Malur AG, Huo Y, De BP, Banerjee AK**. 2002. Characterization of the oligomerization domain of the phosphoprotein of human parainfluenza virus type 3. Virology **302**:373–382.

146. **Chen M, Ogino T, Banerjee AK**. 2006. Mapping and functional role of the self-association domain of vesicular stomatitis virus phosphoprotein. J. Virol. **80**:9511–9518.

147. **Ding HT, Green TJ, Lu SY, Luo M**. 2006. Crystal structure of the oligomerization domain of the phosphoprotein of vesicular stomatitis virus. J. Virol. **80**:2808–2814.

148. **Rahaman A, Srinivasan N, Shamala N, Shaila MS**. 2004. Phosphoprotein of the rinderpest virus forms a tetramer through a coiled coil region important for biological function: a structural insight. J. Biol. Chem. **279**:23606–23614.

149. **Asenjo A, Villanueva N**. 2000. Regulated but not constitutive human respiratory syncytial virus (HRSV) P protein phosphorylation is essential for oligomerization. FEBS Lett. **467**:279–284.

150. **Castagne N, Barbier A, Bernard J, Rezaei H, Huet J-C, Henry C, Da Costa B, Eleouet J-F**. 2004. Biochemical characterization of the respiratory syncytial virus P-P and P-N protein complexes and localization of the P protein oligomerization domain. J. Gen. Virol. **85**:1643–1653.

151. **Chattopadhyay S, Banerjee AK**. 2009. Phosphoprotein, P of human parainfluenza virus type 3 prevents self-association of RNA-dependent RNA polymerase, L. Virology **383**:226–36.

152. **Leyrat C, Renner M, Harlos K, Grimes JM**. 2013. Solution and crystallographic structures of the central region of the phosphoprotein from human metapneumovirus. PLoS One.

153. **Communie G, Crépin T, Maurin D, Jensen MR, Blackledge M, Ruigrok RWH**. 2013. Structure of the tetramerization domain of measles virus phosphoprotein. J. Virol. **87**:7166–7169.

154. **Cox R, Green TJ, Purushotham S, Deivanayagam C, Bedwell GJ, Prevelige PE, Luo M**. 2013. Structural and functional characterization of the mumps virus phosphoprotein. J. Virol. **87**:7558–68.

155. **Curran J, Pelet T, Kolakofsky D**. 1994. An acidic activation-like domain of the Sendai virus P protein is required for RNA synthesis and encapsidation. Virology **202**:875–884.

156. **Curran J, Marq JB, Kolakofsky D**. 1995. An N-terminal domain of the Sendai paramyxovirus P protein acts as a chaperone for the NP protein during the nascent chain assembly step of genome replication. J. Virol. **69**:849.

157. **Smallwood S, Ryan KW, Moyer SA**. 1994. Deletion analysis defines a carboxyl-proximal region of Sendai virus P protein that binds to the polymerase L protein. Virology **202**:154–163.

158. **Kolakofsky D, Le Mercier P, Iseni F, Garcin D**. 2004. Viral RNA polymerase scanning and the gymnastics of Sendai virus RNA synthesis. Virology **318**:463–473.

159. **Ryan KW, Kingsbury DW**. 1988. Carboxyl-terminal region of Sendai virus P protein is required for binding to viral nucleocapsids. Virology **167**:106–112.

160. **Ryan KW, Morgan EM, Portner A**. 1991. Two noncontiguous regions of Sendai virus P protein combine to form a single nucleocapsid binding domain. Virology **180**:126–134.

161. **García-Barreno B, Delgado T, Melero JA**. 1996. Identification of protein regions involved in the interaction of human respiratory syncytial virus phosphoprotein and nucleoprotein: significance for nucleocapsid assembly and formation of cytoplasmic inclusions. J. Virol. **70**:801–808.

162. **De BP, Hoffman MA, Choudhary S, Huntley CC, Banerjee AK**. 2000. Role of NH(2)- and COOH-terminal domains of the P protein of human parainfluenza virus type 3 in transcription and replication. J. Virol. **74**:5886–5895.

163. **Gao Y, Lenard J**. 1995. Cooperative binding of multimeric phosphoprotein (P) of vesicular stomatitis virus to polymerase (L) and template: pathways of assembly. J. Virol. **69**:7718–7723.

164. **Ivanov I, Crépin T, Jamin M, Ruigrok RWH**. 2010. Structure of the dimerization domain of the rabies virus phosphoprotein. J. Virol. **84**:3707–3710.

165. **Chenik M, Schnell M, Conzelmann KK, Blondel D**. 1998. Mapping the interacting domains between the rabies virus polymerase and phosphoprotein. J. Virol. **72**:1925–1930.

166. **Schoehn G, Iseni F, Mavrakis M, Blondel D, Ruigrok RWH**. 2001. Structure of recombinant rabies virus nucleoprotein-RNA complex and identification of the phosphoprotein binding site. J. Virol. **75**:490–498.

167. **Mavrakis M, Méhouas S, Réal E, Iseni F, Blondel D, Tordo N, Ruigrok RWH**. 2006. Rabies virus chaperone: identification of the phosphoprotein peptide that keeps nucleoprotein soluble and free from non-specific RNA. Virology **349**:422–429.

168. **Sourimant J, Rameix-Welti M-A, Gaillard A-L, Chevret D, Galloux M, Gault E, Eléouët J-F**. 2015. Fine mapping and characterization of the L-polymerase-binding domain of the respiratory syncytial virus phosphoprotein. J. Virol. **89**:4421–4433.

169. **Nishio M, Tsurudome M, Ito M, Ito Y**. 2000. Mapping of domains on the human parainfluenza type 2 virus P and NP proteins that are involved in the interaction with the L protein. Virology **273**:241–247.

170. **Navarro J, López-Otín C, Villanueva N**. 1991. Location of phosphorylated residues in human respiratory syncytial virus phosphoprotein. J. Gen. Virol. **72 (Pt 6)**:1455–1459.

171. **Villanueva N, Navarro J, Méndez E, García-Albert I**. 1994. Identification of a protein kinase involved in the phosphorylation of the C-terminal region of human respiratory syncytial virus P protein. J. Gen. Virol. **75 (Pt 3)**:555–65.

172. **Barik S, McLean T, Dupuy LC**. 1995. Phosphorylation of Ser232 directly regulates the transcriptional activity of the P protein of human respiratory syncytial virus: phosphorylation of Ser237 may play an accessory role. Virology **213**:405–412.

173. **Sánchez-Seco MP, Navarro J, Martínez R, Villanueva N**. 1995. C-terminal phosphorylation of human respiratory syncytial virus P protein occurs mainly at serine residue 232. J. Gen. Virol. **76 (Pt 2)**:425–430.

174. **Fuentes SM, Sun D, Schmitt AP, He B**. 2010. Phosphorylation of paramyxovirus phosphoprotein and its role in viral gene expression. Future Microbiol. **5**:9–13.

175. **Lu B, Ma C, Brazas R, Jin H**. 2002. The major phosphorylation sites of the respiratory syncytial virus phosphoprotein are dispensable for virus replication in vitro. J. Virol. **76**:10776–10784.

176. **Lenard J**. 1999. Host cell protein kinases in nonsegmented negative-strand virus (mononegavirales) infection. Pharmacol. Ther. **83**:39–48.

177. **Mazumder B, Adhikary G, Barik S**. 1994. Bacterial expression of human respiratory syncytial viral phosphoprotein P and identification of Ser237 as the site of phosphorylation by cellular casein kinase II. Virology **205**:93–103.

178. **Das T, Schuster A, Schneider-Schaulies S, Banerjee AK**. 1995. Involvement of cellular casein kinase II in the phosphorylation of measles virus P protein: identification of phosphorylation sites. Virology **211**:218–226.

179. **De BP, Gupta S, Banerjee a K**. 1995. Cellular protein kinase C isoform zeta regulates human parainfluenza virus type 3 replication. Proc. Natl. Acad. Sci. U. S. A. **92**:5204–5208.

180. **Huntley CC, De BP, Banerjee AK**. 1997. Phosphorylation of Sendai virus phosphoprotein by cellular protein kinase C ζ. J. Biol. Chem. **272**:16578–16584.

181. **Liu Z, Huntley CC, De BP, Das T, Banerjee AK, Oglesbee MJ**. 1997. Phosphorylation of canine distemper virus P protein by protein kinase C-zeta and casein kinase II. Virology **232**:198–206.

182. **Sun M, Fuentes SM, Timani K, Sun D, Murphy C, Lin Y, August A, Teng MN, He B**. 2008. Akt plays a critical role in replication of nonsegmented negative-stranded RNA viruses. J. Virol. **82**:105–114.

183. **Huppertz HL, Hall WW, Ter Meulen V**. 1977. Polypeptide composition of mumps virus. Med. Microbiol. Immunol. **163**:251–259.

184. **Jensik SC, Silver S**. 1976. Polypeptides of mumps virus. J. Virol. **17**:363–373.

185. **Orvell C**. 1978. Structural polypeptides of mumps virus. J. Gen. Virol. **41**:527–539.

186. **Rima BK, Roberts MW, McAdam WD, Martin SJ**. 1980. Polypeptide synthesis in mumps virus-infected cells. J. Gen. Virol. **46**:501–505.

187. **Hviid A, Rubin S, Mühlemann K**. 2008. Seminar: Mumps. Lancet **371**:932–944.

188. **Richardson M, Elliman D, Maguire H, Simpson J, Nicoll A**. 2001. Evidence base of incubation periods, periods of infectiousness and exclusion policies for the control of communicable diseases in schools and preschools. Pediatr. Infect. Dis. J. **20**:380–391.

189. **Kilham L**. 1948. Isolation of mumps virus from the blood of a patient. Proc. Soc. Exp. Biol. Med. **69**:99–100.

190. **Wolinsky JS, Klassen T, Baringer JR**. 1976. Persistence of neuroadapted mumps virus in brains of newborn hamsters after intraperitoneal inoculation. J. Infect. Dis. **133**:260.

191. **Fleischer RB, Kreth HW**. 1982. Mumps virus replication in human lymphoid cell lines and in peripheral blood lymphocytes: preference for T cells. Infect. Immun. **35**:25–31.

192. **Kilham L**. 1949. Mumps meningoencephalitis with and without parotitis. Am. J. Dis. Child. **78**:324–333.

193. **Maris EP, Enders JF, Stokes J, Kane LW**. 1946. Immunity in mumps : IV. The correlation of the presence of complement-fixing antibody and resistance to mumps in human beings. J. Exp. Med. **84**:323–339.

194. **Philip RN, Reinhard KR, Lackman DB**. 1995. Observations on a mumps epidemic in a "virgin" population. 1958. Am. J. Epidemiol. **142**:233–253.

195. **Krüger N, Hoffmann M, Drexler JF, Müller MA, Corman VM, Sauder C, Rubin S, He B, Örvell C, Drosten C, Herrler G**. 2015. Functional properties and genetic relatedness of the fusion and hemagglutinin-neuraminidase proteins of a mumps virus-like bat virus. J. Virol. **89**:4539–4548.

196. **Kaaijk P, van der Zeijst B, Boog M, Hoitink C**. 2008. Increased mumps incidence in the Netherlands: review on the possible role of vaccine strain and genotype. Euro Surveill. **13**:6–8.

197. **Marin M, Broder KR, Temte JL, Snider DE, Seward JF**. 2010. Use of combination measles, mumps, rubella, and varicella vaccine: recommendations of the Advisory Committee on Immunization Practices (ACIP). MMWR **59**:1–12.

198. **Buynak EB, Hilleman MR**. 1966. Live attenuated mumps virus vaccine. 1. Vaccine development. Proc. Soc. Exp. Biol. Med. **123**:768–775.

199. **Pagano JS, Levine RH, Sugg WC, Finger JA**. 1967. Clinical trial of new attenuated mumps virus vaccine (Jeryl Lynn strain): preliminary report. Prog. Immunobiol. Stand. **3**:196–202.

200. **Buynak EB, Hilleman MR, Leagus MB, Whitman Jr. JE, Weibel RE, Stokes Jr. J**. 1968. Jeryl Lynn strain live attenuated mumps virus vaccine. I. Influence of age, virus dose, lot, and γ-globulin administration on response. J. Am. Med. Assoc. **203**:9–13.

201. **Weibel RE, Stokes Jr. J, Buynak EB, Leagus MB, Hilleman MR**. 1968. Jeryl Lynn strain live attenuated mumps virus vaccine. II. Durability of immunity following administration. J. Am. Med. Assoc. **203**:14–18.

202. **Young ML, Dickstein B, Weibel RE, Stokes J, Buynak EB, Hilleman MR**. 1967. Experiences with Jeryl Lynn strain live attenuated mumps virus vaccine in a pediatric outpatient clinic. Pediatrics **40**:798.

203. **Rubin SA, Afzal MA, Powell CL, Bentley ML, Auda GR, Taffs RE, Carbone KM**. 2005. The rat-based neurovirulence safety test for the assessment of mumps

virus neurovirulence in humans: An international collaborative study. J. Infect. Dis. VO - 191 1123.

204. **Hassan J, Dean J, Moss E, Carr MJ, Hall WW, Connell J**. 2012. Seroepidemiology of the recent mumps virus outbreaks in Ireland. J. Clin. Virol.

205. **Smits G, Mollema L, Hahné S, Melker H de, Tcherniaeva I, Waaijenborg S, Binnendijk R van, Klis F van der, Berbers G**. 2013. Seroprevalence of mumps in The Netherlands: dynamics over a decade with high vaccination coverage and recent outbreaks. PLoS One **8**:e58234–e58234.

206. **Nelson GE, Aguon A, Valencia E, Oliva R, Guerrero ML, Reyes R, Lizama A, Diras D, Mathew A, Camacho EJ, Monforte M-N, Chen T-H, Mahamud A, Kutty PK, Hickman C, Bellini WJ, Seward JF, Gallagher K, Fiebelkorn AP**. 2013. Epidemiology of a mumps outbreak in a highly vaccinated island population and use of a third dose of measles-mumps-rubella vaccine for outbreak control--Guam 2009 to 2010. Pediatr. Infect. Dis. J. **32**:374–380.

207. **Rajčevic´ S, Šeguljev Z, Petrovic V, Medic´ S, Nedelijkovic´ J, Miloševic´ V, Turo L, Ristic´ M**. 2012. Ongoing mumps outbreak in Novi Sad, the autonomous province of Vojvodina, Serbia, January to April 2012. Eurosurveillance **17**:20169.

208. **Jin L, Rima B, Brown D, Örvell C, Tecle T, Afzal M, Uchida K, Nakayama T, Song J-W, Kang C, Rota PA, Xu W, Featherstone D**. 2005. Proposal for genetic characterisation of wild-type mumps strains: Preliminary standardisation of the nomenclature. Arch. Virol. **150**:1903–1909.

209. **Rubin SA, Qi L, Audet SA, Sullivan B, Carbone KM, Bellini WJ, Rota PA, Sirota L, Beeler J**. 2008. Antibody induced by immunization with the Jeryl Lynn mumps vaccine strain effectively neutralizes a heterologous wild-type mumps virus associated with a large outbreak. J. Infect. Dis. **198**:508–515.

210. **Rubin SA, Link MA, Sauder CJ, Zhang C, Ngo L, Rima BK, Duprex WP**. 2012. Recent mumps outbreaks in vaccinated populations: no evidence of immune escape. J. Virol. **86**:615–620.

211. **Tsutsumi H, Chiba Y, Abo W, Chiba S, Nakao T**. 1980. T-cell-mediated cytotoxic response to mumps virus in humans. Infect. Immun. **30**:129–134.

212. **Cusi M, Correale P, Valassina M**. 2001. Comparative study of the immune response in mice immunized with four live attenuated strains of mumps virus by intranasal or intramuscular route. Arch. Virol. **146**:1241–1248.

213. **Hanna-Wakim R, Yasukawa LL, Sung P, Arvin AM, Gans HA**. 2008. Immune responses to mumps vaccine in adults who were vaccinated in childhood. J. Infect. Dis. **197**:1669–1675.

214. **Jokinen S, Osterlund P, Julkunen I, Davidkin I**. 2007. Cellular immunity to mumps virus in young adults 21 years after measles-mumps-rubella vaccination. J. Infect. Dis. **196**:861–867.

215. **Weibel RE, Stokes Jr. J, Buynak EB, Whitman Jr. JE, Hilleman MR**. 1967. Live, attenuated mumps-virus vaccine. 3. Clinical and serologic aspects in a field evaluation. N. Engl. J. Med. **276**:245–251.

216. **Afzal MA, Pickford AR, Forsey T, Heath AB, Minor PD**. 1993. The Jeryl Lynn vaccine strain of mumps virus is a mixture of two distinct isolates. J. Gen. Virol. **74 (Pt 5)**:917–920.

217. **Amexis G, Rubin S, Chizhikov V, Pelloquin F, Carbone K, Chumakov K**. 2002. Sequence diversity of Jeryl Lynn strain of mumps virus: Quantitative mutant analysis for vaccine quality control. Virology **300**:171–179.

218. **Chambers P, Rima BK, Duprex WP**. 2009. Molecular differences between two Jeryl Lynn mumps virus vaccine component strains, JL5 and JL2. J. Gen. Virol. **90**:2973–2981.

219. **Xu P, Chen Z, Phan S, Pickar A, He B**. 2014. Immunogenicity of novel mumps vaccine candidates generated by genetic modification. J. Virol. **88**:2600–10.

220. **Tsurudome M, Yamada A, Hishiyama M, Ito Y**. 1987. Replication of mumps virus in mouse: transient replication in lung and potential of systemic infection. Arch. Virol. **97**:167–179.

221. **Vandermeulen C, Verhoye L, Vaidya S, Clement F, Brown KE, Hoppenbrouwers K, Leroux-Roels G**. 2010. Detection of mumps virus-specific memory B cells by transfer of peripheral blood mononuclear cells into immune-deficient mice. Immunology **131**:33–39.

222. **Young KR, Nzula S, Burt DS, Ward BJ**. 2014. Immunologic characterization of a novel inactivated nasal mumps virus vaccine adjuvanted with Protollin. Vaccine **32**:238–245.

223. **Belser JA, Katz JM, Tumpey TM**. 2011. The ferret as a model organism to study influenza A virus infection. Dis. Model. Mech. **4**:575–579.

224. **Gordon I, Pavri K, Cohen SM**. 1956. Response of ferrets to mumps virus. J. Immunol. **76**:328–333.

225. **Parker L, Gilliland SM, Minor P, Schepelmann S**. 2013. Assessment of the ferret as an in vivo model for mumps virus infection. J. Gen. Virol. **94**:1200–1205.

226. **Flanagan TD, Andrada JA, Barron AL, Witebsky E**. 1971. Response to experimental infection with mumps virus in rhesus monkeys. Infect. Immun. **3**:642–647.

227. **Genco RJ, Flanagan TD, Emmings FG**. 1973. Immunocyte response to experimental mumps virus infection in Rhesus monkeys. Infect. Immun. **7**:520–525.

228. **Goodbourn S, Randall RE**. 2009. The regulation of type I interferon production by paramyxoviruses. J. Interferon Cytokine Res. **29**:539–547.

229. **Centers for Disease Control and Prevention**. 2013. Prevention of measles, rubella, congenital rubella syndrome, and mumps, 2013: summary recommendations of the Advisory Committee on Immunization Practices (ACIP). MMWR **62**:1–34.

230. **Emerson S, Yu Y**. 1975. Both NS and L proteins are required for in vitro RNA synthesis by vesicular stomatitis virus. J. Virol. **15**:1348–1356.

231. **Banerjee AK, Barik S, De BP**. 1991. Gene expression of nonsegmented negative strand RNA viruses. Pharmacol. Ther. **51**:47–70.

232. **Pattnaik a K, Hwang L, Li T, Englund N, Mathur M, Das T, Banerjee a K**. 1997. Phosphorylation within the amino-terminal acidic domain I of the phosphoprotein of vesicular stomatitis virus is required for transcription but not for replication. J. Virol. **71**:8167–8175.

233. **Raha T, Samal E, Majumdar A, Basak S, Chattopadhyay D, Chattopadhyay DJ**. 2000. N-terminal region of P protein of Chandipura virus is responsible for phosphorylation-mediated homodimerization. Protein Eng. **13**:437–444.

234. **Delano W**. 2002. The PyMOL user's manual. Delano Scientific, San Carlos, CA.

235. **Lin Y, Horvath F, Aligo JA, Wilson R, He B**. 2005. The role of simian virus 5 V protein on viral RNA synthesis. Virology **338**:270–280.

236. **Yu Q, Hardy RW, Wertz GW**. 1995. Functional cDNA clones of the human respiratory syncytial (RS) virus N, P, and L proteins support replication of RS virus genomic RNA analogs and define minimal trans-acting requirements for RNA replication. J. Virol. **69**:2412–2419.

237. **Hitoshi N, Ken-ichi Y, Jun-ichi M**. 1991. Efficient selection for high-expression transfectants with a novel eukaryotic vector. Gene **108**:193–199.

238. **Luthra P, Sun D, Wolfgang M, He B**. 2008. AKT1-dependent Aativation of NF-κB by the L protein of parainfluenza virus 5. J. Virol. **82**:10887–10895.

239. **Russell CJ, Jardetzky TS, Lamb RA**. 2001. Membrane fusion machines of paramyxoviruses: capture of intermediates of fusion. EMBO J. **20**:4024–34.

240. **Zengel J, Pickar A, Pei X, Lin A, He B**. 2015. The roles of phosphorylation of the nucleocapsid protein of mumps virus in regulating viral RNA transcription and replication. J. Virol. **89**:7338–7347.

241. **Eckerdt F, Strebhardt K**. 2006. Polo-like kinase 1: target and regulator of anaphase-promoting complex/cyclosome-dependent proteolysis. Cancer Res. **66**:6895–6898.

242. **Elia AEH, Cantley LC, Yaffe MB**. 2003. Proteomic screen finds pSer/pThr-binding domain localizing Plk1 to mitotic substrates. Science **299**:1228–1231.

243. **Silljé HHW, Nigg EA**. 2003. Signal transduction. Capturing polo kinase. Science (80-.). **299**:1190–1191.

244. **Wu Z-Q, Liu X**. 2008. Role for Plk1 phosphorylation of Hbo1 in regulation of replication licensing. Proc. Natl. Acad. Sci. U. S. A. **105**:1919–1924.

245. **Lowery DM, Lim D, Yaffe MB**. 2005. Structure and function of Polo-like kinases. Oncogene **24**:248–259.

246. **Horikami SM, Curran J, Kolakofsky D, Moyer SA**. 1992. Complexes of Sendai virus NP-P and P-L proteins are required for defective interfering particle genome replication in vitro. J. Virol. **66**:4901–4908.

247. **Byrappa S, Pan YB, Gupta KC**. 1996. Sendai virus P protein is constitutively phosphorylated at serine249: high phosphorylation potential of the P protein. Virology **216**:228–34.

248. **Hu C, Gupta KC**. 2000. Functional Significance of Alternate Phosphorylation in Sendai Virus P Protein. Virology **268**:517–532.

249. **Villanueva N, Hardy R, Asenjo A, Yu Q, Wertz G**. 2000. The bulk of the phosphorylation of human respiratory syncytial virus phosphoprotein is not essential but modulates viral RNA transcription and replication. J. Gen. Virol. **81**:129–133.

APPENDIX A

C57BL/6 IFNR1-KO MICE AS A MODEL FOR STUDYING MUV PATHOGENESIS

Introduction

Establishment of an animal model to study MuV pathogenesis has been limited because the only natural host of MuV is the human. Experimental infections have been induced in numerous species, however a small animal model that reflects the human disease has not been established. Mice are an attractive model due to better cost-efficiency, and a broader availability of reagents. MuV is not known to replicate well or cause illness in wild-type adult mice (212, 220), however, C57BL/6 IFNr1-KO mice are susceptible to intracranial (i.c.) MuV infection. Thus, infection of IFNr1-KO mice may be a potential small animal model for studying MuV pathogenesis. There is no established mumps neutralizing antibody titer predictive of protection against infection or disease, therefore the lack of immune correlates to protection makes it difficult to standardize the efficacy of the current MuV vaccine program. IFNr1-KO mice may be used to directly compare vaccine efficacy based on protection against MuV outbreak strains.

Results

Infection of C57BL/6 wild-type and C57BL/6 IFNr1-KO mice with MuV.

To determine if C57BL/6 wild-type and IFNr1-KO mice are susceptible to infection with the $MuV^{Iowa/US/06}$ outbreak strain studied in our lab, three mice each were infected with $1.6x10^7$ PFU i.p. or 1000 PFU i.c.. To monitor disease progression, body weight measurements and behavioral changes were recorded daily. No signs of disease were evident in the C57BL/6 wild-type mice or in the IFNr1-KO i.p. group. At 4 days post infection (dpi), one mouse in the IFNr1-KO i.c. infected group was found dead and the other two mice in this group, MuV-IA-1 and MuV-IA-2, appeared lethargic and lost 15% and 16% of their original body weight, respectively (Fig. A.1A). Brains, spleens, and lungs were collected at 6 dpi. No infectious virus was found in the spleens or lungs, and titers from the brains were $1.1x10^4$ PFU/mL for MuV-IA-1 and $7.1x10^3$ PFU/mL for MuV-IA-2 (Fig. A.1B). Viral RNA was also purified from tissue homogenates for real-time PCR analysis using a MuV-IA NP gene-specific probe. Viral RNA levels in the brains corroborated the infectious virus titers and additionally, MuV RNA was found in the spleen of the MuV-IA-1 mouse (Fig. A.1C). These results suggest that the intracranial route of MuV infection in C57BL/6 IFNr1-KO mice may be used as a tool to study MuV infection and pathogenesis.

C57BL/6 IFNr1-KO intracranial infection kinetics.

To study the kinetics of the C57BL/6 IFNr1-KO mouse i.c. model, mice were infected with 1000 PFU i.c. of a recombinant MuV containing a renilla luciferase reporter gene (rMuV-Rluc). Body weights were measured daily and mice were sacrificed at 3, 5,

7, and 8 dpi. Mice began to appear lethargic and loose weight by 5 dpi, and all remaining mice reached the humane endpoint for weight loss on day 8. Tissue homogenates of lungs, spleens, and brains were collected and used to measure renilla luminescence as a correlate to virus replication. On 5, 7, and 8 dpi, one mouse from each time point had enhanced activity in the lung (Fig. A.2A), and one mouse had significantly enhanced activity in the spleen on 5 dpi (Fig. A.2B). Luciferase activity increased in the brain until 7 dpi, where it then decreased on 8 dpi (Fig. A.2C). These results suggest that peak viral replication for the intracranial route of infection in C57BL/6 IFNr1-KO mice is 7 dpi.

Intranasal and subcutaneous infection of C57BL/6 IFNr1-KO mice with MuV.

To determine if IFNr1-KO mice are susceptible to additional routes of infection, adult IFNr1-KO mice were infected with $3x10^6$ PFU intranasal (i.n.) or infected with $6x10^6$ PFU subcutaneous (s.c.) with rMuV-Rluc. Body weights were measured daily and mice were sacrificed at 4, 7, and 10 dpi. Tissue homogenates of lungs, spleens, and brains were collected and used to measure renilla luminescence as a correlate to virus replication (Fig. A.3). Luciferase activity of all tissue homogenates of s.c. infected mice was not greater than that of mock infected mice, suggesting that MuV did not replicate in IFNr1-KO mice infected by the s.c. route. Luciferase activity of brain and spleen homogenates of i.n. infected mice was not greater than that of mock infected mice, however luciferase activity was enhanced at 4 dpi. These results suggest that rMuV-Rluc replicates early following i.n. infection, followed by viral clearance after 4 dpi in IFNr1-KO mice.

C57BL/6 IFNr1-KO intranasal infection kinetics.

To further characterize the kinetics of the intranasal model, C57BL/6 wild-type and IFNr1-KO mice were infected with $1x10^6$ PFU i.n. of MuV. Body weights were measured daily and mice were sacrificed at 2, 3, and 4 dpi. Body weights of infected mice remained similar to that measured at the time of infection (data not shown). Lung tissue homogenates were collected and used to measure infectious viral titers by plaque assay. No infectious virus was found in the lungs of C57BL/6 wild-type mice (Fig. A.3A). Titers from the lungs of IFNr1-KO mice gradually declined from 2 to 4 dpi. Since the highest average peak titer of 160 PFU/g was measured on 2 dpi, this time point was used for testing MuV antibody protection efficacy in this IFNr1-KO i.n. mouse model.

Development of C57BL/6 IFNr1-KO passive antibody protection model.

To develop an antibody protection model for testing vaccine candidates against a MuV outbreak strain, BALB/c mice were sham vaccinated or vaccinated and boosted at 21 and 35 days post primary vaccination through intramuscular (i.m.) injection with $1x10^6$ PFU of MuV. Serum samples were collected and pooled at 56 days post primary vaccination. The serum neutralization titer was calculated as 1:128 by neutralizing plaque reduction assay.

To examine the importance of the humoral immune response to protection of vaccine candidates against a MuV outbreak strain, passive antibody transfer was examined. Serum from the sham vaccinated mice, or the pooled serum from the MuV vaccinated mice was passively transferred to naïve C57BL/6 IFNr1-KO mice by intraperitoneal (i.p.) injection (Fig. A.4.A). At 24 hours post antibody transfer, mice were

challenged with $1x10^6$ PFU i.n. of MuV. Lungs were collected and homogenized 2 days post challenge (dpc), and viral titers were measured by plaque assay. As observed in Figure A.5.B, mice that received passive antibody treatment with serum from MuV vaccinated mice had reduced viral burden 2 dpc compared to mice that received serum from sham vaccinated mice. These results suggest that humoral immunity plays a role in protection against intranasal MuV infection of C57BL/6 IFNr1-KO mice. This model may be used to examine efficacy of vaccine candidates against a MuV outbreak strain.

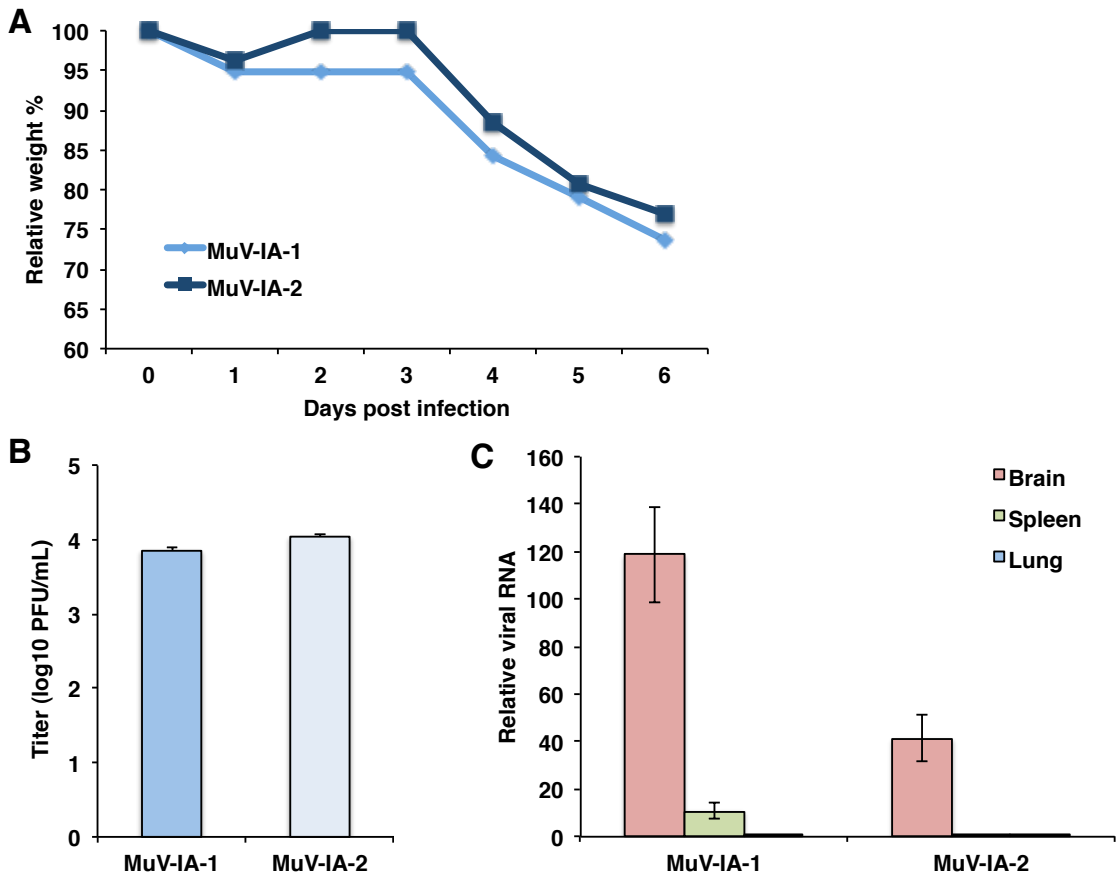

Figure A.1. Susceptibility of C57BL/6 IFNr1-KO mice to intracranial infection with MuV. (A) Body weight measurements of infected mice. C57BL/6 IFNr1-KO mice were infected i.c. with 1000 PFU of MuV. Body weights were measured daily and calculated as the percentage of the original body weight prior to infection. (B) MuV titers in infected mice. Brains were collected and homogenized 6 dpi. Brain homogenates were used for virus titration via plaque assay. (C) Viral RNA in tissues of infected mice. Brains, spleens, and lungs were collected and homogenized 6 dpi and used for viral RNA extraction. Real-time PCR was completed using a MuV-NP specific FAM tagged probe and an actin FAM tagged probe. Relative viral RNA was calculated by normalizing MuV-NP to host actin. Error bars represent the SEM of data from 3 replicates.

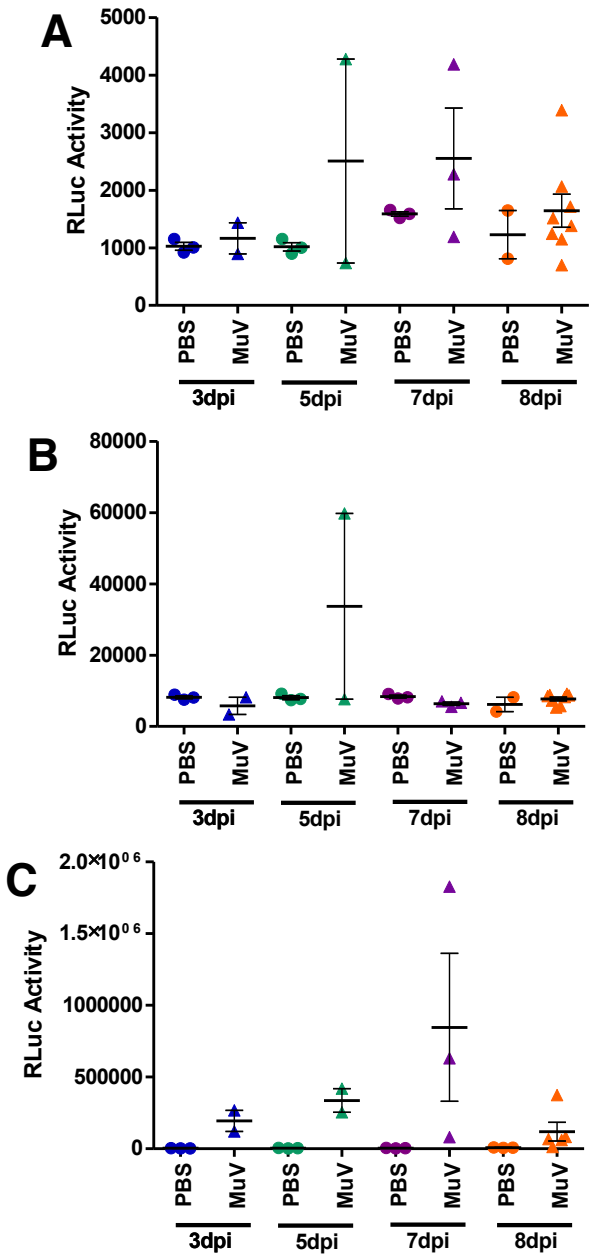

Figure A.2. C57BL/6 IFNr1-KO intracranial infection kinetics. C57BL/6 IFNr1-KO mice were infected i.c. with PBS or 1000 PFU of a recombinant MuV containing a renilla luciferase reporter gene (rMuV-Rluc). (A) Lung, (B) spleen, and (C) brain tissues were collected and homogenized at 3, 5, 7, and 8 dpi. Tissue homogenates were used to measure renilla luciferase activity.

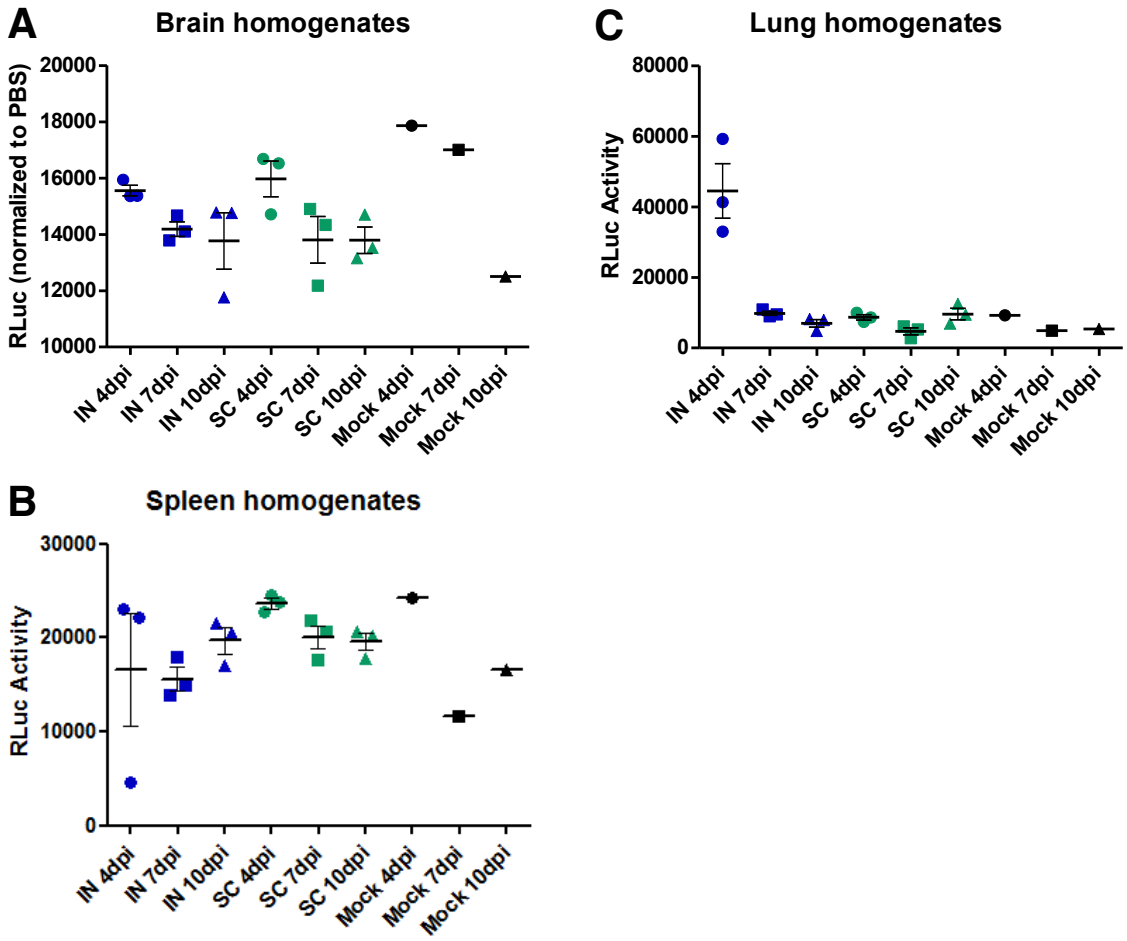

Figure A.3. Susceptibility of C57BL/6 IFNr1-KO mice to intranasal and subcutaneous infections with MuV. C57BL/6 IFNr1-KO mice were infected with PBS or $3x10^6$ PFU i.n. or $6x10^6$ PFU s.c. with rMuV-Rluc. (A) Brain, (B) spleen, and (C) lung tissues were collected and homogenized at 4, 7, and 9 dpi. Tissue homogenates were used to measure renilla luciferase activity.

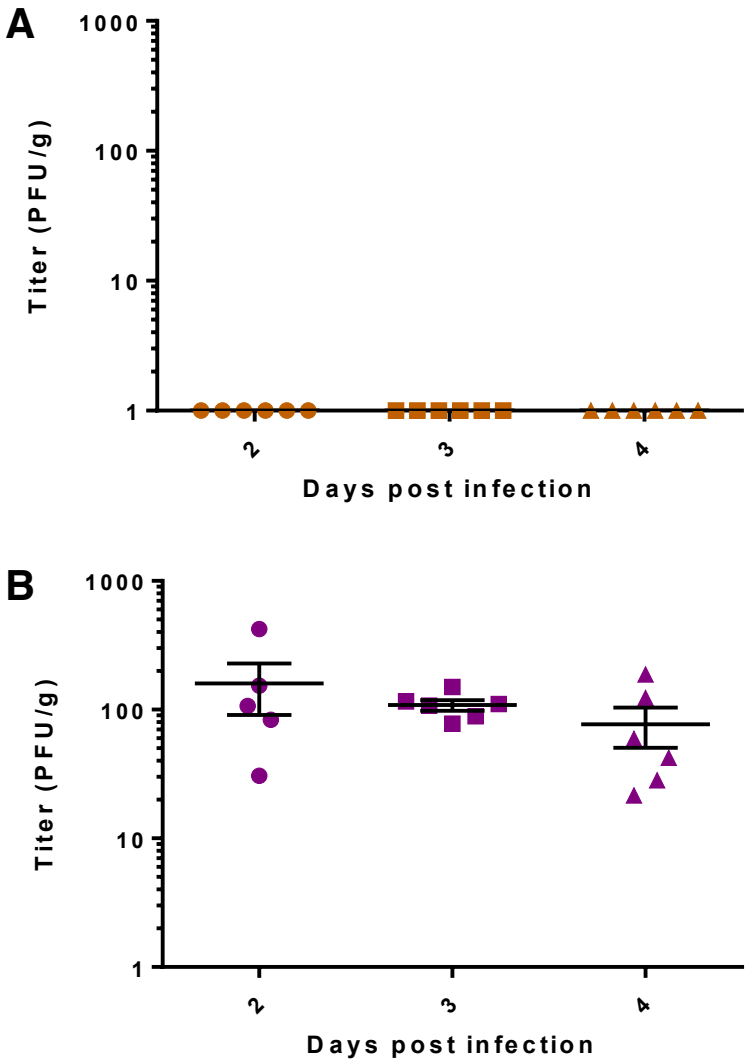

Figure A.4. C57BL/6 IFNr1-KO intranasal infection kinetics. C57BL/6 wild-type (A) or IFNr1-KO (B) mice were infected i.n. with $1x10^6$ PFU of MuV. Lung tissues were collected and homogenized 2, 3, and 4 dpi. Lung homogenates were used for virus titration via plaque assay.

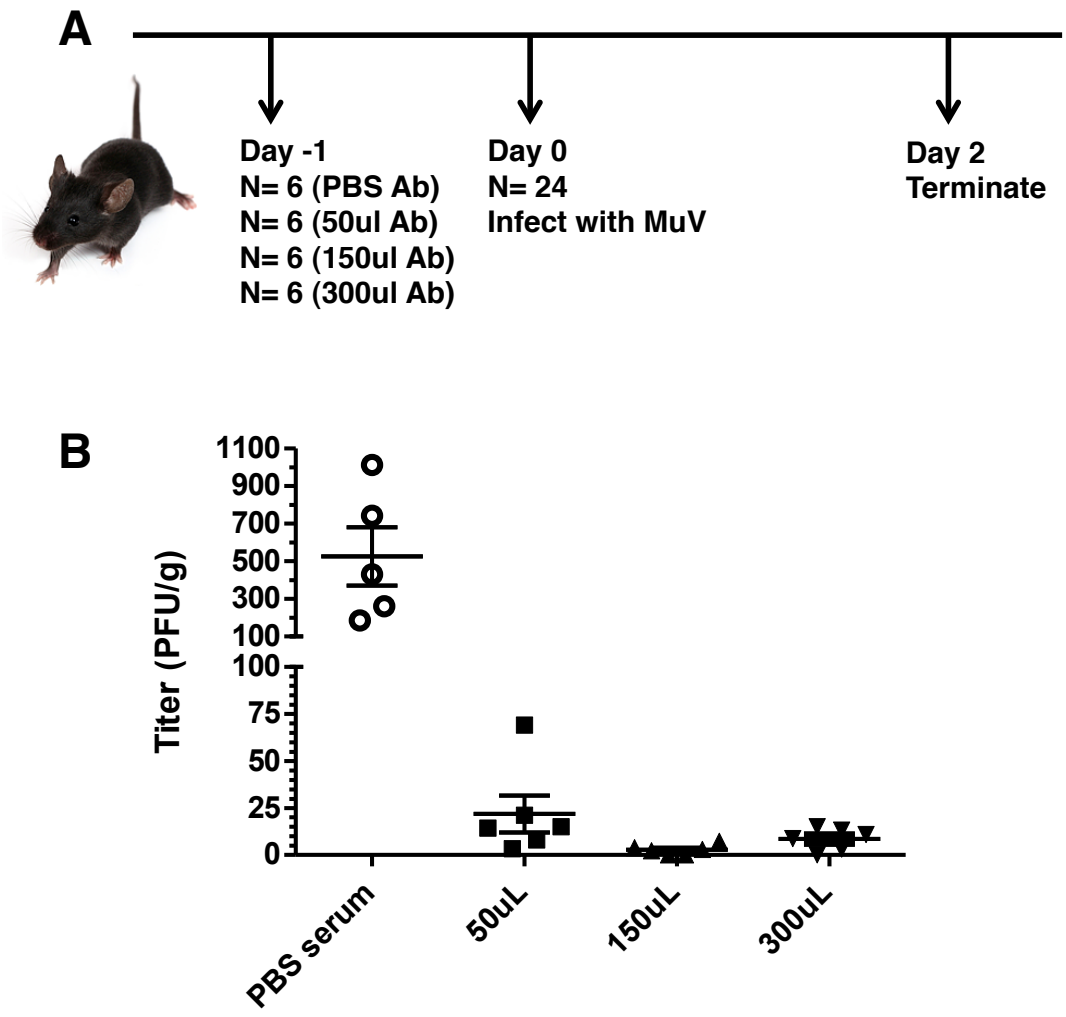

Figure A.5. Reduced viral burden in IFNr1-KO i.n. infected mice that received passive MuV neutralizing antibody treatment. (A) Schematic of passive antibody transfer experiment schedule. Serum from sham vaccinated or MuV vaccinated BALB/c mice was pooled and administered to naïve C57BL/6 IFNr1-KO mice i.p. After 24 hours post antibody transfer, mice were infected with $1x10^6$ PFU i.n. of MuV. Lung tissues were collected and homogenized 2 dpi. (B) Viral titers in lungs. Lung homogenates were used for virus titration via plaque assay.